Heterogeneous Cellular Networks Mixed with LoS and NLoS Transmissions

Jiaqi Wang

Department of Electronic and Electrical Engineering
University of Sheffield

A thesis submitted in partial fulfillment of the requirements
for the degree of

Doctor of Philosophy

April, 2019

Abstract

In the last decades, the rapid increase of user traffic demand for better user experience has pushed the traditional macrocell-only networks being evolving to modern heterogeneous networks(HetNets) with a multi-tier structure. The dense deployment of small-cell base stations (BSs) implies short distances between BSs and users. It is therefore likely that users will see line-of-sight (LoS) links from its serving BS and even nearby interfering BSs, which has not been considered in performance analysis for multi-tier HetNets yet.

In this thesis, the dense multi-tier HetNet with LoS and non-line-of-sight (NLoS) transmissions based on a multi-slope path loss model is analyzed. The spatial locations of BSs of any given network tier and those of mobile users are modeled as independent spatial Poisson point processes (PPPs). The expressions of downlink coverage probability are divided for a multi-tier HetNet, based on that the calculations of the area spectral efficiency (ASE) and energy efficiency (EE) are further proposed. The results demonstrate that in an extremely dense HetNet, both the ASE and EE of the HetNet will drop quickly with further increase of the small-cell density due to the dominance of LoS interfering small-cell links.

Following that, the investigation is moved to the probabilistic events of LoS and NLoS transmissions. Four transmission scenarios are simulated with different path loss models, including a linear LoS probability function, a suburban area, a millimetre wave transmission and a 3D path loss model. Accordingly, a user-centric BS clustering strategy is proposed for a non-coherent joint transmissions (JTs) in dense small-cell networks, based on the idea of grouping the BSs with their LoS probabilities to such user above a predefined threshold. The proposed BS clustering strategy is evaluated in the above four transmission environments. Our simulation results show that the coverage probability and spectrum efficiency (SE) achieved by the proposed user-centric BS clustering strategy achieve a rapid growth rate with the

increasing BS density, and even at extremely high BS densities in all four considered environments.

Lastly, following the proposed BS clustering strategy above, a further developed clustering strategy called multi-BS multi-user-equipment (UE) clustering is proposed to allow multiple BSs to serve multiple UEs simultaneously. The main idea of this clustering strategy is to boost network performance in terms of coverage probability and SE at high BS density without sacrificing the ASE. Utilizing stochastic geometry, the closed form expressions of the network performance in terms of coverage probability, SE, ASE and EE are derived in a downlink small-cell network. The results show that the proposed clustering strategy achieves high coverage probability and linear increasing SE and ASE in ultra dense networks at same time.

Acknowledgements

Firstly, I would like to express the deepest appreciation to my supervisor Dr. Xiaoli Chu for the continuous support of my Ph.D study, for her patience and motivation. Without her guidance and persistent help this thesis would not have been possible. I am also grateful to my second supervisor Prof. Jie Zhang for his sincere support and encouragement. I would also like to thank Dr. Ming Ding and Dr. David López-Pérez for as well for their brilliant comments and suggestions. At last, I would like to thank my family for their endless love and support.

List of Publications

1. J. Wang, X. Chu, M. Ding, and D. López-Pérez, "On the performance of multi-tier heterogeneous networks under los and nlos transmissions," in *2016 IEEE Globecom Workshops (GC Wkshps)*. IEEE, 2016, pp. 1–6
2. J. Wang, X. Chu, M. Ding, and D. López-Pérez, "The effect of los and nlos transmissions on base station clustering in dense small-cell networks," in *2019 IEEE 90th Vehicular Technology Conference (VTC2019-Fall)*, 2019, pp. 1–6

Contents

List of Tables

List of Figures

List of Abbreviations

3D Three dimensional

ASE Area spectral efficiency

AWGN Additive white Gaussian noise

BS Base station

CCDF Complementary cumulative distribution function

CDF Cumulative distribution function

CoMP Coordinated multi-point

CSI Channel state information

EE Energy efficiency

HetNet Heterogeneous network

JT Joint transmission

LoS Line-of-sight

MIMO Multiple-input-multiple-output

NLoS Non-line-of-sight

PDF Probability density function

QoS Quality of service

RS Received signal

RSS Received signal strength

SE Spectral efficiency

SINR Signal-to-interference-plus-noise ratio

SNR Signal-to-noise ratio

UE User equipment

Chapter 1

Introduction

In this chapter, the background of deployment of heterogeneous network (HetNets) is presented. The future HetNets with dense deployment of the small-cell base station (BS) is seem to be a promising approach to meet the fast increasing data demand. However, the dense deployment of HetNets faces new challenges. This thesis aims to investigate the limitation of current HetNets and looking for technology for enhancement of the future cellular networks. The contributions and structures of the thesis are then presented.

1.1 Background

In the last decades, the wireless communication has been pushed into a fast evolution from 3G to 4G, and now coming into 5G era! The reason behind is due to the rapid increase of user traffic demand for better user experience. According to the traffic forecast in [3], the growth rate of mobile data traffic in 2017 was 12 exabytes per month, which will have a seven-fold increase until 2022.

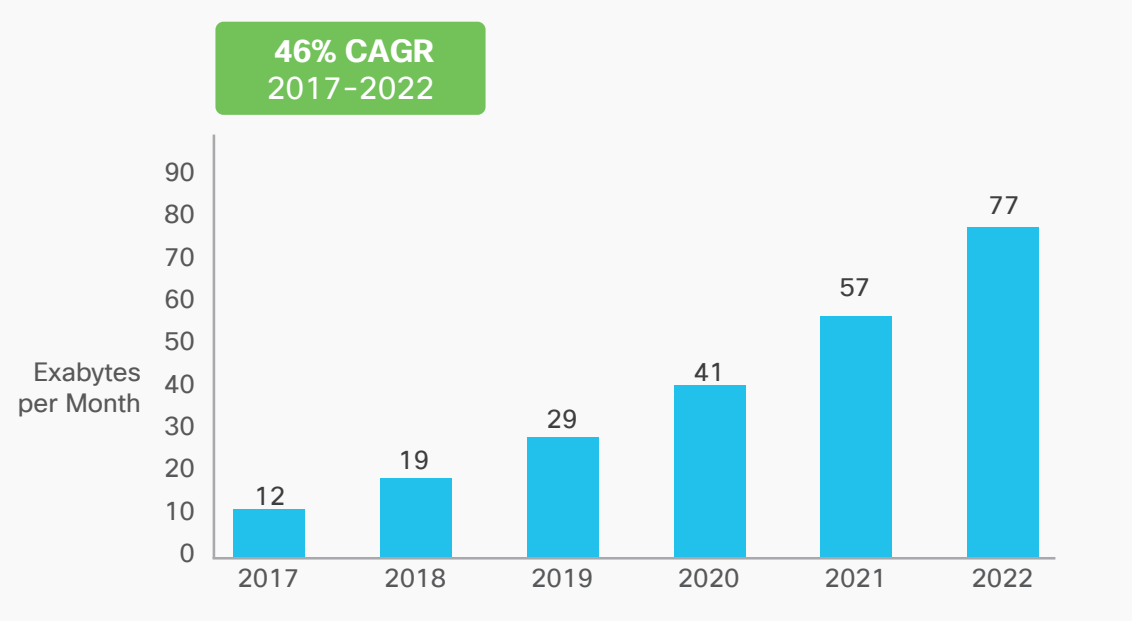

Figure 1.1: Global mobile data traffic growth rate prediction from 2017 to 2022, [Source: Cisco VNI Mobile, 2019]

1.1.1 Deploying HetNets

In order to meet the exponentially increasing traffic demands, the traditional macrocell-only cellular networks are being evolving to modern HetNets which consists of a large number of small cells which are in various types, e.g., microcells, metrocells, picocells, or femtocells. Distinguish from their achievable functions and working transmitting power levels, they are suitable for different local environments. Moreover they are designed to be simple structure with a low install and operating cost, which is ideal for large amount of deployment. In this case, the dense deployment of the small cells reuses the spectrum locally and provides most of the capacity at mobile user equipments (UEs) while macrocells provide an umbrella coverage for UEs.

Despite the benefits, the operators face the challenges to manage the interference

from the dense BS deployment in HetNets, especially inter-cell interference from small-cell BSs.

1.1.2 LoS and NLoS transmission

In traditional cellular networks, the Non-line-of-sight (NLoS) propagation is in charged for most cases. The powerful macrocells are deployed in a sparse grid of the cellular network to provide to cover more area. UEs are usually experiencing a relatively large distance of transmission links to macrocell BS, which results obstacles like, buildings, trees and uneven terrain occurs. The transmitting signal from a macrocell BS may experience reflection, diffraction and absorption in some cases. Therefore, the users are usually suffered from the low received power because of the relatively large distance of transmission links. The techniques, such as multi-path signal propagation and relays, are investigated to overcome such issues.

In contrast, the modern HetNets consists of a large number of small cells. The transmitting distances between UEs and BSs are dramatically reduced. The UEs may located a few meters to BSs. In this case, line-of-sight (LoS) propagation in wireless communication is no longer considered for indoor Wi-Fi network only. People are able to find the small cells BSs on street lamp posts, traffic lights, top of house roof (as shown in Fig. 1.2), etc.

The LoS transmission refers to a transmitting signal travelling at direct path from the transmitter at BS to the receiver at user. Without reflection, diffraction and absorption through the propagation. The LoS transmission link is expected with the high signal power at the receiver to improve the quality of service (QoS) for users. Therefore, the more sophisticated and practical path loss models are worth

Figure 1.2: 5G small-cell BS on house roof [4]

to be considered in the analysis of cellular networks.

1.2 Motivation of the Thesis

In widely considered traditional cellular networks, the sparse deployment of macro-cell BSs leads to the relatively large transmission distances. The transmission links between BSs to UEs and interfering links between BSs to BSs in the outdoor environment are modelled as NLoS propagation only. By utilizing the mathematical tractable tool of stochastic geometry, the network performance is able to theoretically evaluated. To meet the rapidly increasing user demand, the cellular networks evolve from single tier networks to the HetNets with multi-tier structure containing

macrocell BSs and a large number of small-cell BSs. The dense deployment of the small cells in HetNets triggers occurrence of the LoS transmissions in the outdoor environment.

It is challenging to theoretically model the HetNets with the re-defined complicated path loss model. The previous research [5] has shown a path for considering the probabilistic LoS and NLoS transmissions in a single tier cellular network. Base on that, the first research focuses to facilitate a more complicated path loss in a multi-tier HetNets to consider both LoS and NLoS transmissions. The performance of the HetNets from the theoretical results in terms of coverage probability, ASE and EE is expected to demonstrate the characteristic of the effects of LoS transmissions in HetNets.

Following that, the further consideration of more outdoor transmission environments are expected to in the LoS and NLoS path loss model. Since the high transmitting power from LoS links causing the severe interference in densely deployed small-cell BSs leads to negative effects on network performance. In order to mitigate the LoS interference, the BS clustering strategy of joint transmissions (JTs) would be introduced which has the significant effect on mitigating the cell edge interference.

Lastly, the more advanced BS clustering strategy is worth to study in order to further enhance the performance of the cellular networks.

1.3 Contributions of the Thesis

The research contributions of this thesis are listed as follows:

- In Chapter 4, the path loss model with LoS and NLoS transmissions are de-

fined for multi-tier HetNets. Accordingly, the tractable approach by utilizing stochastic geometry is proposed to evaluate the network performance in terms of coverage probability, ASE and EE.

- In Chapter 5, the further investigation are studied for LoS and NLoS path loss model in different transmission environments. A user-centric BS clustering strategy for non-coherent JT is proposed to mitigate inter-cell interference. The proposed BS clustering strategy regarding to a LoS probability threshold is compared to the existing RSS-based BS clustering in the network performance.
- In the Chapter 6, following the research in Chapter 5, the further enhancement of clustering strategy called multi-BS multi-UE clustering strategy is proposed in dense small-cell networks. The tractable approach is developed for theoretical analysis of the network performance in terms of average coverage probability, SE, ASE and EE.

1.4 Structure of the Thesis

The structure of this thesis is presented as follows:

- **Chapter 2: Literature Reivew**

  This chapter firstly reviews the performance analysis of current HetNets in stochastic geometry, and then introduces the importance role of LoS and NLoS model in network performance analysis. Following that, a technologies called coordinated multi-point (CoMP) transmission is reviewed as a potential enhancement for cellular networks.

- **Chapter 3: Stochastic Geometry in Cellular Networks**

In this chapter, stochastic geometry is reviewed as the methodology in theoretical analysis for cellular networks. The concept of stochastic geometry is firstly stated for adaptation to randomness located BSs in networks. The characteristics of point process are determined in a number of definitions. Furthermore, the point process is adapted in wireless network environment for general elaboration.

- **Chapter 4: HetNets in LoS/NLoS Transmissions**

  In this chapter, the path loss model with LoS and NLoS is facilitated in a HetNet. A tractable approach by using stochastic geometry is proposed for theoretical analysis of a K-tier HetNet. The proposed analytical approach is then considered in a simplified 2-tier (macro and small cells) network for more practical simulation. The performance analysis of the HetNets is presented in terms of coverage probability, ASE and EE. The results discuss the performance degradation at high BS density.

- **Chapter 5: LoS/NLoS Transmissions in BS Clustering**

  In this chapter, the LoS and NLoS path loss model is considered in a number of transmission environments, including linear LoS probability function in a theoretical model, isolate picocells in a suburban area, millimetre wave in outdoor environment and urban micro cells in a 3D scenario. The coverage probability and spectral efficiency (SE) of the small-cell network are evaluated in all mentioned cases. The performance degradation of LoS transmission model at high BS density is further proved.

  Correspondingly, a BS clustering strategy is proposed to mitigate the LoS interference at high BS density in order to enhance the network performance.

The analysis in terms of coverage probability and SE are repeated for comparison without BS clustering. The complexity of proposed clustering strategy is further discussed by the number of BSs in a proposed cluster for JTs.

- **Chapter 6: Multi-BS Multi-UE Clustering**

  Following the above the BS clustering strategy research, a new clustering strategy called multi-BS multi-UE clustering is then proposed to improve the utilizing efficiency in spatial domain. The corresponding tractable approach is developed in stochastic geometry in small-cell networks. The performance analysis of a small-cell network is discussed in terms of coverage probability, average data rate, ASE and EE.

- **Chapter 7: Conclusions and Future Works**

  This chapter summarizes the thesis and discusses the future works.

Chapter 2

Literature Review

In this chapter, the topics of current HetNets is introduced in terms of performance features. Due to the channel model have a significant effect on network performance, the critical role of LoS and NLoS transmissions in path loss model is then introduced. Finally, the BS clustering strategy in co-operative transmission for enhancement of network performance is reviewed.

2.1 Review of HetNets Performance Analysis

Dense deployments of small cells are widely considered as the most promising approach to provide high quality of service to mobile users. Thus, future cellular networks are likely to have a multi-tier structure composed of macrocell base stations (BSs) and overlaid small-cell BSs, known as HetNets [7–9].

2.1.1 Performance Analysis in Cellular Networks

The cellular networks are widely evaluated by the characteristics in terms of coverage probability, Spectral efficiency (SE), Area spectral efficiency (ASE) and Energy

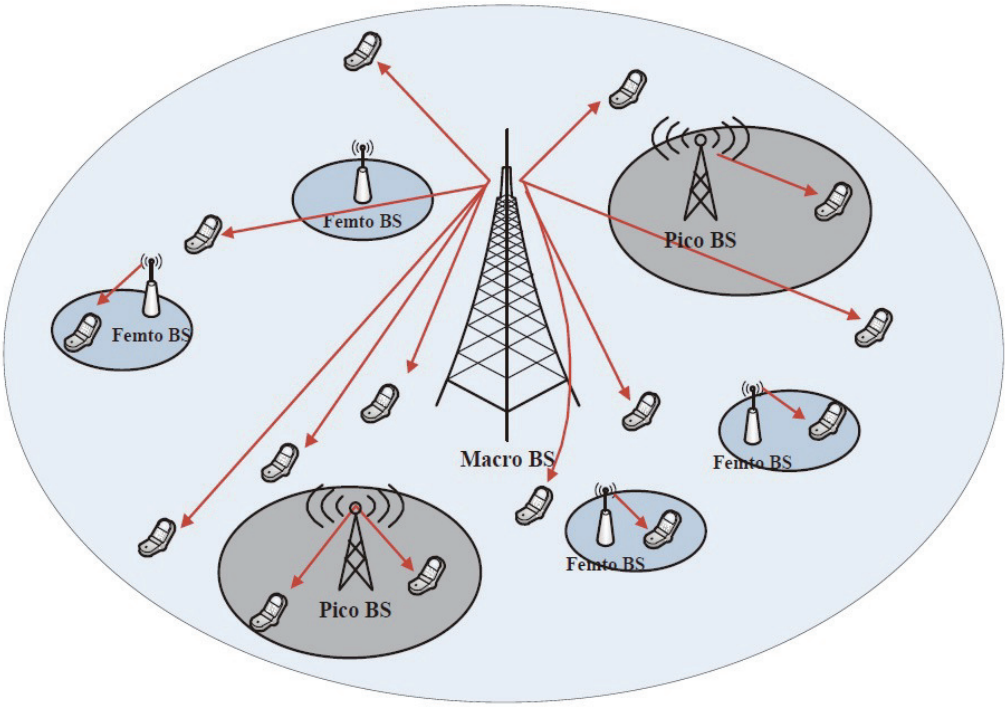

Figure 2.1: Illustration of a three-tier heterogeneous cellular network [6]

efficiency [10–14].

- *Coverage probability*: It is defined as the probability that the signal-to-interference-plus-noise ratio (SINR) at a given UE can achieve a target threshold. The coverage probability can be viewed as the complementary of the outage probability [15, 16]. The coverage probability $\mathcal{C}$ can be given by a mathematical definition as following,

$$\mathcal{C} = \mathbb{P}[\text{SINR} > T] \tag{2.1}$$

  for a SINR threshold T.

- *Spectral efficiency*: It refers to the data rate that can be transmitted to a UE over a given bandwidth in a specific cellular network with the unit of bits/sec/Hz (or bps/Hz) [17]. When the UEs in the cellular network are assumed to share

same spectrum, it is also know as average data rate. The SE denoted by $\mathcal{R}$ is shown in the equation as,

$$\mathcal{R} = \mathbb{E}[\ln(\text{SINR} + 1)]. \tag{2.2}$$

- *Area spectral efficiency*: By considering the cellular network in a defined geographic area, the spatial domain is included. The SE is further introduced by a given covered area with the unit of bits/sec/Hz/km^2 (or bps/Hz/km^2).

$$\text{ASE} = \frac{\mathcal{R}}{\text{Area}} \tag{2.3}$$

- *Energy efficiency*: It is defined as the ratio of the total network throughput over the energy consumption, and the unit is in bits/Joule [18]. To analyze one sub-channel, the EE can be also calculated by the following equation with its unit bps/Hz/W [19].

$$\text{EE} = \frac{\text{ASE}}{P/\text{Area}} \tag{2.4}$$

where P/Area is the average networks power consumption in unit area.

2.1.2 HetNets Performance of Coverage Probability and SE

In many works, HetNets have been modeled as Poisson point process (PPP) for performance analysis by capturing the impact of path loss, composite shadowing and fading, transmit power, traffic loads in multi-tier structure, partial and full spectral reuse among different tiers ($K > 1$), arbitrary locations and deployment densities of all types of BSs. Using the stochastic geometry, the coverage probability

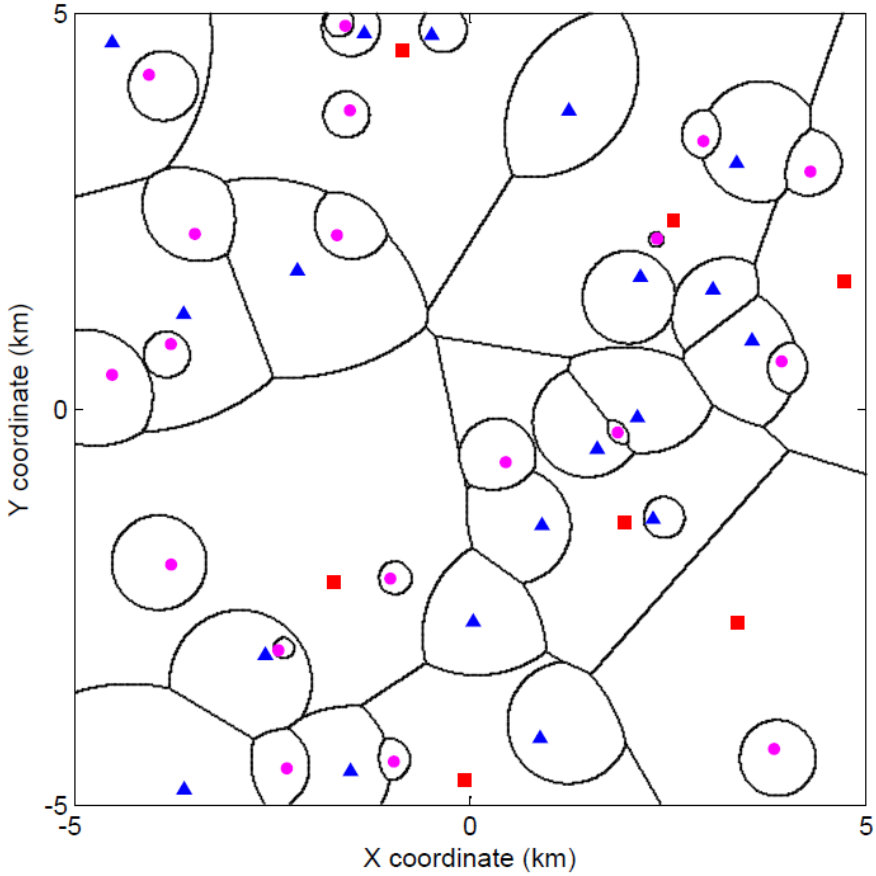

Figure 2.2: Example of downlink HetNet with three tiers of BSs: a high-power macrocell BS (red square) is overlaid with successively denser and lower power picocells (blue triangle) and femtocells (magenta circle) [20]

of the is able to theoretically analyzed through the equation [21–24].

$$\mathcal{C} = \sum_{k=1}^{K} \mathbb{P}[\mathrm{SINR}_k(r) > \gamma] \tag{2.5}$$

In [20], the coverage of different BSs is shown in Fig. 2.2, where black lines show the border of cell coverage. By taking advantage of the tractability offered by PPP

modeling [24–26], the tractable framework is then established to model cellular networks. In a multi-tier HetNets, the tractable approach for coverage probability and achievable data rate, in which a flexible cell association is introduced in term of received signal power and bias factor in different tiers [20, 27].

Furthermore, the authors in [28] show that a positive range expansion bias of the small cells will encourage users to discard the macrocells and associate with lightly loaded small cells. The HetNets will then be improved in coverage probability. Moreover, this coverage can be further optimized by tuning the parameters of BS densities and bias factor of small cells [29]. Offloading UEs towards small cells is an effective way to meet the high data rate demand in two-tier HetNets, but offloaded users suffer from strong inter-tier interference, which reduces the benefits of offloading [30].

The small cells with various types of BSs can achieve large performance gain through aggressive spectrum reuse [31–33]. By deploying more small cells in a HetNets, it has a potential to improve SE by reducing inter-cell interference if the small cells can partially open theirs channels for external UEs to access. In [31], the SE of a multi-tier HetNet is analytically derived in both open and closed access schemes of small cells.

$$\mathcal{R} = \mathbb{E}[\ln(\mathrm{SINR} + 1)] \tag{2.6}$$

The PPP is modelled to prove its accuracy by comparing the coverage probability in the traditional grid deployment and real-world random deployment.

In [32,34], the problem of optimizing the rate coverage is analyzed from the tier association probability and spectrum portioning is addressed in a multi-tier network. By utilizing tools of stochastic geometry, the significantly improved coverage is shown

in rate coverage of the system. In [33, 35], the data rate in both spectrum reuse and shared spectrum access scenarios are modeled for uplink transmission in the HetNet. The data rate in small cells degrades severely due to co-tier interference. The optimal factor of partial spectrum reuse defined as the portion of spectrum reused by small cells in two-tier HetNets is further analyzed in [36].

2.1.3 HetNets performance of ASE

Unlike the traditional cellular network with macro cells only, the dense deployment of small cells in current HetNets brings the concern of efficiency evaluation in sptial domain [37]. The SE of a network system is further introduced in a unit area as the ASE as,

$$\text{ASE} = \frac{\mathcal{R}}{\text{Area}} = \lambda_{\text{BS}}\mathcal{R} \tag{2.7}$$

where λ_{BS} is the BS density.

In [38, 39], the ASE is modeled in a multi-tier HetNet with macro and femto BSs, where the deployment of low power femtocell BSs are around the edge of the macro-cells. Then, the HetNets is suited in uplink transmission with location based power control mechanism [40]. A analytical bounds on the uplink ASE of is derived for the cell edge user by the approach of the moment generating function. In [41–43], it has been shown that the ASE of a downlink HetNet increases with the additional deployment of small-cell BSs. However, more small-cell BSs raise the energy cost and limit network flexibility and performance.

2.1.4 HetNets performance of EE

It is worth noting that a rapid increasing number of deployed small-cell BSs lead to an increase in the total energy consumption of the HetNets, growing environmental awareness and economic sustainability [44–48]. These foreseeing impacts of EE in cellular networks is motivating the standardization authorities and network operators to continuously explore future technologies [46].Thus, the more comprehensive performance analyses of HetNets gains the focus on energy efficiency. The analytical equation of EE is then presented in [49, 50] as,

$$\mathrm{EE} = \frac{\mathrm{ASE}}{\sum_{k=1}^{K} \lambda_k P_k}. \tag{2.8}$$

In [51,52], a framework of theoretical analysis is derived to evaluate EE in a two-tier multiple-input-multiple-output(MIMO) HetNet while considering wireless backhaul in both uplink and downlink transmissions. In [36], by analyzing partial spectrum reuse in two-tier HetNets. the UE association choice of preferable BSs is suggested in term of BS energy cost. In order to further improve the energy efficiency and interference mitigation in HetNets, [53] proposed an iterative power allocation algorithms between primary macrocells and small cells. It maximized the sum energy efficiency of the small cells while respecting the interference limits at the macrocell UEs. In [54], the authors investigate the method to enhance EE in cognitive uplink wireless system. By considering the uncertainty of the channel state information (CSI) between the primary and secondary UEs, the energy efficiency is maximized. In [55], the authors proposed an energy efficiency model for Poisson-Voronoi tessel-

lation cellular networks, in which the spatial distribution of traffic load and power consumption are considered for a typical BS. The energy efficiency is evaluated in both numerical and Monte Carlo simulations by taking into account traffic load, channel effects and interference.

2.1.5 Effect of Path Loss in Network Performance

The path loss model with equation form as PathLoss $= r^{-\alpha}$ is widely accepted in analysis of cellular networks to model the decay of transmitted signal power. In [56], the outage probability of the cellular network is demonstrate in Fig. 2.3 as a function of the path loss exponent β. The figure indicates that the system

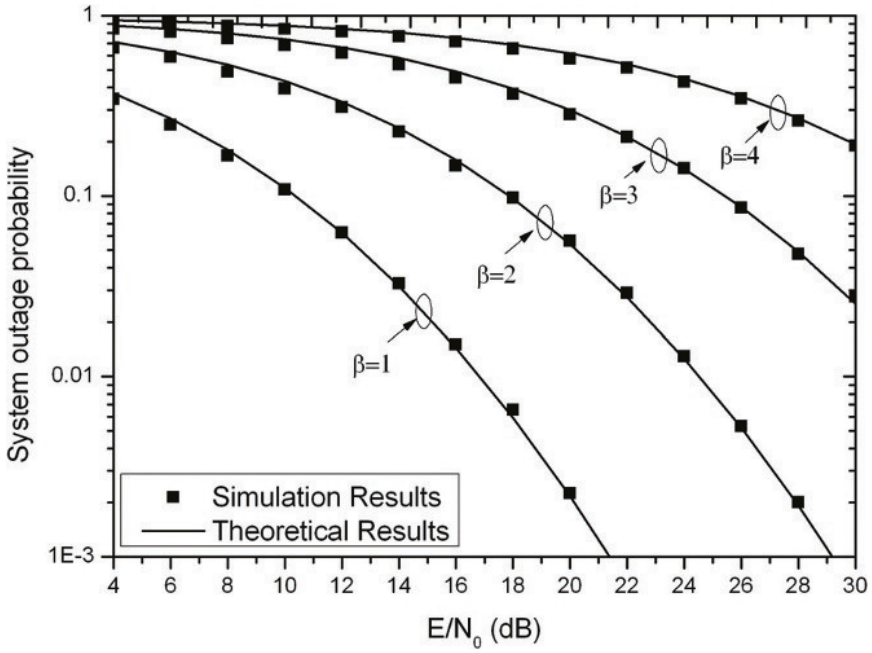

Figure 2.3: System outage probability versus the transmit SNR with different path loss exponents [56]

outage performance can be improved with the decrease of β. That's because the path loss increases with the decrease of β, and then the channel gain will increase

correspondingly, which results a lower outage probability of the system. In [57–59], The coverage probability, potential throughput and ASE are shown in path loss models of various path loss exponents in dense cellular networks. The disappointed results predict the limit of cellular network densification. Since, significant effects of path loss model in analysis of cellular network, the more practical model for current dense HetNets is in required.

2.2 Review of LoS and NLoS Transmissions

Traditionally, NLoS transmissions would usually occur in cellular communications. By introducing dense deployment of the small cells in HetNets, the distance of transmission link largely reduced bewteen the UEs and their serving BSs. It is likely that UEs will see LoS links from serving BSs and even nearby interfering BSs. Traditionally, NLoS transmissions with single slope would usually occur in the cellular communications model [60]. Compared to NLoS interfering links, the LoS interfering links with slow attenuation of the signal power can lead to severer interference to the user.

In [61–63], the LoS and NLoS path loss models have gained significant interest in the design of dense small-cell networks. In [61], the 3GPP suggested different outdoor path loss models for urban, suburban, and rural environments. In [62], a linear function for the LoS probability was considered as a special case for a tractable analysis of small-cell network performance. In [63], 3 dimensional (3D) path loss models covering both LoS and NLoS transmissions were proposed for both indoor and outdoor environments, where the heights of BSs and users play an important role.

From stochastic geometry, the analytical framework for small cell networks was proposed in [64], where the more accurate path loss model is taken into account for both the LoS and NLoS transmissions as shown in equation.

$$l(r) = \begin{cases} l^{\mathrm{L}}(r) = A^{\mathrm{L}} r^{-\alpha^{\mathrm{L}}} & \text{with } \mathrm{Pr}_1^{\mathrm{L}}(r) \\ l^{\mathrm{NL}}(r) = A^{\mathrm{NL}} r^{-\alpha^{\mathrm{NL}}} & \text{with } 1 - \mathrm{Pr}_1^{\mathrm{L}}(r) \end{cases} \tag{2.9}$$

The results indicated the dense networks will suffer from high outage probability under both LoS and NLoS transmissions. It brought the concern to justify the benefit of future dense cellular networks. Furthermore, the ASE and on the energy efficiency of dense small-cell networks were evaluated in the effect of LoS and NLoS transmissions in [65]. It is interesting to notice that the ASE behave two linear increase rates at low and high BS densities. The EE exhibits a a global maximum value in LoS and NLoS transmissions, which in contrast of monotonically increasing in the case of LoS or NLoS scenarios. In addition, the LoS and NLoS transmissions is introduced in millimeter wave cellular networks [66]. The closed-form formulas from stochastic geometry is addressed to compute coverage probability and the average rate.

2.2.1 Multi-slope path loss model

In traditional single path loss model, the fixed path loss exponent can lead to magnitude differences in received and interference powers against the true values in practical. The uplink dense small cell networks under both LoS and NLoS transmissions is analyzed in the network performance of ASE [67], which conclude that a significant improvement of the ASE can be realized by introducing a small power compensation factor in uplink transmission. In [68], multi-slope path loss models are

modelled by a piece-wise power law and continuous and accurately approximates, where different distance ranges are subject to different path loss exponents within each distance slope.

$$l(r) = \begin{cases} l_1(r) = A_1 r^{-\alpha_1} & \text{when } 0 < r \leq d_1 \\ l_2(r) = A_2 r^{-\alpha_2} & \text{when } d_{n-1} < r \leq d_n \\ ... & \\ l_N(r) = A_N r^{-\alpha_N} & \text{when } r > d_{N-1} \end{cases} \tag{2.10}$$

A more comprehensive multi-slope path loss model was used to model LoS and NLoS transmissions in a single-tier homogeneous small-cell network [5,69]. The analytical results were obtained by utilizing stochastic geometry, which showed the existence of an optimum BS density to maximise the achievable coverage probability. Once this optimum point is reached, the coverage probability decreases fast with the small cell density. This is because the LoS transmissions from nearby interfering BSs collectively cause a tremendous amount of interference to the users. In this case, the gains of techniques such as coordinated multi-point (CoMP) can be expected to increase in dense networks.

2.3 BS Clustering Strategy

HetNets is seemed to be the key feature for future cellular networks, which is able to meet the ever-increasing mobile user data demand. However, the the dense deployment of small cells are randomly located and operated in uncoordinated state. The more organized coordinated operation is thus required for network enhancement. User-centric BS co-operation can play a important role in managing interference in

HetNets, which provide a guarantee for the improvement of user data rate [70].

2.3.1 Review of Joint Transmissions

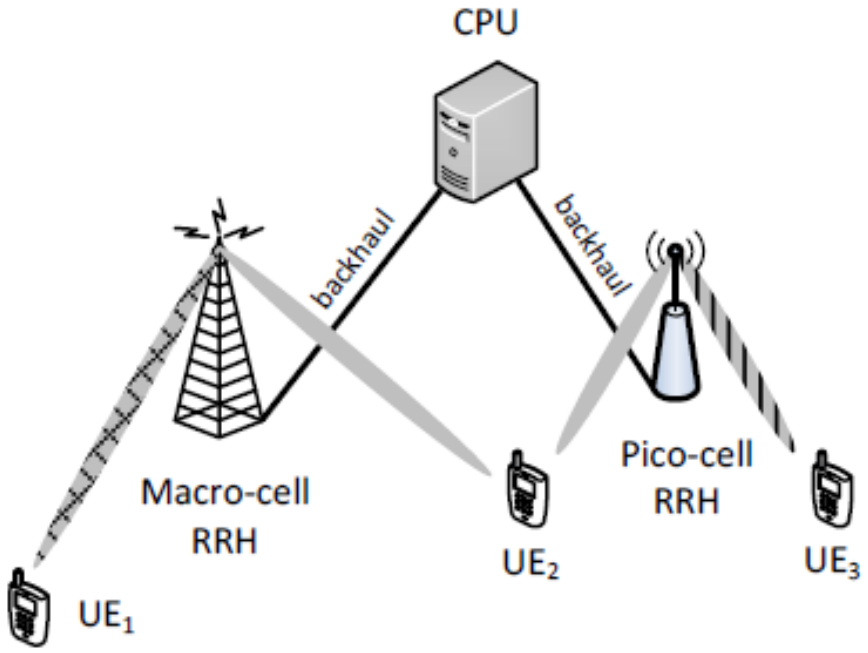

Figure 2.4: Illustration of CoMP [71]

CoMP with JT is considered as one of the key technology enhancements for future cellular networks to improve user data rate and SE. CoMP transmission as shown in Fig. 2.4 is realized by exchanging coordination information between a set of transmission BSs, forming a so-called CoMP cluster [71, 72]. Interference can be mitigated by cooperation between different sites of BSs. Significant gains can be rewarded for both the uplink and downlink transmissions [73].

In [43, 74, 75], the outage probability of a user is studied in CoMP to mitigate inter-cell interference in dense cellular networks. The practical factors are included as the irregular locations of Poisson distributed BSs, the resultant path loss, multi-antenna

BSs for mitigating mutual interference in the same cluster and different sub-channel for nearby BSs.

A closed-form expressions and accurate approximations of average data rate of CoMP cluster with imperfect CSI is derived in [76], subjected to the small-scale Rayleigh fading, path loss attenuation, and interference from outside CoMP cluster. In order to improve performance of the coverage and data rate especially for cell edge UEs, the cellular networks are considered in multi-tier structure. The network performance of the coverage probability is enhanced by CoMP transmission techniques in [77]. In [78, 79], the overlaying macro BSs and small-cell BSs are deployed in co-channel. The cross-tier interference have a significantly negative effects in network performance due to multiple tiers of BSs operating shared spectrum. CoMP with JT show the effectiveness in mitigating cross-tier interference in multi-tier networks.

Moreover, in [80], it considers the power optimization problem for downlink transmission in CoMP systems, aims to minimum weighted EE with QoS constraint. However, the performance of CoMP systems heavily depends on the feedback quality and channel imperfections.

2.3.2 Coherent and Non-coherent Joint Transmissions

For interference limited cellular networks, CoMP with JT has been widely considered as a promising technique to increase the network performance [81]. Ideal backhaul of the network is assumed, which allow randomly deployed BSs jointly transmit user data. The signals from different BSs are well synthesized. The inter-cell interference is thus mitigated and hence improve SINR at the UEs and resulting better coverage

probability and SE of the whole network.

Coherent Joint Transmissions

In coherent JT, it is assumed that CSI of the serving links from the BSs in the cooperation set is shared in the BSs in the cooperation set. Based on the CSI shared among all cooperating BSs, the potential serving BSs for one typical UE is a subset of all BSs. The transmitted signals from different BSs in the subset are jointly pre-coded with prior phase alignment and tight synchronized to transmit the same message to the target UE on the same time and frequency resource [82–86]. In [87], coherent JT in downlink heterogeneous cellular networks is further proposed with a tight approximation and closed form of coverage probability by utilizing stochastic geometry. The results indicate a significant positive gains in coverage probability in coherent JT scenario. A further study of coherent JT is produced in [83]. A Gamma distribution is introduced in PPP of stochastic geometry, which provide an tight upper bound of network coverage probability and approximation is tight in interference limited HetNets.

Non-coherent Joint Transmissions

One popular BS cooperation technology is non-coherent JT, where multiple BSs collaboratively transmit to a user without prior phase-mismatch correction or tight synchronization [70,88–90]. It presented in [88] that a tractable model from stochastic geometry is approached by taking into account the BS density, channel fading, average path loss, and interference in non-coherent JT. In [89], non-coherent JT was then analyzed in HetNets, where any BS with the received signal strength (RSS) above a pre-defined threshold is selected to perform user-centric BS clustering. It

was shown that for small cooperative clusters of small-cell BSs, non-coherent JT among small cells can provide SE gains without significantly increasing the traffic load per cell. In [70], stochastic geometry tools were used to analyze non-coherent JT models, where each user is served by either one or two BSs. In [90], the non-coherent JT was combined with frequency reuse to improve the utilisation efficiency of spectrum resources.

2.3.3 User-Centric BS clustering

According to the random location of all UEs, the BS set of JT is usually formed in term of UE-BS association constraint, such as RSS threshold. Where any BS with the RSS above a pre-defined threshold is selected to perform in JT [89]. In spatial area of BS set, there is one typical UE located at the origin surround by BSs in JT, which forms a disk area, so called user-centric BS clustering.

In [91], user-centric BS clustering is facilitated in a multi-cell HetNet a large number of distributed small-cell BSs. By considering each UE is served a small number of potentially overlapping BSs, this work investigated interference management problem. A tractable model using Poisson cluster process (PCP) was presented for coverage probability analysis in [92] to modeling the irregularities in the locations of cellular BSs. In [93], the mean achievable rate per user is study in coordinated BS downlink transmission as clustered cellular networks, with transmit power constraints of the BSs. The interference within the cluster is blocked among users, while the interference from other clusters still remains. The average achievable rate per user is evaluate by the impact of the main parameters, such as the singal-to-noise ratio (SNR), the antenna configuration and the path loss.

We note that none of the above works on coherent or non-coherent JT has considered the challenges and opportunities brought by the LoS links in dense cellular networks, in which case the LoS links widely appears in outdoor transmission environment.

2.4 Summary

In this chapter, three main sections are reviewed as the performance analysis in HetNets, the key role of LoS and NLoS transmissions and BS Clustering Strategy.

In the review of performance analysis in HetNets, the key features of a HetNets is related to the performance of coverage probability, SE, ASE and EE. Various scenarios and technologies are derived in related closed form expressions by stochastic geometry to enhance these features.

In the review of LoS and NLoS transmissions, the LoS transmission links are determined to usually occur in dense deployment of small-cell networks. In the analysis of dense deployment of small cells, more practical multi-slope path loss model with probabilistic LoS and NLoS transmissions is required. The HetNet coverage and ASE hold in a more comprehensive path loss model

In the review of BS clustering strategy, the CoMP is first introduced as a primeval co-operative transmission technology. Following that, the coherent and non-coherent JTs are introduced for more recent researches. Lastly, the user-centric BS clustering in JTs is considered as a effective way to mitigate a interference in cellular network.

Chapter 3

Stochastic Geometry in Cellular Networks

In this chapter, stochastic geometry is reviewed as the mathematic methodology in theoretical analysis for cellular networks. The point process is introduced and further adapted for wireless network environment by a series of definitions and derivations in [94, 95].

3.1 Concept of Stochastic Geometry

Unlike the hexagonal deployment of traditional cellular networks, the modern HetNets especially the dense deployment of small cells consists BSs in random locations. The theoretical analysis of the cellular network raise the question that how can one derive statistical properties of a collection of BS points? Stochastic geometry subjected to point process provides the answer to explain the characteristics of the random spatial patterns.

3.2 Point Process

Consider the d-dimensional space $\mathbb{R}^d$. There are several ways to describe A spatial point process Φ which is the collection of points $(x_1, x_2, ...)$

- Direct characterization of the points x_i.
- Using the intervals $S_i = x_i + 1 - x_i$, $i \in N$. Here it is assumed that the points are ordered in ascending index, i.e., $x_1 \leq x_2 \leq ....$ The increments S_i are independent in this renewal processes.
- Counting the infinite points falling in a set $B \subset \mathbb{R}$:

$$N(B) = \sum_{i=1}^{\infty} 1(x_1 \in B). \tag{3.1}$$

3.2.1 One-dimensional Poisson Process

Definition 3.1 *A one-dimensional Poisson point process (PPP) is a point process in* $\mathbb{R}$ *with constant intensity* λ. $N([a, b))$ *has the Poisson distribution with mean* $\lambda(b - a)$ *in each interval* $[a, b)$,

$$\mathbb{P}(N([a, b)) = k) = \exp(-\lambda(b - a))\frac{(\lambda(b - a))^k}{k!} \tag{3.2}$$

Due to the intensity is not a function of the location, so the process is called homogeneous or uniform.

3.2.2 Poisson Point Process

Definition 3.2 *For a PPP in finite-dimension* $\mathbb{R}^d$ *with intensity measure* Λ *and density* λ, *the Poisson distribution* $N(B)$ *is defined by its means* $\Lambda(B)$ *for every set*

$B \subset \mathbb{R}^d$,

$$\mathbb{P}(N(B) = k) = \exp\big(- \int_B \lambda(x)\mathrm{d}x\big) \frac{(\int_B \lambda(x)\mathrm{d}x)^k}{k!} \tag{3.3}$$

If $\Lambda(b) = \lambda|B|$ *in* $\mathbb{R}$*, we call* Φ *is a homogeneous PPP and* λ *is the intensity parameter.*

3.2.3 Mean of Sum in Point Process

Theorem 3.1 *From Campbell's theorem, for a point process* $\Phi = x = x_1, x_2, ... \subset \mathbb{R}^d$ *and a measurable function* f*:* $\mathbb{R}^d \to \mathbb{R}$*, the sum*

$$S = \sum_{x \in \Phi} f(x) \tag{3.4}$$

further calculate the expectations of sums of function f *with ranges on the real line, the mean of sum in function* f *over the point process is given as,*

$$\mathbb{E}(S) = \int_{\mathbb{R}^d} f(x)\Lambda(\mathrm{d}x) \tag{3.5}$$

If the point process Phi has a density of λ*, it becomes,*

$$\mathbb{E}(S) = \int_{\mathbb{R}^d} f(x)\lambda(x)\mathrm{d}x \tag{3.6}$$

Furthermore, in a stationary point process Phi with uniform or constant intensity, it can be written as,

$$\mathbb{E}(S) = \lambda \int_{\mathbb{R}^d} f(x)\mathrm{d}x \tag{3.7}$$

3.2.4 Moment-Generating Function of Point Process

Theorem 3.2 *From Campbell's theorem, for homogeneous PPP with intensity λ in $\mathbb{R}^d$ and a measurable function f: $\mathbb{R}^d \to \mathbb{R}$, the sum*

$$S = \sum_{x \in \Phi} f(x) \tag{3.8}$$

is absolutely convergent, if and only if

$$\int_{\mathbb{R}}^{d} \min(|f(x)|, 1) \mathrm{d}x < \infty. \tag{3.9}$$

In this case, we have the moment-generating function as,

$$\mathbb{E}(e^{tS}) = \exp\Big(\int_{\mathbb{R}^d} \lambda(e^{tf(x)} - 1) \mathrm{d}x \Big) \tag{3.10}$$

The obtained equation is a function of f. If setting $t = 1$, the characteristic functional of the PPP is obtained.

$$\mathbb{E}(e^{S|f|}) = \exp\Big(\int_{\mathbb{R}^d} \lambda(e^{f(x)} - 1) \mathrm{d}x \Big) \tag{3.11}$$

3.2.5 Probability Generating Function of Point Process

A PPP denoted by Φ has $\Phi = x = x_1, x_2, ... \subset \mathbb{R}^d$ and a measurable function f: $\mathbb{R}^d \to \mathbb{R}$. The sum of $f(x)$ over Φ is given as

$$\sum_{x \in \Phi} f(x) = \int_{\mathbb{R}^d} f(x) \Phi(\mathrm{d}x) = \int_{\mathbb{R}^d} f(x) p(x) \mathrm{d}x \tag{3.12}$$

where

$$p(x) = \sum_{y \in \Phi} \delta(x - y) \tag{3.13}$$

$\delta(\dot{})$ is the Dirac delta function. The mean value of the sum is derived in expectation operation.

$$\mathbb{E}\big(\sum_{x \in \Phi} f(x)\big) = \int_{\mathcal{N}} \int_{\mathbb{R}^d} f(x)\varphi(\mathrm{d}x)P(\mathrm{d}\varphi) \tag{3.14}$$

where $\mathcal{N}$ counts the number of points in Phi.

Definition 3.3 *Let $\mathcal{V}$ be the family of all measurable functions v, $\mathbb{R}^d \to [0, 1]$. For $v \in \mathcal{V}$, the probability generating functional (pgfl) of the point process Φ is defined as*

$$G\,[v] = \mathbb{E}\big(\sum_{x \in \Phi} v(x)\big) = \int_{\mathcal{N}} v(x)P(\mathrm{d}\varphi) \tag{3.15}$$

From the derivation above, the result is shown as,

$$G\,[v] = \mathbb{E}\big[\exp\big(\int_{\mathcal{R}^d} \log v(x)\Phi(\mathrm{d}x)\big)\big] \tag{3.16}$$

3.3 Point Process in Cellular Networks

3.3.1 Interference in Point Process

The transmitter is modelled as a point process $Phi \subset \mathbb{R}^d$ with the intensity of λ. Due to the fact that $\mathbb{E}_I(y) = \mathbb{E}_I 0)$, thus the origin is picked as the reference point to calculate the expectation over the point process. Following the power law $l(x) = ||x||^{-\alpha}$. the mean interference is given as

$$\mathbb{E}_I = \mathbb{E}\Big(\sum_{x \in \Phi} ||x||^{-\alpha}\Big) \tag{3.17}$$

From the Campbell's formula,

$$\mathbb{E}_I = \lambda \int_{\mathbb{R}^d} ||x||^{-\alpha} \mathrm{d}x \tag{3.18}$$

3.3.2 Coverage Probability in Poisson Network

In this section, a receiver is assumed to be able to decode the message from the a working transmitter, and located with the distance r to the transmitter. By considering the power law and Rayleigh fading, the signal power arrived at the receiver is exponential with mean $r - \alpha$. The coverage probability of the considered transmission link is determined in a PPP with interferers of intensity λ.

$$p_s = \mathbb{P}(SIR > \theta) = \mathbb{P}(S > I\theta) = \mathbb{E}_I(\exp(-I\theta)) \tag{3.19}$$

Further include the distance r in above equation, it gives,

$$p_s(r) = \mathbb{P}(SIR > \theta | r) = \mathbb{E}_I(\exp(-Ir^{\alpha}\theta)) \tag{3.20}$$

3.3.3 Shannon throughput

The Shannon throughput is based on the coverage probability of the system, due to the fact that only successful transmissions counts. Recall the coverage probability in above equation and consider p is a function of threshold θ, the Shannon throughput is then derived as,

$$\mathbb{E}\log(SINR + 1) = -\int_0^{\infty} \log(1+\theta)\mathrm{d}p_s(\theta) \tag{3.21}$$

If the complementary cumulative distribution function (cdf) of the random variable $X = \log(1 + SINR)$, we have,

$$\mathbb{P}(X > x) = \mathbb{P}(SINR > e^x - 1) = p_s(d^x - 1) \tag{3.22}$$

Substitute the results in above equation, it gives,

$$\mathbb{E}\log(SINR + 1) = -\int_0^\infty p_s(d^x - 1)\mathrm{d}x \tag{3.23}$$

Chapter 4

HetNets in LoS/NLoS Transmissions

In this chapter, the path loss is considered in a practical model with multi slops considering both LoS and NLoS transmissions. A tractable approach is then developed in a mult-tier HetNets, in which the UE is associated to serving BS with a maximum biased received power. A simplified two-tier HetNets is modelled in the closed form equations for verification. The performance of the HetNets is analyzed in terms of coverage probability, ASE and EE.

4.1 Introduction

Dense deployments of small cells are widely considered as the most promising approach to provide high quality of service to mobile users.

Thus, future cellular networks are likely to have a multi-tier structure with various types of BSs. In many existing works, HetNets have been modeled as spatial PPPs

for performance analysis. By taking advantage of the tractability offered by PPP modeling, the authors show that a positive small-cell range expansion bias that encourages users to associate with lightly loaded small cells can enhance the HetNet coverage [20], and that this coverage can be optimized by tuning the density and bias factor of small cells. It has been shown that the ASE of a HetNet increases with the increase of small-cell density when a single-slope path loss model is considered [41].

However, the possibility of LoS transmissions has not be considered in HetNets yet. Although NLoS transmissions would usually occur in cellular communications, with the dense deployment of small-cell BSs and the resulting short distances between BSs and users, it is likely that users will see LoS links from its serving BS and even nearby interfering BSs. In [5], a multi-slope path loss model is used to model LoS and NLoS transmissions in a single-tier homogeneous small-cell network. The analytical results show both the existence of a maximum coverage probability and the non-linear increase or even decrease of the ASE with the small cell density. These probabilistic LoS transmissions have not been considered in the performance analysis for multi-tier HetNets yet. Moreover, in light of the results in [5], it is not clear whether or not the conclusions of HetNet coverage in [20] and ASE in [41] hold for a more comprehensive path loss model.

It is also worth noting that most HetNet performance analysis does not focus on energy efficiency (EE), and that a rapid increase in the number of deployed small-cell BSs may lead to an increase in the total energy consumption of a HetNet, affecting its environmental friendliness or economic sustainability [44]. Thus, there is a need for comprehensive HetNet performance analyses, considering also HetNet EE.

In this chapter, we study the network performance of a dense multi-tier HetNet

under a practical multi-slope path loss model that covers LoS and NLoS transmissions. The spatial locations of BSs of any given network tier and those of mobile users are modeled as independent PPPs. A user is associated to the BS that offers the highest biased downlink received power, which is the downlink received power multiplied by the bias factor of the corresponding network tier. Under this practical yet tractable system model, we analyze and derive the expression of downlink coverage probability for a multi-tier HetNet, and then use it to calculate its ASE and EE. Numerical results are provided for a two-tier HetNet to verify the obtained analytical expressions and shed new light on the performance gains achievable by dense deployment of small cells in a HetNet.

The rest of this chapter is organized as follows. In Section 4.2, the path loss model is introduced, followed by defining user association in Section 4.3. In Section 4.4, we analyze the coverage probability, ASE and EE for multi-tier HetNets under LoS and NLoS transmissions. Then, we simplify the derived analytical equation to fit in a two-tier HetNets in Section 4.5. In Section 4.6, we present the numerical results. In Section V, the conclusions are drawn.

4.2 Multi-Slope Path Loss Model

In this section, we consider a K-tier ($K > 2$) HetNet with all the K tiers sharing the same frequency spectrum. The spatial distribution of the k^{th} tier BSs follows an independent homogeneous PPP with intensity of $\lambda_k, k \in 1, 2, ..., K$. The indexes of all the k^{th} tier BSs are contained in the set Φ_k. The users are distributed over the K-tier HetNet area following another independent PPP with intensity of λ_u, where λ_u is large enough to ensure that each BS has at least one user.

We use a multi-slope path loss model considering both LoS and NLoS transmissions as probabilistic events, where the path loss of a link is segmented into N slopes depending on the range of the link. Accordingly, the path loss between a k^{th} tier BS and a user at distance r is given by

$$l_k(r) = \begin{cases} l_{k,1}(r) = \begin{cases} l_{k,1}^{\text{L}}(r) = A_{k,1}^{\text{L}} r^{-\alpha_{k,1}^{\text{L}}} & \text{with } \Pr_1^{\text{L}}(r) \\ l_{k,1}^{\text{NL}}(r) = A_{k,1}^{\text{NL}} r^{-\alpha_{k,1}^{\text{NL}}} & \text{with } 1 - \Pr_1^{\text{L}}(r) \end{cases} & 0 < r \leq d_1 \\ \ldots \\ l_{k,n}(r) = \begin{cases} l_{k,n}^{\text{L}}(r) = A_{k,n}^{\text{L}} r^{-\alpha_{k,n}^{\text{L}}} & \text{with } \Pr_n^{\text{L}}(r) \\ l_{k,n}^{\text{NL}}(r) = A_{k,n}^{\text{NL}} r^{-\alpha_{k,n}^{\text{NL}}} & \text{with } 1 - \Pr_n^{\text{L}}(r) \end{cases} & d_{n-1} < r \leq d_n \\ \ldots \\ l_{k,N}(r) = \begin{cases} l_{k,N}^{\text{L}}(r) = A_{k,N}^{\text{L}} r^{-\alpha_{k,N}^{\text{L}}} & \text{with } \Pr_N^{\text{L}}(r) \\ l_{k,N}^{\text{NL}}(r) = A_{k,N}^{\text{NL}} r^{-\alpha_{k,N}^{\text{NL}}} & \text{with } 1 - \Pr_N^{\text{L}}(r) \end{cases} & r > d_{N-1} \end{cases} \tag{4.1}$$

where $d_n (n = 1, 2, \ldots, N-1)$ are the segment breaking points, $\Pr_n^{\text{L}}(r) (n = 1, 2, \ldots, N-1)$ is the probability of LoS transmission of the n^{th} slope, $1 - \Pr_n^{\text{L}}(r)$is the probability of NLoS transmission of the n^{th} slope, and $\alpha_{k,n}^{\text{L}}$, $\alpha_{k,n}^{\text{NL}}$, $A_{k,n}^{\text{L}}$ and $A_{k,n}^{\text{NL}}$ are the LoS and NLoS path loss exponents and path loss constants of the n^{th} slope in the k^{th} tier, respectively. 3rd Generation Partnership Project (3GPP) has suggested some expressions for $\Pr_n^{\text{L}}(r)$ [5, 61].

4.3 User Association scheme

We consider a user association scheme based on the maximum biased received power [20], i.e.,

$$(i^*, k^*) = \arg \max_{k \in 1,2,\ldots,K, i \in \Phi_k} P_k B_k l_k(r_i) \tag{4.2}$$

For brevity of notation, we omit $*$ from i^* and k^* hereafter. P_k is the transmit power of a k^{th} tier BS. r_i is the distance from the i^{th} BS in the k^{th} tier to the user. B_k is the bias factor of k^{th} tier BS, which allows to manipulate the load balancing between different tiers or cell range expansion.

Therefore, the user is associated to the $i^{*\text{th}}$ BS in the k^{th} tier , and the downlink SINR is given by

$$\text{SINR}_k(r_i) = \frac{P_k h_{r_i} l_k(r_i)}{I_{k,i} + \sigma^2} \tag{4.3}$$

where h_{r_i} is the channel model of the fading power gain between the i^{th} BS in the k^{th} tier and the user, which follows a unit-mean exponential distribution, $I_{k,i}$ is the interference power received from cross-tier and co-tier BSs and is expressed as

$$I_{k,i} = I_{cross} + I_{co} = \sum_{j=1, j \neq k}^{K} \sum_{x \in \Phi_j} P_j h_{r_x} l_j(r_x) + \sum_{x \in \Phi_k, x \neq i} P_k h_{r_x} l_k(r_x) \tag{4.4}$$

and σ^2 is the additive White Gaussian Noise (AWGN) power at the user.

4.4 Theoretical Analysis in Multi-tier HetNets

In this section, we analyze the coverage probability of a multi-tier HetNet under the system model given in Section II, and then use the obtained coverage probability to

calculate its ASE and EE.

4.4.1 Coverage Probability

The downlink coverage probability is defined as the probability that the downlink SINR of a user is above a pre-defined threshold [22], i.e.,

$$\begin{aligned}\mathcal{C} &= \sum_{k=1}^{K} \mathbb{P}[\mathrm{SINR}_k(r_i) > \gamma, k = k^*] \\ &= \sum_{k=1}^{K} \mathcal{C}_k(\lambda_k, \gamma)\rho_k\end{aligned} \tag{4.5}$$

where $\mathcal{C}_k(\lambda_k, \gamma)$ is the coverage probability offered by the kth tier [22], γ is the SINR threshold, and ρ_k, which is equal to $\mathbb{P}[k = k^*]$, is the probability of a typical user being associated with a k^{th} tier BS, and the expression of ρ_k is given by (4.10).

According to the multi-slope path loss model in (4.1), the coverage probability of a user associated with a k^{th} tier BS can be further expressed as

$$\mathcal{C}_k(\lambda_k, \gamma) = \sum_{n=1}^{N} (T_{k,n}^{\mathrm{L}} + T_{k,n}^{\mathrm{NL}}) \tag{4.6}$$

where the coverage probability of the nth slope in the k^{th} tier is composed of the following two parts [5],

$$\begin{aligned}T_{k,n}^{\mathrm{L}} &= \int_{d_{n-1}}^{d_n} \mathbb{P}[\mathrm{SINR}_k^{\mathrm{L}}(r) > \gamma] f_{k,n}^{\mathrm{L}}(r) dr \\ T_{k,n}^{\mathrm{NL}} &= \int_{d_{n-1}}^{d_n} \mathbb{P}[\mathrm{SINR}_k^{\mathrm{NL}}(r) > \gamma] f_{k,n}^{\mathrm{NL}}(r) dr\end{aligned} \tag{4.7}$$

The probability of a downlink user with LoS transmission from the serving BS having

SINR greater than the threshold γ is given by

$$\begin{aligned}
&\mathbb{P}[\mathrm{SINR}_k^{\mathrm{L}}(r) > \gamma] = \mathbb{P}\Big[\frac{P_k h_{r_x} l_{k,n}^{\mathrm{L}}(r)}{I_{k,i} + \sigma^2} > \gamma\Big] \\
&= \mathbb{E}_{I_{k,i}}\Big\{\mathbb{P}\Big[h_{r_x} > \frac{\gamma(I_{k,i} + \sigma^2)}{P_k l_{k,n}^{\mathrm{L}}(r)}\Big]\Big\} \\
&\overset{(a)}{=} \mathbb{E}_{I_{k,i}}\Big\{\exp\Big(-\frac{\gamma(I_{k,i} + \sigma^2)}{P_k l_{k,n}^{\mathrm{L}}(r)}\Big)\Big\} \\
&= \exp\Big(-\frac{\gamma\sigma^2}{P_k l_{k,n}^{\mathrm{L}}(r)}\Big)\mathbb{E}_{I_{\mathrm{cross}}}\Big\{\exp\Big(-\frac{\gamma I_{\mathrm{cross}}}{P_k l_{k,n}^{\mathrm{L}}(r)}\Big)\Big\}\mathbb{E}_{I_{\mathrm{co}}}\Big\{\exp\Big(-\frac{\gamma I_{\mathrm{co}}}{P_k l_{k,n}^{\mathrm{L}}(r)}\Big)\Big\} \\
&\overset{(b)}{=} \exp\Big(-\frac{\gamma\sigma^2}{P_k l_{k,n}^{\mathrm{L}}(r)}\Big)\mathcal{L}_{I_{\mathrm{co}}}\Big(\frac{\gamma r^{\alpha_{k,n}^{\mathrm{L}}}}{P_k A_{k,n}^{\mathrm{L}}}\Big)\prod_{j=1, j\neq k}^{K}\mathcal{L}_{I_{\mathrm{cross}}}\Big(\frac{\gamma r^{\alpha_{k,n}^{\mathrm{L}}}}{P_k A_{k,n}^{\mathrm{L}}}\Big) \\
&= \exp\Big(\frac{\gamma\sigma^2 r^{\alpha_{k,n}^{\mathrm{L}}}}{P_k A_{k,n}^{\mathrm{L}}}\Big)\prod_{j=1}^{K}\mathcal{L}_{I_{k,i}}\Big(\frac{\gamma r^{\alpha_{k,n}^{\mathrm{L}}}}{P_k A_{k,n}^{\mathrm{L}}}\Big)
\end{aligned} \tag{4.8}$$

where (a) follows the independence of h_{r_x}, (b) follows the exponential distributed h_{r_x}, and (c) follows from the probability generating functional of a PPP.

According to the computation in [5], $\mathrm{SINR}^{\mathrm{L}}$ and $\mathrm{SINR}^{\mathrm{NL}}$ are the coverage probability offered by LoS and NLoS links, respectively, and are given by

$$\begin{aligned}
\mathbb{P}[\mathrm{SINR}_k^{\mathrm{L}}(r) > \gamma] &= \exp\Big(-\frac{\gamma\sigma^2 r^{-\alpha_{k,n}^{\mathrm{L}}}}{P_k A_{k,n}^{\mathrm{L}}}\Big)\prod_{j=1}^{K}\mathcal{L}_{I_{k,i}}\Big(\frac{\gamma r^{-\alpha_{k,n}^{\mathrm{L}}}}{P_k A_{k,n}^{\mathrm{L}}}\Big) \\
\mathbb{P}[\mathrm{SINR}_k^{\mathrm{NL}}(r) > \gamma] &= \exp\Big(-\frac{\gamma\sigma^2 r^{-\alpha_{k,n}^{\mathrm{NL}}}}{P_k A_{k,n}^{\mathrm{NL}}}\Big)\prod_{j=1}^{K}\mathcal{L}_{I_{k,i}}\Big(\frac{\gamma r^{-\alpha_{k,n}^{\mathrm{NL}}}}{P_k A_{k,n}^{\mathrm{NL}}}\Big)
\end{aligned} \tag{4.9}$$

where $\mathcal{L}_{I_j}(s)$ is the Laplace transform of interference I_j [20].

Moreover, $f_{k,n}^{\mathrm{L}}(r)$ and $f_{k,n}^{\mathrm{NL}}(r)$ are the probability density functions (PDFs) of the link between a user and a k^{th} tier BS being LoS and NLoS, respectively, conditioned on the range r of the link satisfying $d_{n-1} < r \leq d_n$.

[ht]

Corollary 4.1 ***Computation of*** ρ_k

The probability of a typical user being associated with a k^{th} *tier BS is the combination of two events. Firstly, if the user is associated to a LoS BS, its biased received power is greater than that in any other LoS and NLoS links, i.e.,* $\mathbb{P}[P_k B_k l^{\text{L}}_{k,n}(r) > P_j B_j l_j(x)]$*. Similarly, if the user is associated to a NLoS BS, its biased received power is also greater than that in any other LoS and NLoS links in all tiers, i.e.,* $\mathbb{P}[P_k B_k l^{\text{NL}}_{k,n}(r) > P_j B_j l_j(x)]$*. The calculation is further referenced from subsection of "Computation of* $f^{\text{L}}_{k,n}(r)$*" in 4.2.*

$$
\begin{aligned}
&\rho_k = \mathbb{P}[k = k^*] \\
&= \mathbb{E}\Big[\mathbb{P}\big[P_k B_k l^{\text{L}}_{k,n}(r) > P_j B_j l_j(x) \bigcup P_k B_k l^{\text{NL}}_{k,n}(r) > P_j B_j l_j(x)\big]\Big] \\
&= \int_0^\infty \left\{ \begin{array}{l} \prod_{j=1, j\neq k}^{K} \mathbb{P}[P_k B_k l^{\text{L}}_{k,n}(r) > P_j B_j l^{\text{L}}_j(x)] \\ \times \prod_{j=1}^{K} \mathbb{P}[P_k B_k l^{\text{L}}_{k,n}(r) > P_j B_j l^{\text{NL}}_j(x)] \end{array} \right\} f_{R^{\text{L}}_k(r)dr} \\
&+ \int_0^\infty \left\{ \begin{array}{l} \prod_{j=1, j\neq k}^{K} \mathbb{P}[P_k B_k l^{\text{NL}}_{k,n}(r) > P_j B_j l^{\text{NL}}_j(x)] \\ \times \prod_{j=1}^{K} \mathbb{P}[P_k B_k l^{\text{NL}}_{k,n}(r) > P_j B_j l^{\text{L}}_j(x)] \end{array} \right\} f_{R^{\text{L}}_k(r)dr} \\
&= 2\pi\lambda_k \int_0^\infty \left\{ \begin{array}{l} r \exp\Big(- \int_0^r \Pr^{\text{L}}_n(u) 2\pi u \lambda_k du \Big) \\ \times \prod_{j=1, j\neq k}^{K} \exp\Big(- \int_0^a \Pr^{\text{L}}_n(u) 2\pi u \lambda_j du \Big) \\ \times \prod_{j=1}^{K} \exp\Big(- \int_0^b \big[1 - \Pr^{\text{L}}_n(u)\big] 2\pi u \lambda_j du \end{array} \right\} dr\} \\
&+ 2\pi\lambda_k \int_0^\infty \left\{ \begin{array}{l} r \exp\Big(- \int_0^r \big[1 - \Pr^{\text{L}}_n(u)\big] 2\pi u \lambda_k du \Big) \\ \times \prod_{j=1, j\neq k}^{K} \exp\Big(- \int_0^c \big[1 - \Pr^{\text{L}}_n(u)\big] 2\pi u \lambda_j du \Big) \\ \times \prod_{j=1}^{K} \exp\Big(- \int_0^d \Pr^{\text{L}}_n(u) 2\pi u \lambda_j du \end{array} \right\} dr\}
\end{aligned}
\tag{4.10}
$$

where $a = \left(\frac{P_j B_j A^{\text{L}}_{j,n}}{P_k B_k A^{\text{L}}_{k,n}}\right)^{1/\alpha^{\text{L}}_{j,n}} r^{\alpha^{\text{L}}_{k,n}/\alpha^{\text{L}}_{j,n}}$, $b = \left(\frac{P_j B_j A^{\text{NL}}_{j,n}}{P_k B_k A^{\text{L}}_{k,n}}\right)^{1/\alpha^{\text{NL}}_{j,n}} r^{\alpha^{\text{L}}_{k,n}/\alpha^{\text{NL}}_{j,n}}$,
$c = \left(\frac{P_j B_j A^{\text{NL}}_{j,n}}{P_k B_k A^{\text{NL}}_{k,n}}\right)^{1/\alpha^{\text{NL}}_{j,n}} r^{\alpha^{\text{NL}}_{k,n}/\alpha^{\text{NL}}_{j,n}}$ *and* $d = \left(\frac{P_j B_j A^{\text{L}}_{j,n}}{P_k B_k A^{\text{NL}}_{k,n}}\right)^{1/\alpha^{\text{L}}_{j,n}} r^{\alpha^{\text{NL}}_{k,n}/\alpha^{\text{L}}_{j,n}}$.

Calculation of PDFs $f^{\mathrm{L}}_{k,n}(r)$ and $f^{\mathrm{NL}}_{k,n}(r)$

The expression of $f^{\mathrm{L}}_{k,n}(r)$ is given by

$$\begin{aligned} f^{\mathrm{L}}_{k,n}(r) = \frac{\mathrm{Pr}^{L}_{n}(r)2\pi r\lambda_k}{\rho_k}\exp\Big(-\int_0^r \mathrm{Pr}^{\mathrm{L}}_{n}(u)2\pi u\lambda_k du\Big) \\ \times \prod_{j=1,j\neq k}^{K}\exp\Big(-\int_0^a \mathrm{Pr}^{\mathrm{L}}_{n}(u)2\pi u\lambda_j du\Big) \\ \times \prod_{j=1}^{K}\exp\Big(-\int_0^b \big[1-\mathrm{Pr}^{\mathrm{L}}_{n}(u)\big]2\pi u\lambda_j du\Big) \end{aligned} \tag{4.11}$$

where $a = \Big(\frac{P_jB_jA^{\mathrm{L}}_{j,n}}{P_kB_kA^{\mathrm{L}}_{k,n}}\Big)^{1/\alpha^{\mathrm{L}}_{j,n}} r^{\alpha^{\mathrm{L}}_{k,n}/\alpha^{\mathrm{L}}_{j,n}}$ and $b = \Big(\frac{P_jB_jA^{\mathrm{NL}}_{j,n}}{P_kB_kA^{\mathrm{L}}_{k,n}}\Big)^{1/\alpha^{\mathrm{NL}}_{j,n}} r^{\alpha^{\mathrm{L}}_{k,n}/\alpha^{\mathrm{NL}}_{j,n}}$. The calculation of (4.11) is provided in following section 4.2.

The expression of $f^{\mathrm{NL}}_{k,n}(r)$ is given by

$$\begin{aligned} f^{\mathrm{NL}}_{k,n}(r) = \frac{\big[1-\mathrm{Pr}^{\mathrm{L}}_{n}(r)\big]2\pi r\lambda_k}{\rho_k}\exp\Big(-\int_0^r \big[1-\mathrm{Pr}^{\mathrm{L}}_{n}(u)\big]2\pi u\lambda_k du\Big) \\ \times \prod_{j=1,j\neq k}^{K}\exp\Big(-\int_0^c \big[1-\mathrm{Pr}^{\mathrm{L}}_{n}(u)\big]2\pi u\lambda_j du\Big) \\ \times \prod_{j=1}^{K}\exp\Big(-\int_0^d \mathrm{Pr}^{\mathrm{L}}_{n}(u)2\pi u\lambda_j du\Big) \end{aligned} \tag{4.12}$$

where $c = \Big(\frac{P_jB_jA^{\mathrm{NL}}_{j,n}}{P_kB_kA^{\mathrm{NL}}_{k,n}}\Big)^{1/\alpha^{\mathrm{NL}}_{j,n}} r^{\alpha^{\mathrm{NL}}_{k,n}/\alpha^{\mathrm{NL}}_{j,n}}$ and $d = \Big(\frac{P_jB_jA^{\mathrm{L}}_{j,n}}{P_kB_kA^{\mathrm{NL}}_{k,n}}\Big)^{1/\alpha^{\mathrm{L}}_{j,n}} r^{\alpha^{\mathrm{NL}}_{k,n}/\alpha^{\mathrm{L}}_{j,n}}$. By plugging (4.9), (4.11) and (4.12) into (4.7), we can calculate the coverage probability of LoS and NLoS links for the n^{th} slope in the k^{th} tier. By substituting the calculated (4.7), (4.6) and (4.10) into (4.5), we obtain the coverage probability of the K-tier.

Corollary 4.2 ***Computation of*** $f_{R_k}(r)$

The probability of a user being R_k away from its serving BS with the LoS link is regarded to r, which can be expressed by the combination of the probability of any LoS BS located outside the distance R_k^{L} and any NLoS BS located outside the distance R_k^{NL} conditioned on the probability of the LoS BS belonging to the k^{th} tier [96]. The probability is given by

$$\begin{aligned}\mathbb{P}[R_k > r] &= \mathbb{P}[R_k^{\mathrm{L}} > r, R_k^{\mathrm{NL}} > r | k = k^*] \\ &= \frac{\mathbb{P}[R_k^{\mathrm{L}} > r, R_k^{\mathrm{NL}} > r, k = k^*]}{\mathbb{P}[k = k^*]} \\ &= \frac{\mathbb{P}[R_k^{\mathrm{L}} > r, R_k^{\mathrm{NL}} > r, k = k^*]}{\rho_k}\end{aligned} \tag{4.13}$$

$\rho_k = \mathbb{P}[k = k^*]$, and the numerator is expressed as

$$\begin{aligned}&\mathbb{P}[R_k^{\mathrm{L}} > r, R_k^{\mathrm{NL}} > r, k = k^*] = \int_r^{\infty} \mathbb{P}[R_k^{\mathrm{L}} > r, R_k^{\mathrm{NL}} > r] f_{R_k}(r) \\ &\int_r^{\infty} \left\{ \begin{array}{l} \prod_{j=1, j\neq k}^{K} \mathbb{P}[P_k B_k l_{k,n}^{\mathrm{L}}(r) > P_j B_j l_{j,n}^{\mathrm{L}}(x)] \\ \times \prod_{j=1}^{K} \mathbb{P}[P_k B_k l_{k,n}^{\mathrm{L}}(r) > P_j B_j l_{j,n}^{\mathrm{NL}}(x)] \end{array} \right\} dr\}\end{aligned} \tag{4.14}$$

Following the eq. (4.13), we first consider the Computation of $f_{R_k}(r)$. The nearest BS with a LoS path to the user is located at R_k away from the user. The complementary cumulative distribution function (CCDF) of R_k is

$$F_{R_k}(r) = \exp(-\int_0^r \mathrm{Pr}_n^{\mathrm{L}}(u) 2\pi u \lambda_k du) \tag{4.15}$$

The PDF of R_k is

$$f_{R_k}(r) = \mathrm{Pr}_n^{\mathrm{L}}(r) 2\pi r \lambda_k \exp(-\int_0^r \mathrm{Pr}_n^{\mathrm{L}}(u) 2\pi u \lambda_k du) \tag{4.16}$$

Corollary 4.3 ***Computation of*** $\mathbb{P}[P_k B_k l^{\mathrm{L}}_{k,n}(r) > P_j B_j l^{\mathrm{L}}_{j,n}(x)]$

The probability of $\mathbb{P}[P_k B_k l^{\mathrm{L}}_{k,n}(r) > P_j B_j l^{\mathrm{L}}_{j,n}(x)]$ *in (4.13) is calculated to be the probability of no BS being closer to the user than* $a = \left(\frac{P_j B_j A^{\mathrm{L}}_{j,n}}{P_k B_k A^{\mathrm{L}}_{k,n}}\right)^{1/\alpha^{\mathrm{L}}_{j,n}} r^{\alpha^{\mathrm{L}}_{k,n}/\alpha^{\mathrm{L}}_{j,n}}$ *in the* j^{th} *tier,*

$$\begin{aligned}
&\mathbb{P}[P_k B_k l^{\mathrm{L}}_{k,n}(r) > P_j B_j l^{\mathrm{L}}_{j,n}(x)] \\
&= \mathbb{P}\Big[A^{\mathrm{L}}_{k,n} r^{-\alpha^{\mathrm{L}}_{k,n}} > \frac{P_j B_j}{P_k B_k} A^{\mathrm{L}}_{j,n} r^{-\alpha^{\mathrm{L}}_{j,n}}\Big] \\
&= \mathbb{P}\Big[x > \Big(\frac{P_j B_j A^{\mathrm{L}}_{j,n}}{P_k B_k A^{\mathrm{L}}_{k,n}}\Big)^{1/\alpha^{\mathrm{L}}_{j,n}} r^{\alpha^{\mathrm{L}}_{k,n}/\alpha^{\mathrm{L}}_{j,n}}\Big] \\
&= \exp(-\int_0^a \mathrm{Pr}^{\mathrm{L}}_n(u) 2\pi u \lambda_j du)
\end{aligned} \tag{4.17}$$

where $a = \left(\frac{P_j B_j A^{\mathrm{L}}_{j,n}}{P_k B_k A^{\mathrm{L}}_{k,n}}\right)^{1/\alpha^{\mathrm{L}}_{j,n}} r^{\alpha^{\mathrm{L}}_{k,n}/\alpha^{\mathrm{L}}_{j,n}}$.

Corollary 4.4 ***Computation of*** $\mathbb{P}[P_k B_k l^{\mathrm{L}}_{k,n}(r) > P_j B_j l^{\mathrm{NL}}_{j,n}(x)]$

Following similar computation of (4.17), we have

$$\mathbb{P}[P_k B_k l^{\mathrm{L}}_{k,n}(r) > P_j B_j l^{\mathrm{NL}}_{j,n}(x)] = \exp(-\int_0^b [1 - \mathrm{Pr}^{\mathrm{L}}_n(u)] 2\pi u \lambda_j du) \tag{4.18}$$

where $b = \left(\frac{P_j B_j A^{\mathrm{NL}}_{j,n}}{P_k B_k A^{\mathrm{L}}_{k,n}}\right)^{1/\alpha^{\mathrm{NL}}_{j,n}} r^{\alpha^{\mathrm{L}}_{k,n}/\alpha^{\mathrm{NL}}_{j,n}}$.

From (4.16), (4.17) and (4.18) the cumulative distribution function (CDF) of R_k is

$F^{\mathrm{L}}_{k,n}(r) = 1 - \mathbb{P}[R_k > r]$. Thus, the PDF is shown as,

$$\begin{aligned} f^{\mathrm{L}}_{k,n}(r) &= \frac{d\big(1 - F^{\mathrm{L}}_{k,n}(r)\big)}{dr} \\ &= \frac{\mathrm{Pr}^{L}_{n}(r) 2\pi r \lambda_k}{\rho_k} \exp\Big(- \int_0^r \mathrm{Pr}^{\mathrm{L}}_{n}(u) 2\pi u \lambda_k du \Big) \\ &\times \prod_{j=1, j\neq k}^{K} \exp\Big(- \int_0^a \mathrm{Pr}^{\mathrm{L}}_{n}(u) 2\pi u \lambda_j du \Big) \\ &\times \prod_{j=1}^{K} \exp\Big(- \int_0^b \big[1 - \mathrm{Pr}^{\mathrm{L}}_{n}(u)\big] 2\pi u \lambda_j du \Big) \end{aligned} \tag{4.19}$$

4.4.2 Area Spectral Efficiency and Energy Efficiency

From [11], the ASE (in bps/Hz/m^2) of a K-tier HetNet is the summation of the ASE offered by each tier, i.e.,

$$\text{ASE of all tiers} = \sum_{k=1}^{K} \lambda_k \log_2(1+\gamma) \rho_k \mathcal{C}_k(\lambda_k, \gamma) \tag{4.20}$$

Following [12], the EE (in bps/Hz/W) of the K-tier HetNet is defined as

$$\mathrm{EE} = \frac{\text{ASE of all tiers}}{\sum_{k=1}^{K} \lambda_k P_k} \tag{4.21}$$

where $\sum_{k=1}^{K} \lambda_k P_k$ is the average spatial transmitting power consumption [44]. By substituting (4.10) into (4.8), we have the EE of a K-tier as

$$\mathrm{EE} = \frac{\sum_{k=1}^{K} \lambda_k \log_2(1+\gamma) \rho_k \mathcal{C}_k(\lambda_k, \gamma)}{\sum_{k=1}^{K} \lambda_k P_k} \tag{4.22}$$

4.5 Two-Tier HetNets in LoS/NLoS Transmissions

In this section, a two-tier HetNet ($k \in \{1, 2\}$) composed of macrocells and small cells is facilitated in above analytical model, $K = 2$. We use a path loss model with the LoS probability given as [5]

$$\Pr^{\mathrm{L}}(r) = \begin{cases} 1 - \frac{r}{d_1} & \text{when} \quad 0 < r \leq d_1 \\ 0 & \text{when} \quad r > d_1 \end{cases} \tag{4.23}$$

According to this function of LoS probability, we naturally consider a two slopes path loss ($N = 2, n \in \{1, 2\}$) as $0 < r \leq d_1$ and $d_1 < r < \infty$. Moreover, the path loss exponents and constants of each slope in each tier are assumed to be same for simplification, i.e., $\alpha^{\mathrm{L}}_{k,n} = \alpha^{\mathrm{L}}$, $\alpha^{\mathrm{NL}}_{k,n} = \alpha^{\mathrm{NL}}$, $A^{\mathrm{L}}_{k,n} = A^{\mathrm{L}}$, $A^{\mathrm{NL}}_{k,n} = A^{\mathrm{NL}}$.

From eq. (4.6), in a two-tier HetNet with a two-slope path loss model, the coverage probability of the k^{th} is written as, σ^2

$$\begin{aligned} \mathcal{C} &= \mathcal{C}_1 + \mathcal{C}_2 \\ &= T^{\mathrm{L}}_{1,1} + T^{\mathrm{NL}}_{1,1} + T^{\mathrm{L}}_{1,2} + T^{\mathrm{NL}}_{1,2} + T^{\mathrm{L}}_{2,1} + T^{\mathrm{NL}}_{2,1} + T^{\mathrm{L}}_{2,2} + T^{\mathrm{NL}}_{2,2} \\ &\overset{(a)}{=} T^{\mathrm{L}}_{1,1} + T^{\mathrm{NL}}_{1,1} + T^{\mathrm{NL}}_{1,2} + T^{\mathrm{L}}_{2,1} + T^{\mathrm{NL}}_{2,1} + T^{\mathrm{NL}}_{2,2} \end{aligned} \tag{4.24}$$

where (a) is due to that there is no LoS BS in the slope of $r > d_1$, which means $T^{\mathrm{L}}_{2,2} = 0$. In order to calculate $T^{\mathrm{L}}_{1,1}$, we recall the eq. (4.7),

$$\begin{aligned} T^{\mathrm{L}}_{1,1} &= \int_{d_1}^{0} \mathbb{P}[\mathrm{SINR}^{\mathrm{L}}_1(r) > \gamma] f^{\mathrm{L}}_{1,1}(r) dr \\ &= \int_{d_1}^{0} \exp(-s\sigma^2) \mathcal{L}_{I^{\mathrm{L}}_1}(s) \mathcal{L}_{I^{\mathrm{L}}_2}(s) \mathcal{L}_{I^{\mathrm{NL}}_1}(s) \mathcal{L}_{I^{\mathrm{NL}}_2}(s) f^{\mathrm{L}}_{1,1}(r) \end{aligned} \tag{4.25}$$

where $s = \frac{\gamma r^{-\alpha^{\mathrm{L}}}}{P_1 A^{\mathrm{L}}}$. The $\mathcal{L}_{I_1^{\mathrm{L}}}(s)$, $\mathcal{L}_{I_1^{\mathrm{NL}}}(s)$, $\mathcal{L}_{I_2^{\mathrm{L}}}(s)$ and $\mathcal{L}_{I_2^{\mathrm{NL}}}(s)$ are interference from LoS BSs in 1^{th} tier and 2^{th} tier and NLoS BSs in 1^{th} tier and 2^{th} tier, respectively.
In the eq. (4.25), we first solve the $f_{1,1}^{\mathrm{L}}$. Recalling the eq. (4.11) and facilitating in current two-tier HetNet with two-slope path loss model.

$$\begin{aligned} f_{1,1}^{\mathrm{L}} = (1-\frac{r}{d_1})\frac{2\pi\lambda_1 r}{\rho_1}\exp\Big(-\int_0^r (1-\frac{u}{d_1})2\pi u\lambda_1 du\Big) \\ \times \underbrace{\exp\Big(-\int_0^a (1-\frac{u}{d_1})2\pi u\lambda_2 du\Big)}_{\tilde{a}} \\ \times \underbrace{\exp\Big(-\int_0^b \frac{u}{d_1}2\pi u\lambda_1 du\Big)}_{\tilde{b}} \\ \times \underbrace{\exp\Big(-\int_0^c \frac{u}{d_1}2\pi u\lambda_2 du\Big)}_{\tilde{c}} \end{aligned} \tag{4.26}$$

where $a = \big(\frac{P_2 B_2}{P_1 B_1}\big)^{1/\alpha^{\mathrm{L}}} r$, $b = \big(\frac{A^{\mathrm{NL}}}{A^{\mathrm{L}}}\big) r^{\alpha^{\mathrm{L}}/\alpha^{\mathrm{NL}}}$ and $c = \big(\frac{P_2 B_2 \alpha^{\mathrm{NL}}}{P_1 B_1 \alpha^{\mathrm{L}}}\big)^{1/\alpha^{\mathrm{NL}}} r^{\alpha^{\mathrm{L}}/\alpha^{\mathrm{NL}}}$.

Since the numerical relationship between a and d_1 affects the calculation of the first multiplier in eq. (4.26), i.e. $\tilde{a}$, we then discuss the cases of $0 < a \leq d_1$ and $a > d_1$.

4.5.1 Discussion of parameter a

According to the value of parameter a, the calculation of section $\tilde{a}$ in eq. 4.26 have two scenarios.

Scenario 1: If $0 < a \leq d_1$

If $0 < a \leq d_1$, the first multiplier in eq. (4.26), i.e. section $\tilde{a}$ in eq. 4.26 remains the same.

$$\tilde{a} = \exp\Big(-\int_0^a (1-\frac{u}{d_1})2\pi u\lambda_2 du\Big) \tag{4.27}$$

The intuition behind is due to that no interfering BSs with LoS links in 2^{th} tier ($k = 2$) is possible to be located in the range of $[0, a]$. In this case, there is possible interfering LoS BSs in 2^{th} tier located in the range of $a \leq d_1$. Then, we have

$$\begin{aligned}\mathcal{L}_{I_2^{\text{L}}} &= \exp\Big(-2\pi\lambda_2 \int_a^{d_1} \big(1 - \frac{u}{d_1}\big) \frac{u}{1 + (sP_2A^{\text{L}})^{-1}u^{\alpha^{\text{L}}}} du\Big) \\ &= \exp\Big(-2\pi\lambda_2 \Big\{ \xi_1 \left[\alpha^{\text{L}}, 1, (\frac{P_2}{P_1}\gamma r^{\alpha^{\text{L}}})^{-1}, d_1\right] - \xi_1 \left[\alpha^{\text{L}}, 1, (\frac{P_2}{P_1}\gamma r^{\alpha^{\text{L}}})^{-1}, a\right] \Big\} \\ &+ \frac{2\pi\lambda_2}{d_1} \Big\{ \xi_1 \left[\alpha^{\text{L}}, 2, (\frac{P_2}{P_1}\gamma r^{\alpha^{\text{L}}})^{-1}, d_1\right] - \xi_1 \left[\alpha^{\text{L}}, 2, (\frac{P_2}{P_1}\gamma r^{\alpha^{\text{L}}})^{-1}, a\right] \Big\}\Big)\end{aligned} \tag{4.28}$$

The detailed computation of the Laplace Transform is provided in following subsection of "Computation of the Laplace Transform" and "Hyper-geometric Functions".

Theorem 4.1 ***Computation of the Laplace Transform***

The calculation of Laplace Transform of interference is shown as

$$\begin{aligned}\mathcal{L}_{I_j}(s) &= \mathbb{E}_{I_j}\Big[\exp\big(-\sum_{x\in\Phi_j} sP_j l(r_x) h_j\big)\Big] \\ &= \mathbb{E}_{l(r_x),h_j}\Big[\prod_{x\in\Phi_j} \exp\big(-sP_j l(r_x) h_j\big)\Big] \\ &\overset{(a)}{=} \mathbb{E}_{l(r_x)}\Big[\prod_{x\in\Phi_j} \mathbb{E}_{h_j}\exp\big(-sP_j l(r_x) h_j\big)\Big] \\ &\overset{(b)}{=} \prod_{x\in\Phi_j} \mathbb{E}_{l(r_x)}\Big[\frac{1}{1 + sP_j l(r_x)}\Big] \\ &\overset{(c)}{=} \exp\Big(-2\pi\lambda_j \int_r^{\infty} \big(1 - \frac{1}{1 + sP_j l(r_x)}\big) du\Big)\end{aligned} \tag{4.29}$$

where (a) follows the independence of h_j, (b) is from the exponential distributed h_j and (c) follows from the probability generating functional of PPP.

Theorem 4.2 ***Hyper-geometric Functions***

The integration can be then transformed in following forms,

$$\xi_1(\alpha,\beta,t,d)=\Big[\frac{d^{(\beta+1)}}{\beta+1}\Big]\,{}_2F_1\left[1,\frac{\beta+1}{\alpha};1+\frac{\beta+1}{\alpha};-td^{\alpha}\right] \tag{4.30}$$

and

$$\xi_2(\alpha,\beta,t,d)=\Big[\frac{d^{-(\alpha-\beta-1)}}{t(\alpha-\beta-1)}\Big]\,{}_2F_1\left[1,1-\frac{\beta+1}{\alpha};2-\frac{\beta+1}{\alpha};-\frac{1}{td^{\alpha}}\right] \tag{4.31}$$

where ${}_2F_1\left[\cdot,\cdot;\cdot;\cdot\right]$ *is the hyper-geometric function.*

Scenario 2: If $a > d_1$

If $a > d_1$, the possible interfering LoS BSs located in 2^{th} tier can only fall in the range of $[d_1,\infty]$, we have

$$\tilde{a}=\exp\Big(-\int_0^{d_1}(1-\frac{u}{d_1})2\pi u\lambda_2 du\Big) \tag{4.32}$$

Moreover, due to the linear function LoS probability reaches 0 when the $r > d_1$, $\mathcal{L}_{I_2^{\mathrm{L}}}(s)=1$ thus vanishes in the equation. The similar discussions of parameter b and c are attached in Appendix.

The rest of derivations in eq. (4.25) are omitted because of repeating process showing above. Computation the coverage probability in the two-tier HetNet with LoS and NLoS transmission is then completed, and last to ASE and EE by following eq. (4.20 and 4.22).

Table 4.1: Simulation Parameter in the two-tier HetNets

Parameter	Values
AWGN power	$\sigma^2 = -95\,\text{dBm}$
d_1	300 m
Macro BS transmit power	$P_1 = 53\,\text{dBm}$
Small-cell BS transmit power	$P_2 = 23\,\text{dBm}$
Bias factor ratio	$B_1/B_2 = 1$
Small scale fading gain	$h \sim \exp(1)$
LoS path loss exponent	$\alpha^{\text{L}} = 2.09$
NLoS path loss exponent	$\alpha^{\text{NL}} = 3.75$
LoS path loss constant	$A^{\text{L}} = 10^{-3.29}$
NLoS path loss constant	$A^{\text{NL}} = 10^{-4.11}$

4.6 Numerical Results

In this section, we present numerical results to verify the obtained analytical formulas. To simplify the calculation, an unbiased network is considered, i.e., $B_1/B_2 = 1$. The rest of parameter values used in the simulation is listed in Table 4.1.

4.6.1 Coverage Probability

Fig. 4.1 shows the coverage probability versus the SINR threshold for different small cell densities (λ_2), where the then density of macrocells $\lambda_1 = 1/(250^2\pi)$. For a given ratio between 2 and 1, the coverage probability decreases with the SINR threshold. This is because the coverage definition becomes more challenging. For a given SINR threshold, the coverage probability decreases with the ratio between λ_2 and λ_1. This is because as the ratio between small cell density and macrocell density increases, it is more likely that a user will see LoS transmissions from nearby small-cell BSs. Since a LoS link causes much less attenuation of signal power than a NLoS link, the cross-tier interference caused by small cells to macrocells and the co-tier interference between small cells becomes more severe with the increase of λ_2. Thus, the coverage

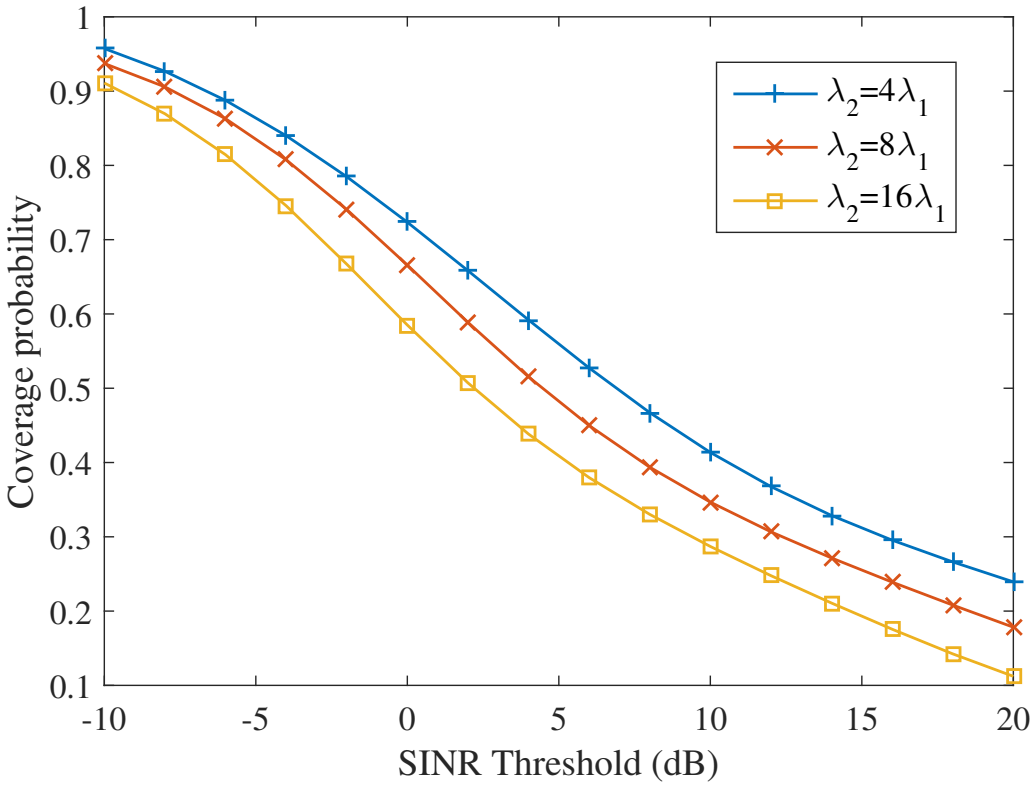

Figure 4.1: Coverage probability vs. SINR threshold in the two-tier HetNets

probability decreases.

Fig. 4.2 shows the coverage probability versus the density of small cells for different macrocell densities, where the SINR threshold is 0dB. For a given density of small cells (less than 0.01 BSs per m^2), the coverage probability increases with the density of macrocells. This is because a higher density of macrocells leads to a shorter average distance from a macro BS to a user, thus a higher macrocell coverage probability. For a given λ_1, the coverage probability first increases with λ_2 and then decreases with it after reaching a maximum value. This is because at relatively low small-cell densities, small-cell links are likely to be NLoS and the small-cell link quality (thus coverage probability) increases with the small-cell density; while at relatively high

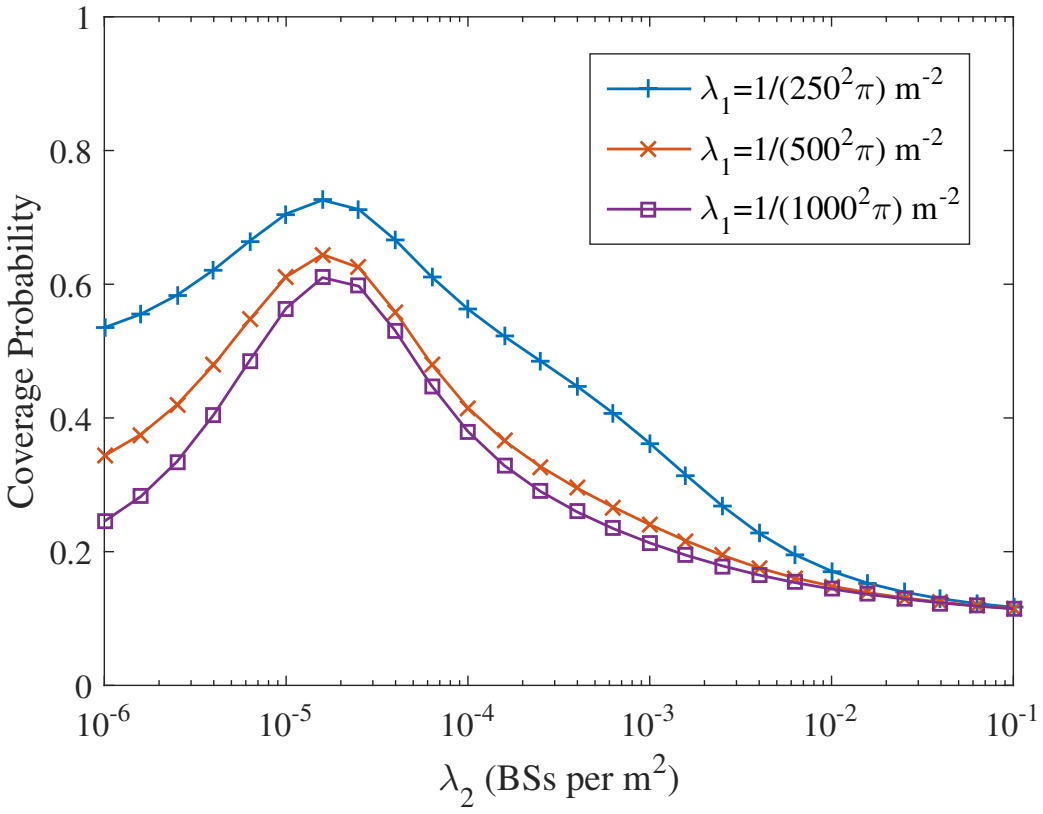

Figure 4.2: Coverage probability vs. small-cell density for different macrocell densities in the two-tier HetNets

small-cell densities, small-cell links are likely to be LoS and the interfering small-cell links become more dominant, leading to reduced coverage probability. It is interesting to note that for different values of λ_1, the maximum coverage probability occurs at approximately the same value of λ_2, i.e., 2×10^{-5} BS per m^2. At very high densities of small cells (larger than 0.01 BSs per m^2), the coverage probabilities for different values of λ_1 converge to the same low value, because all links are LoS dominated.

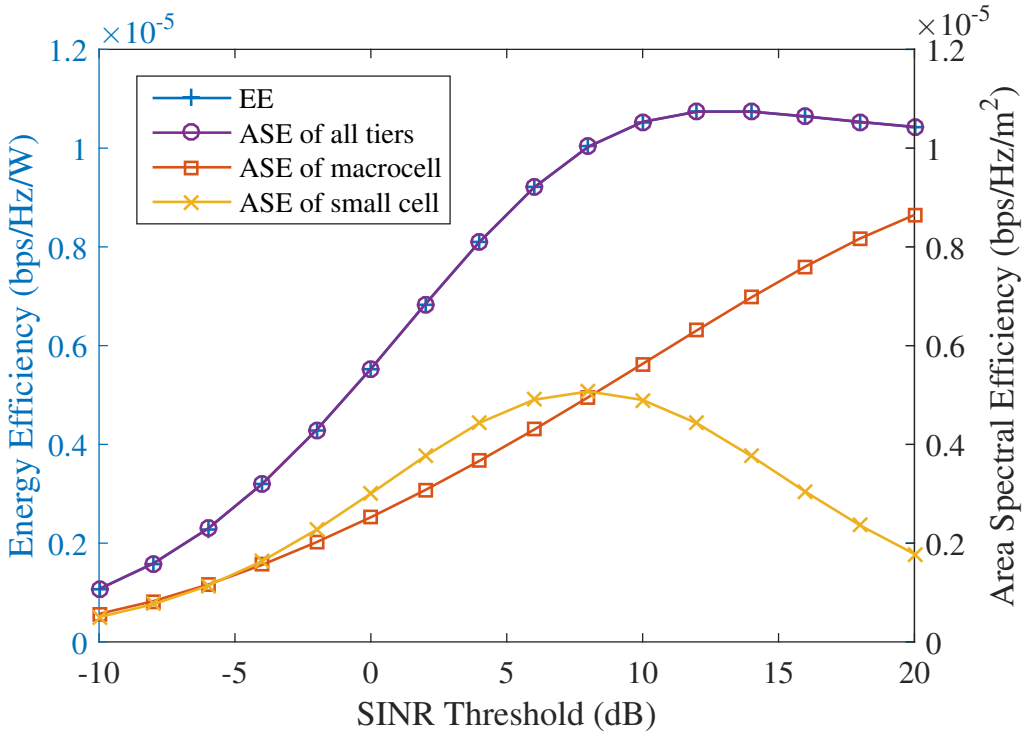

Figure 4.3: ASE and EE vs. SINR threshold

4.6.2 ASE and EE

In Fig. 4.3 and Fig. 4.4, we set $\lambda_1 = 1/(250^2\pi) and \lambda_2 = 2\lambda_1$.

Fig. 4.3 shows the ASE and the EE of the two-tier HetNet versus the SINR threshold. As can be seen, the ASE of small cells first increases with the SINR threshold and then decreases with it after reaching a maximum value. This is mainly due to the NLoS-to-LoS transition of interference links as described in [5]. In contrast, the ASE of macrocells increases almost linearly with the SINR threshold, since such transition does not occur. Following (4.20), the ASE of the HetNet (as the summation of per-tier ASE) also first increases with the SINR threshold and then slowly decreases after reaching a maximum value. Given the parameters in Table I and

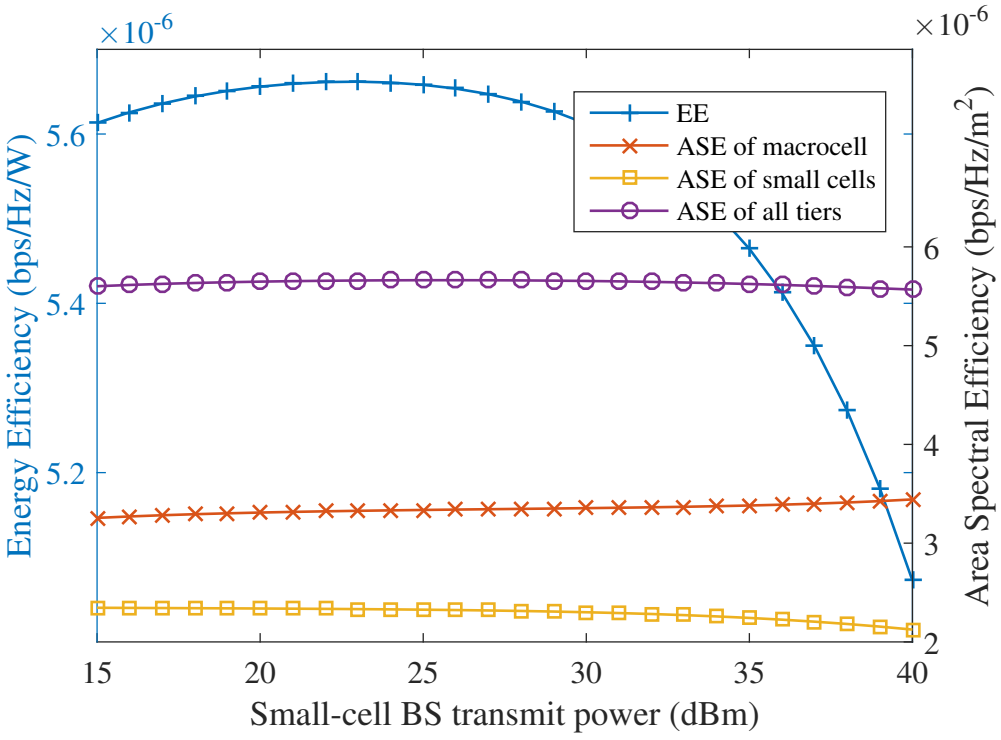

Figure 4.4: ASE and EE vs. transmit power of small cells in the two-tier HetNets

above, the spatial power consumption is approximately 1 W/m^2, and the EE is thus equal to the overall ASE.

Fig. 4.4 shows the ASE and the EE of the two-tier HetNet versus the transmit power of small cells, where the SINR threshold is 0dB. The ASE of macrocells increases slightly with the growth of small-cell BS transmit power, while the ASE of small cells slightly decreases, because the cross-tier interference caused by small cells increases with the small-cell transmit power. As a result, the overall ASE of the HetNet is roughly constant over the different transmit power levels of small cells. Moreover, we observe that the EE of the HetNet first slightly increases with the small-cell transmit power and then drops quickly when the transmit power of small cells is above 25dBm. Thus, high transmit powers should be avoid for densely

deployed small cells, because it will not improve the ASE but will degrade the EE significantly.

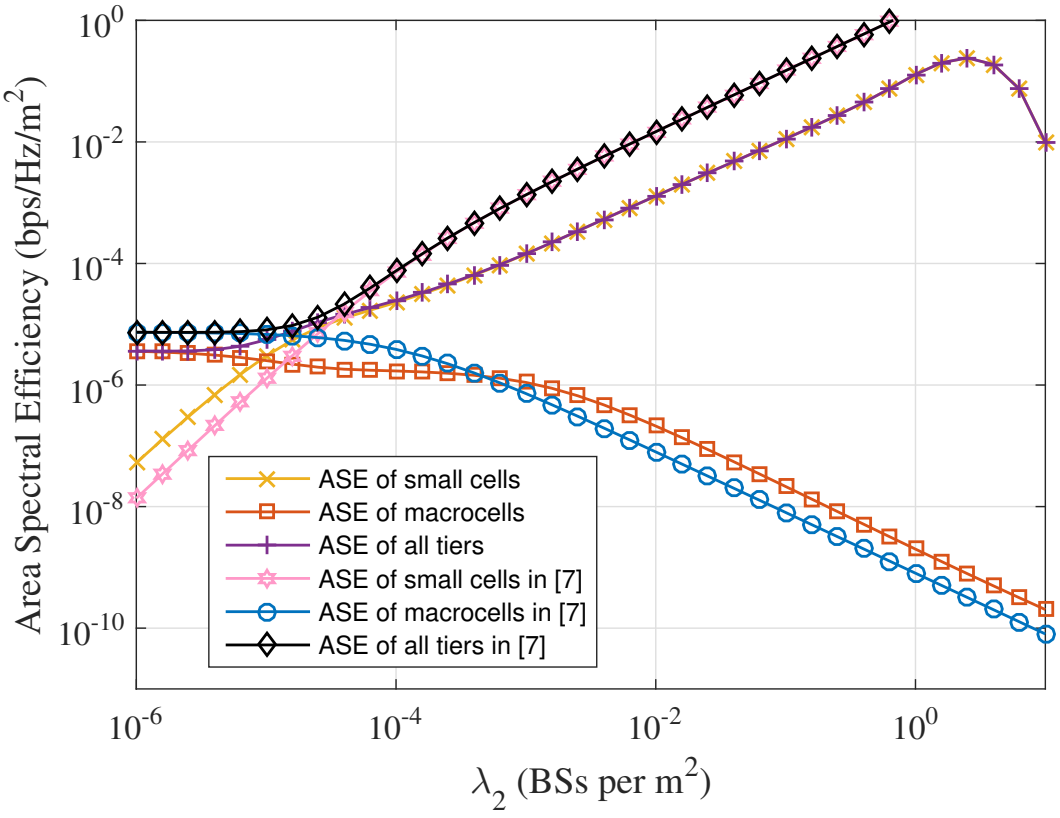

Figure 4.5: ASE of macrocell and small cell vs. small cell density in the two-tier HetNets

Fig. 4.4 compares the ASE of macrocells, small cells and all tiers calculated using our formula with those calculated in [20] versus λ_2, for $\lambda_1 = 1/(250^2\pi)$. The SINR threshold is 0dB. In [20], no possible LoS transmission is considered and the path loss model follows $r^{-\alpha}$, where r is the link range and the path loss exponent $\alpha = 4.5$. As Fig. 4.5 shows, both our formula and that in [20] predict that the ASE of small cells (macrocells) increases (decreases) with λ_2 at a smaller (higher) rate when λ_2 is larger than a certain value, but the value of λ_2 predicted by our calculations at

which the increase rate of small-cell ASE reduces is smaller than that predicted by [20], while the value of λ_2 predicted by our formula at which the decrease rate of macrocell ASE increases is larger than that predicted by [20]. This is because for the same low or moderate value of λ_2, the inter-cell interference caused by small cells is severer with possible LoS transmissions than without. When λ_2 becomes extremely large, in contrary to the result of [20], the ASE of all tiers calculated by our formula decreases quickly with λ_2, because the ASE of all tiers is now dominated by the small-cell ASE, which decreases quickly with λ_2. This is because the domination of LoS transmissions in ultra-dense small-cell deployment results in extremely high inter-cell interference from small cells, which blocks most desired transmission links.

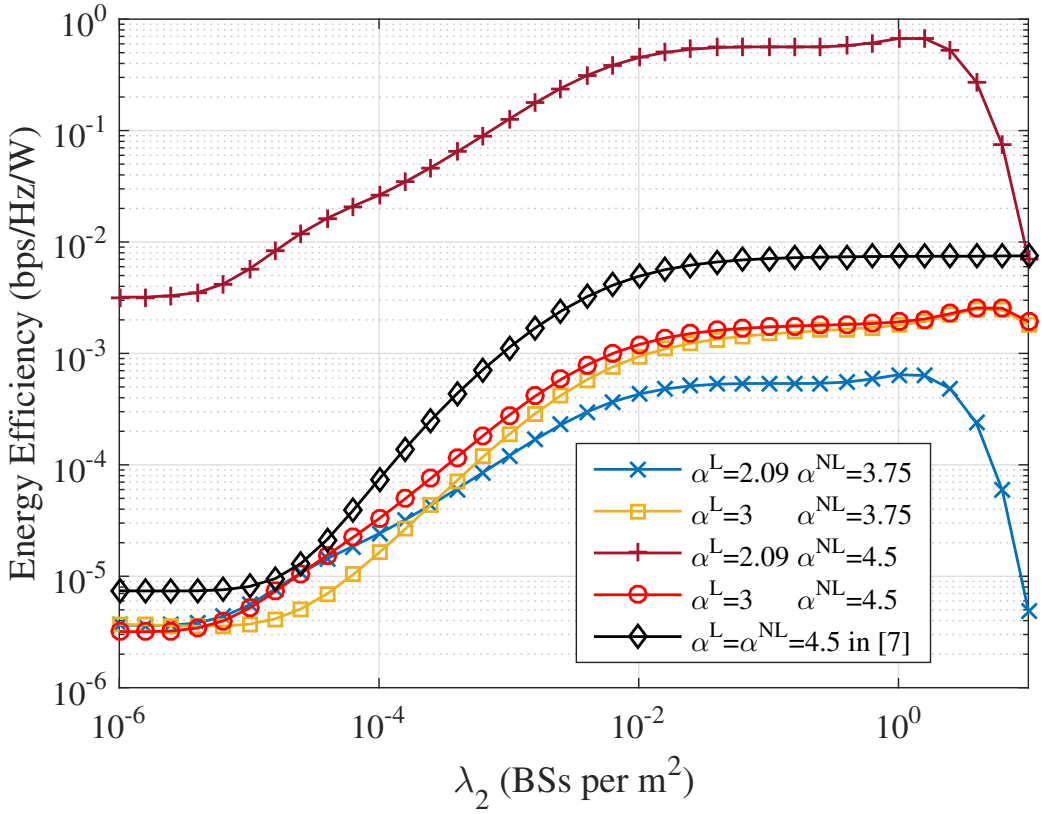

Figure 4.6: EE vs. small cell density at different path loss exponents

Fig.4.6 shows the EE calculated by our formula and that calculated by [20] versus λ_2 for $\lambda_1 = 1/(250^2\pi)$, for a SINR threshold of 0dB and different path loss exponents. We can see that the highest EE is achieved with the smaller α^{L} and the larger α^{NL} at specific small cell densities. This is due to the fact that for such small cell densities, most interfering links are likely to be NLoS and only downlinks from serving BSs are possibly LoS, then for a small α^{L} and a large α^{NL}, the possibly LoS desired links would be strong while most interfering links would be relatively weak, thus leading to the highest EE.

For a small value of λ_2 ($< 3 \times 10^{-4}$ BSs per m^2), the lowest EE is obtained with the larger L and the smaller NL. This is because at low density of small cells, most interfering links are likely to be NLoS and only downlinks from serving BSs are possibly LoS, then for a large α^{L} and a small α^{NL}, any possible LoS desired links would be weak while most interfering links would be strong, resulting in the lowest EE.

For a moderate or large value of λ_2 (i.e., $3 \times 10^{-4} < \lambda_2 < 1$ BSs per m^2), the lowest EE is obtained with the small L and the small NL. This is because for a relatively large density of small cells, most interfering small cell links are likely to be LoS while interfering macrocell links are likely to be NLoS, then with small values of α^{L} and α^{NL}, the interference caused by both small cells and macrocells becomes strong, leading to the lowest EE.

At extremely large values of λ_2, our formula predicts that the EE decreases with the further increase of λ_2, especially fast for the smaller value of α^{L}. This is because with densely deployed small cells, most small cell links are likely to be LoS, making the cross-tier and co-tier interference caused by small cells very strong (especially

for a small α^{L}), and thus a higher λ_2 leads to a lower EE. However, such decrease of EE at extremely large λ_2 is not captured by formulas in [20].

In each considered pair of α^{L} and α^{NL} or for the given , the EE increases very slightly with λ_2 at low or large values of λ_2, but increases fast with λ_2 at moderate values of λ_2. The reason is that as each small cell can serve only a small number of users, a moderate density of small cells is required to noticeably improve the overall network ASE (and thus EE).

4.7 Summary

Based on a multi-slope path loss model, we have derived the formulas of coverage probability, ASE and EE for a K-tier HetNet considering LoS and NLoS transmissions. Our analytical and numerical results demonstrate that at relatively high small-cell densities, the transition of small cell interference links from NLoS to LoS will cause excessive inter-cell interference, which blocks almost all desired links. When small-cell BSs are densely deployed, increasing small-cell transmit power will not improve the ASE, but will degrade the EE significantly. Moreover, our results predict that in an extremely dense HetNet, both the ASE and EE of the HetNet will drop quickly with further increase of the small-cell density due to the dominance of LoS interfering links.

Chapter 5

BS Clustering under LoS/NLoS Transmissions

In this chapter, we further investigate the effects of path loss with LoS and NLoS transmission in four different cases, including linear LoS probability function in analytical model, isolated picocells in a suburban area, millimetre wave propagation in outdoor environment and urban micro cells in a 3D scenario. The degradation of network performance at high BS density in above research is verified in all cases. We propose a user-centric BS clustering strategy in order to mitigate severe LoS interference and enhance the network performance at high BS density.

5.1 Introduction

To meet the explosive growth of mobile data traffic, the dense deployment of small cells is widely considered as a promising approach to provide high QoS to mobile users. However, the resulting dense short-range LoS links bring new challenges to interference management in cellular networks [97]. Compared to NLoS interfering

links, the LoS interfering links with slow attenuation of the signal power can lead to severer interference to the user.

In [61–63], the LoS and NLoS path loss models have gained significant interest in the design of dense small-cell networks. In [61], the 3GPP suggested different outdoor path loss models for urban, suburban, and rural environments. In [62], a linear function for the LoS probability was considered as a special case for a tractable analysis of small-cell network performance. In [63], 3D path loss models covering both LoS and NLoS transmissions were proposed for both indoor and outdoor environments, where the heights of BSs and users play an important role.

For interference limited cellular networks, BS cooperation has been widely considered as a promising technique to increase the SINR at the user. BS cooperation of non-coherent JT is the one popular technology where multiple BSs collaboratively transmit to a user without prior phase-mismatch correction or tight synchronization [70, 89, 90]. Non-coherent JT was also analyzed in HetNets [89], where any BS with the RSS above a pre-defined threshold is selected to perform user-centric BS clustering. It was shown that for small cooperative clusters of small-cell BSs, non-coherent JT among small cells can provide spectral efficiency gains without significantly increasing the traffic load per cell. In [70], stochastic geometry tools were used to analyze non-coherent JT models, where each user is served by either one or two BSs. In [90],the non-coherent JT was combined with frequency reuse to improve the utilisation efficiency of spectrum resources.

We note that none of the above works on non-coherent JT has brought the consideration of LoS transmissions in dense small-cell networks. Through cooperative BS transmissions, the LoS links from nearby BSs to a user can be combined. Ideally,

all BSs within the cluster transmit to the user through LoS links, while any BS left outside the cluster cause interference to the user though NLoS links.

In this chapter, we propose a new user-centric BS clustering strategy for non-coherent JT in dense small-cell networks, where users may see both LoS and NLoS transmissions from nearby BSs. In order to convert as many LoS links as possible into useful transmissions to a user, our proposed user-centric BS clustering strategy selects a small-cell BS into the BS cluster only if the LoS probability of its link to the user is above a predefined threshold. Moreover, we consider four different path loss models with different LoS/NLoS characteristics to evaluate the performance of our proposed user-centric BS clustering strategy. The resulting coverage probability and achievable spectrum efficiency are evaluated through system level simulations, in comparison to the existing RSS-based BS clustering. User association schemes without BS clustering, such as the nearest BS association and the maximum received signal based user-BS association, are also considered.

5.2 Path Loss Model in Different Environments

We consider a homogeneous dense small-cell network, where each small-cell BS transmits at the same power level. The spatial distribution of the small-cell BSs, which are grouped in the BS set Φ, follows a spatial PPP with a spatial density of λBS/km^2. Users are distributed over the network area following another independent homogeneous PPP. We use a path loss model that includes both LoS and NLoS transmissions as probabilistic events, where $\Pr^{\mathrm{L}}(r)$ and $\Pr^{\mathrm{NL}}(r)$ denote the probabilities of the link being LoS and NLoS, respectively. We assume that r is the link range, and $\Pr^{\mathrm{L}}(r) + \Pr^{\mathrm{NL}}(r) = 1$.

The path loss between a BS and a user at distance r (in meter) is given by

$$l(r) = \begin{cases} l^{\mathrm{L}}(r) = A^{\mathrm{L}} + 10\alpha^{\mathrm{L}}\log_{10}(r) & \text{with } \Pr^{\mathrm{L}}(r) \\ l^{\mathrm{NL}}(r) = A^{\mathrm{NL}} + 10\alpha^{\mathrm{NL}}\log_{10}(r) & \text{with } 1 - \Pr^{\mathrm{L}}(r) \end{cases} \tag{5.1}$$

where α^{L}, α^{NL}, A^{L} and A^{NL} are the LoS and NLoS path loss exponents and LoS and NLoS path loss constants, respectively.

5.2.1 Four Path Loss Models

In the following, we discuss four different models for $\Pr^{\mathrm{L}}(r)$ and the associated path loss models that have been proposed in the literature.

5.2.2 Case 1: Linear LoS probability

The 3GPP has suggested the following expression for the LoS probability $\Pr^{\mathrm{L}}(r)$

$$\Pr^{\mathrm{L}}(r) = \begin{cases} 1 - \frac{r}{d_1} & \text{when} \quad 0 < r < d_1 \\ 0 & \text{when} \quad r > d_1, \end{cases} \tag{5.2}$$

where d_1 is the decreasing slope of the LoS probability function. The values of α^{L}, α^{NL}, A^{L} and A^{NL} are 2.09, 3.75, 41.1 dB and 32.9 dB, respectively. This linear function of LoS probability was used in [5] to analyse small-cell networks with $d_1 = 300$m.

5.2.3 Case 2: Isolated Picocell in A Suburban Area

The 3GPP has also suggested the following LoS probability $\Pr^{\mathrm{L}}(r)$ from a picocell BS to a user for a suburban area [61]:

$$\begin{aligned}\Pr^{\mathrm{L}}(r) = 0.5 - \min(0.5, 3\exp(-300/r)) \\ + \min(0.5, 3\exp(-r/95)),\end{aligned} \tag{5.3}$$

where the corresponding path loss model is given by,

$$l(r) = \begin{cases} l^{\mathrm{L}}(r) = 41.1 + 20.9\log_{10}(r) \\ l^{\mathrm{NL}}(r) = 32.9 + 37.5\log_{10}(r). \end{cases} \tag{5.4}$$

5.2.4 Case 3: Millimetre Wave Outdoor Environment

In [62], the millimetre wave propagation at a 73GHz carrier frequency was modelled based on real-world measurements in an outdoor environment. The resulting LoS probability $\Pr^{\mathrm{L}}(r)$ is given by,

$$\Pr^{\mathrm{L}}(r) = [\min(\frac{d_{\mathrm{BP}}}{r}, 1)(1 - \exp(-\frac{r}{\delta})) + \exp(-\frac{r}{\delta})]^2, \tag{5.5}$$

where r is the distance between the BS and the user, d_{BP} is the breaking distance (i.e. 27m), and δ is the decay parameter (i.e. 71m). The LoS path loss model in [62] uses the following free space propagation model:

$$l^{\mathrm{L}}(r) = 20\log_{10}(\frac{4\pi}{\Lambda}) + 20\log_{10}(r), \tag{5.6}$$

where Λ is the carrier wavelength, where $\Lambda = 4.1$mm at carrier frequency $f_c = 73$GHz. For the NLoS propagation, a floating intercept method is used to model

the path loss in a given range of measured transmitter and receiver separations [62]. The resulting path loss model is given as:

$$l(r) = \begin{cases} l^{\mathrm{L}}(r) = 69.7 + 20\log_{10}(r) \\ l^{\mathrm{NL}}(r) = 80.6 + 29\log_{10}(r). \end{cases} \tag{5.7}$$

5.2.5 Case 4: Urban Micro Cell in A 3D Scenario

A 3D channel model in the 2GHz frequency (f_c) band was suggested by the 3GPP in [63]. In this scenario, urban microcells are below the surrounding buildings with their BS antenna height (h_{BS}) at 10m and the UE's antenna height (h_{UE}) at 1.5m. The LoS probability is a function of the 2D distance ($d_{2\mathrm{D}}$), which is the distance between the BS and the user measured in the ground plane, i.e.,

$$\mathrm{Pr}^{\mathrm{L}}(d_{2\mathrm{D}}) = \begin{cases} 1, & d_{2\mathrm{D}} < 18m \\ \frac{18}{d_{2\mathrm{D}}} + \exp(-\frac{d_{2\mathrm{D}}}{36})(1 - \frac{18}{d_{2\mathrm{D}}}), & d_{2\mathrm{D}} > 18m. \end{cases} \tag{5.8}$$

The path loss model in [63] consists of LoS and NLoS propagation, depending on the 3D distance ($d_{3\mathrm{D}}$) as follows,

$$\begin{aligned} l^{\mathrm{L}}(d_{3\mathrm{D}}) &= 22\log_{10}(d_{3\mathrm{D}}) + 28 + 20\log_{10}(f_c) \\ &= 34.02 + 22\log_{10}(d_{3\mathrm{D}}), \end{aligned} \tag{5.9}$$

$$\begin{aligned} l^{\mathrm{NL}}(d_{3\mathrm{D}}) &= 36.7\log_{10}(d_{3\mathrm{D}}) + 22.7 + 26\log_{10}(f_c) \\ &\quad - 0.3(h_{\mathrm{UE}} - 1.5) \\ &= 30.53 + 36.7\log_{10}(d_{3\mathrm{D}}), \end{aligned} \tag{5.10}$$

where d_{3D} is calculated by,

$$d_{3D} = \sqrt{{d_{2D}}^2 + (h_{BS} - h_{UE})^2}. \tag{5.11}$$

Table 5.1: LoS/NLoS channel models

	Case 1	Case 2	Case 3	Case 4
Models	Linear LoS probability	Isolated pico cell in a suburban area	Millimetre wave outdoor environment	Urban micro cell in a 3D scenario
Working frequency	2GHz	2GHz	73GHz, 28GHz	2GHz
2D/3D	2D	2D	2D	3D
BS antenna type	Omni-directional antenna			
BS/UE antenna height	No height information	No height information	No height information	h_{BS} = 10m h_{UE} = 1.5m
Inter-site distance (ISD) (recommended)	N/A	40m	N/A	200m

Table 5.1 lists the information about the four channel models considered in terms of frequency band, BS antenna type, BS/UE antenna height, and recommended BS densification level.

Fig. 5.1 shows the LoS probability of the transmission link between a small-cell BS and a user for a BS intensity of 150 BS/km^2 under the four path loss models discussed above. The linear function for the LoS probability in Case 1 facilitates analytical tractability, as shown in [5]. The LoS probability of an outdoor suburban environment in Case 2 gradually decreases with the increase of the distance between the small-cell BS and the user.

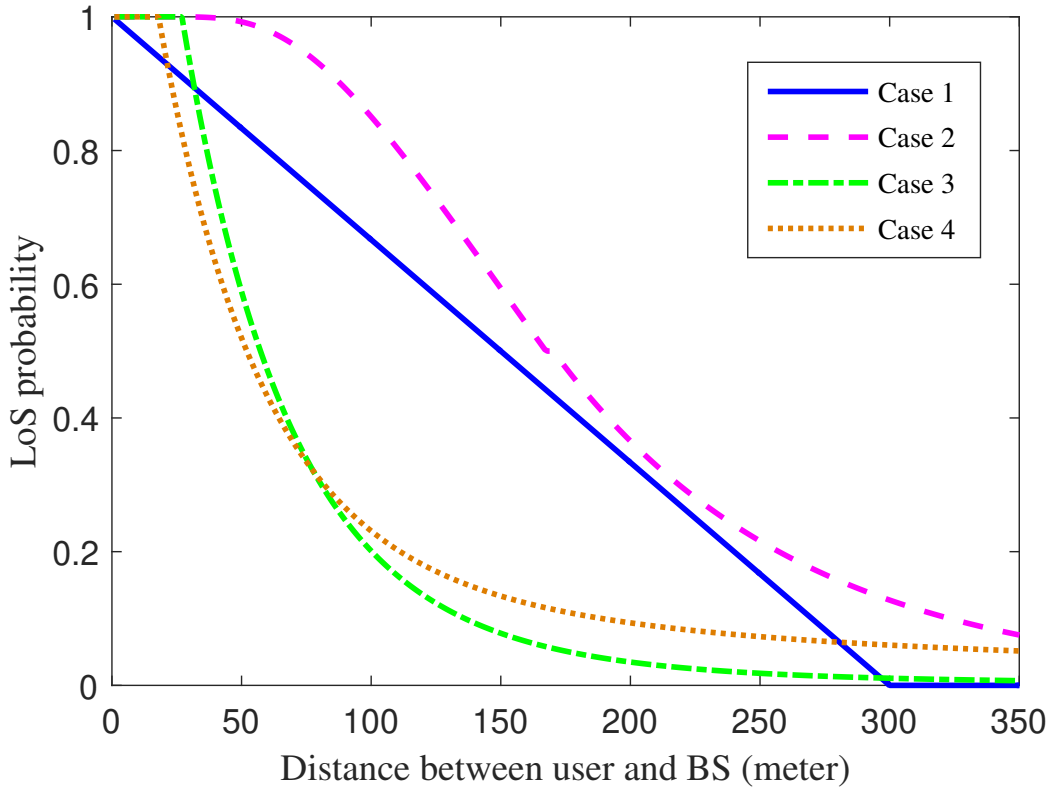

Figure 5.1: LoS probability against distance between user and BS

For a typical user served by a BSs with nearest distance or maximum received signal (RS), the downlink SINR at the user is given by

$$\text{SINR} = \frac{ph_i l(r_i)}{\sum_{j\in\Phi, j\neq i} ph_j l(r_j) + \sigma^2} \tag{5.12}$$

where p is the small-cell BS transmit power, h_i is the channel fading power gain of the link between the i^{th} BS and the user, which follows a unit-mean exponential distribution, r_i is the distance from the i^{th} BS to the user (d_{3D} in case 4), and σ^2 is the additive white Gaussian noise (AWGN) power at the receiver.

5.2.6 Simulation Results of Four Path Loss Models

In this section, we present Monte Carlo simulation results to evaluate the coverage probability (i.e., $\mathcal{C} = \mathbb{P}[\text{SINR} > T]$) for a SINR threshold ($T$) of 0dB and the achievable spectrum efficiency (i.e., $\mathcal{R} = \mathbb{E}[\ln(\text{SINR} + 1)]$ in nats/sec/Hz) of the small-cell network. In the simulation, the typical user is located at the origin, maximum RS based BS association and the nearest BS association are compared in all four cases. The rest of the parameters are listed in Talbe 5.2.

Table 5.2: Simulation Parameter

Parameter	Values
AWGN power	$\sigma^2 = -95\,\text{dBm}$
Small-cell BS transmit power	$P_2 = 23\,\text{dBm}$
Small scale fading gain	$h \sim \exp(1)$
SINR threshold (T)	$0\,\text{dB}$

Fig. 5.2 shows the coverage probability versus the small-cell BS density under maximum-RS and nearest-BS user association in four cases. The coverage probabilities for the maximum RS based BS association and the nearest BS association first increase with the BS density, and then decrease with the BS density after reaching their maximum values. This is because the increasing number of low-attenuation LoS links at higher BS densities cause severe interference to the user, thus degrading the received SINR. The similar trend with the minor gap between case 1 and 2 are observed in both figures, which is due to the similar value of LoS probability as shown in Fig. 5.1. The values in case 3 and 4 results in difference. In Fig. 5.2(a), the peak value of coverage probability in case 3 achieves at higher BS density, compared with case 1, 2 and 4. This is because the fast drop of LoS probability (as shown in Fig. 5.1) combined with high attenuation path loss (as shown in eq. 7) causes

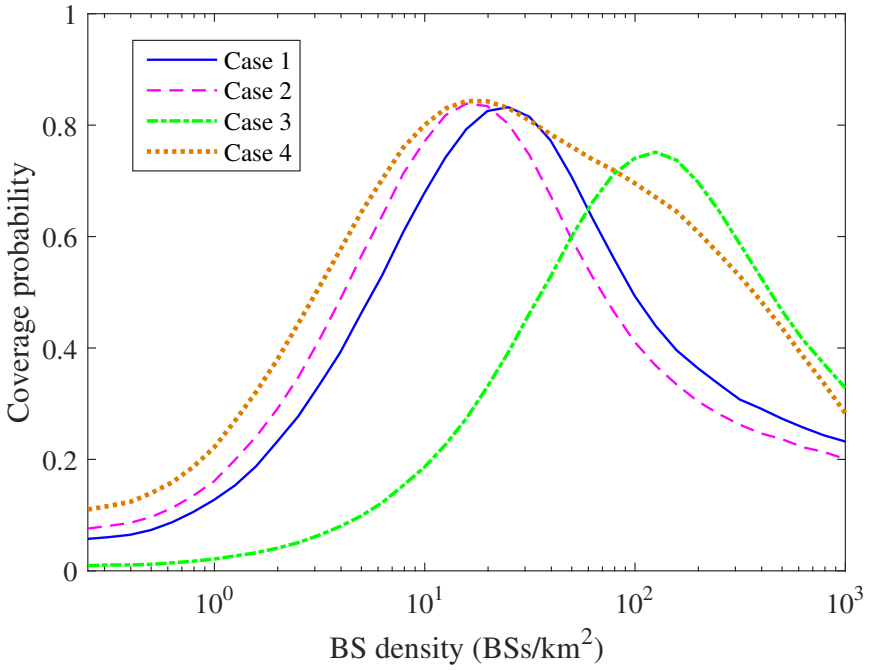

(a) Maximum RS user association

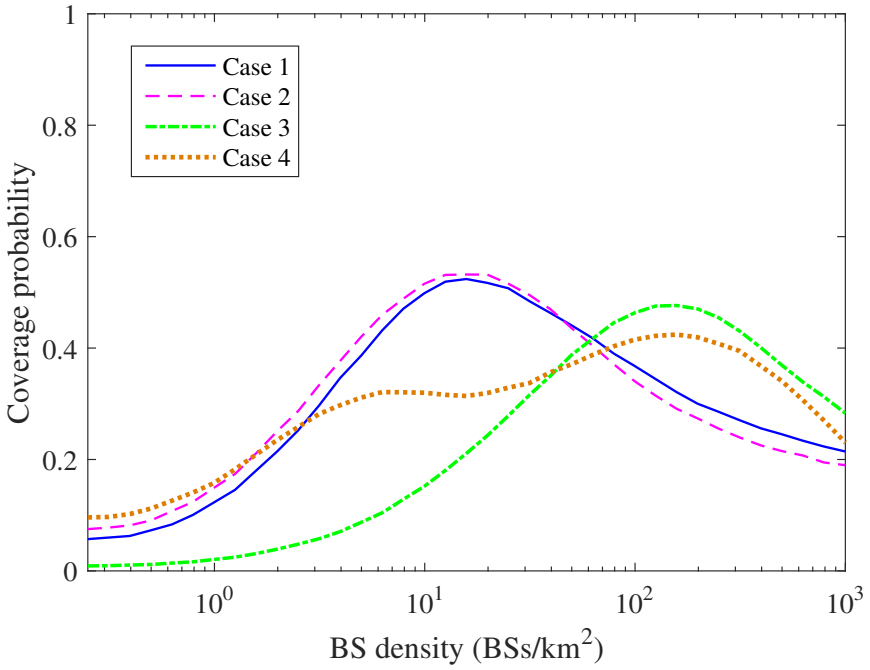

(b) Nearest BS user association

Figure 5.2: Coverage probability vs. BS density in four Cases

less LoS interference to the user. In Fig. 5.2(b), a worse performance in case 4 is observed with its lower decreasing rate at at a relatively high BS density. This is due to the 3D path loss model in Case 3 results in longer transmission links, which results in worse received signal powers at the user, thus causes a worse performance in terms of SINR and coverage probability. However, it overtakes the value in case 1 and 2 at higher BS density. It is because when LoS links become dominated at high BS density, the longer 3D transmission links is crucial for much lower receiving interference at user.

Fig. 5.3 shows the achievable spectral efficiency versus the small-cell BS density under maximum-RS and nearest-BS user association in four cases. It is obvious that the peak value in case 3 is much lower than in case 4, and even half of that in case 1 and 2 in Fig. 5.3(a) This is because when the user is covered by the BS, the RS power is crucial to determine the achievable spectral efficiency. The RS power in case 3 experiences the worst scenario at a certain distance in all cases. In Fig. 5.3(a), the peak value in case 4 drop to the same level as in case 3. The practical 3D transmission link has longer distance than 2D distance used to determine the LoS probability, which results lower SINR and thus worse spectral efficiency.

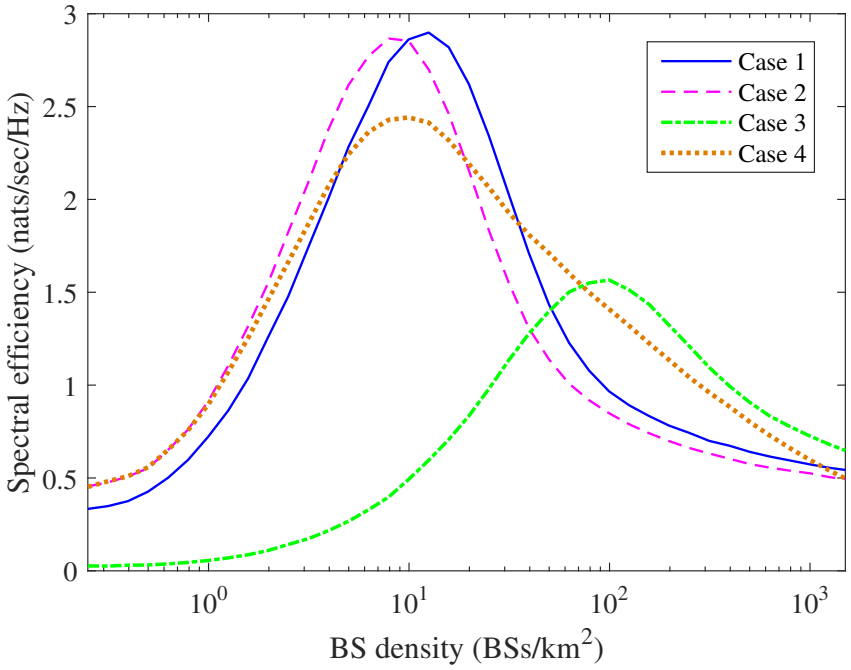

(a) Maximum RS user association

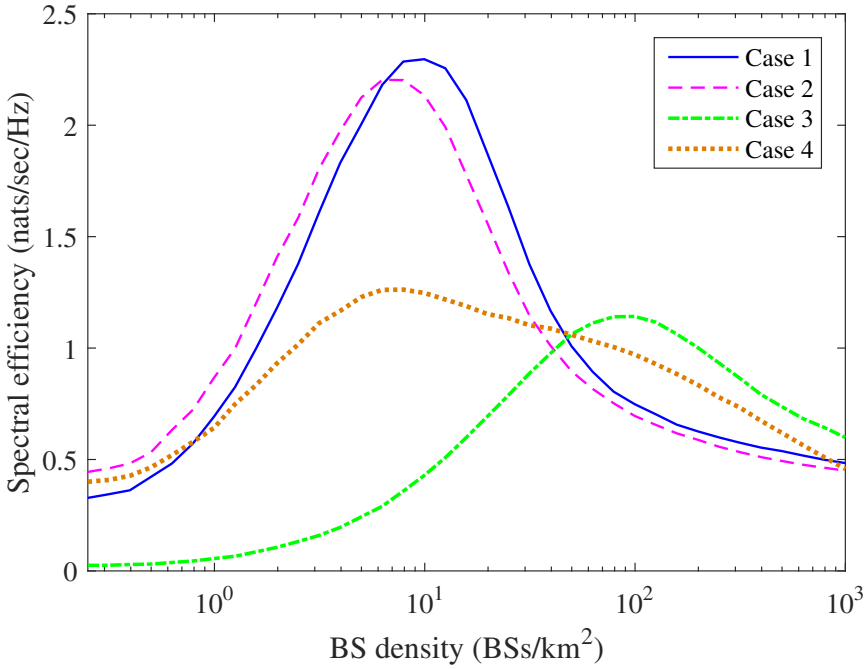

(b) Nearest BS user association

Figure 5.3: Spectral efficiency vs. BS density in four Cases

5.3 User-Centric BS Clustering Strategy

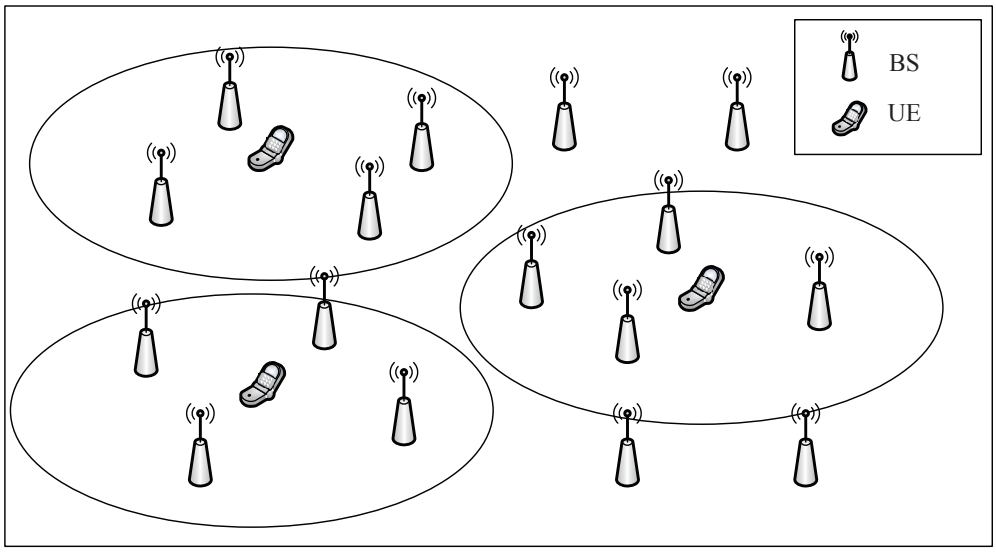

Figure 5.4: Illustration of a user-centric BS Cluster

Since LoS links are usually of a relatively good channel quality, we propose to form a cooperative transmission BS cluster for a user based on the LoS probability of a BS link to it, so that as many LoS links from nearby BSs as possible can be aggregated into desirable transmissions to the user. More specifically, the i^{th} BS is included in the cooperative BS cluster Φ^C for a typical user, if the LoS probability of its link to the user being LoS is greater than a threshold τ, i.e.,

$$\Pr^{\mathrm{L}}(r_i) > \tau \tag{5.13}$$

where r_i is the distance from the user to the i^{th} BS (i.e. $d_{2\mathrm{D}}$ in case 4), and $0 \leqslant \tau < 1$.

If there is no BS meeting the condition in (13), then the user will be served by the nearest BS without BS clustering. The user-BS association decision process in

support of the proposed user-centric BS clustering strategy is illustrated in Fig. 5.5.

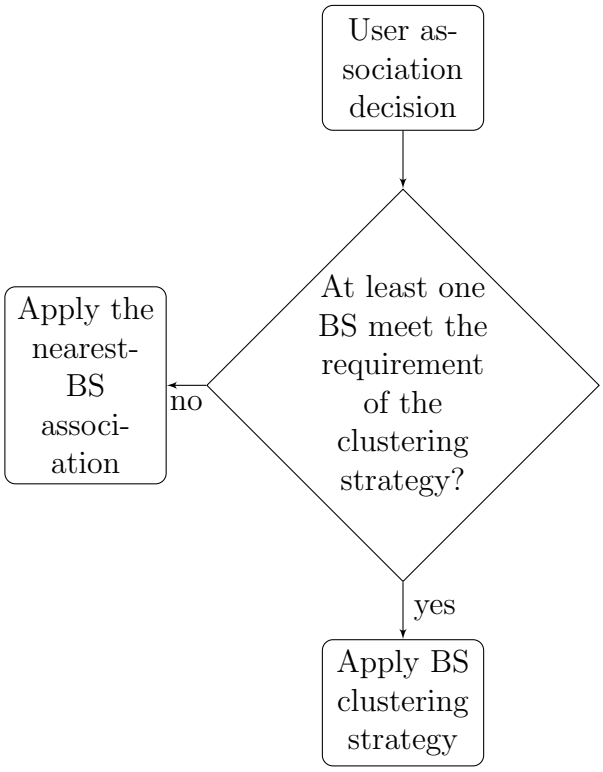

Figure 5.5: User association decision

With the proposed user-centric BS clustering, each user is served by a cluster of nearby BSs. The BSs outside the cluster are the potential interfering sources to the user. For a typical user served by the cooperative cluster Φ^C of BSs, the downlink SINR at the user is rewrited by

$$\text{SINR} = \frac{\sum_{i \in \Phi^C} p h_i l(r_i)}{\sum_{j \notin \Phi^C} p h_j l(r_j) + \sigma^2}. \tag{5.14}$$

5.4 Simulation Results of Clustering Strategy

In this section, we present Monte Carlo simulation results to evaluate the coverage probability and achievable spectrum efficiency of the proposed user-centric BS clustering strategy in a small-cell network. The simulation system is set up similarly with section 5.2.6 where the typical user is located at the origin. In addition, the proposed user-centric BS clustering strategy is compared with the RSS-based BS clustering strategy [89], the maximum RS based BS association and the nearest BS association.

Fig. 5.5 shows the coverage probability versus the small-cell BS density of all the BS clustering or user association schemes under comparison in the four cases discussed in Section II. In case 1, for the RSS-based BS clustering [89], the coverage probability shows a sharp increase in the middle range of the BS density and finally reaches 1. This is because at higher BS densities, more BSs can be clustered to give a higher aggregated received signal power at the user, thus resulting in a higher SINR and a better coverage probability. For our proposed user-centric BS clustering strategy, with the high LoS probability threshold $\tau = 0.3$ and 0.5, the coverage probabilities maintain a fast increasing rate until reaching 1. This is because when the BS density is increasing, nearby BSs are more likely to have a LoS probability higher than the given threshold and are grouped into the BS cluster. We also observe that for ($\tau = 0.7$), the coverage probability first reaches a local maximum value at about 0.6, then decreases, and then increases again with the higher BS densities. This is because the high LoS probability threshold may limit the number of BSs that can be selected for BS clustering, especially when the BS density is relatively low. Consequently for moderate values of the BS density, the increased interference from BSs outside the cooperative cluster counteracts the limited SINR improvement

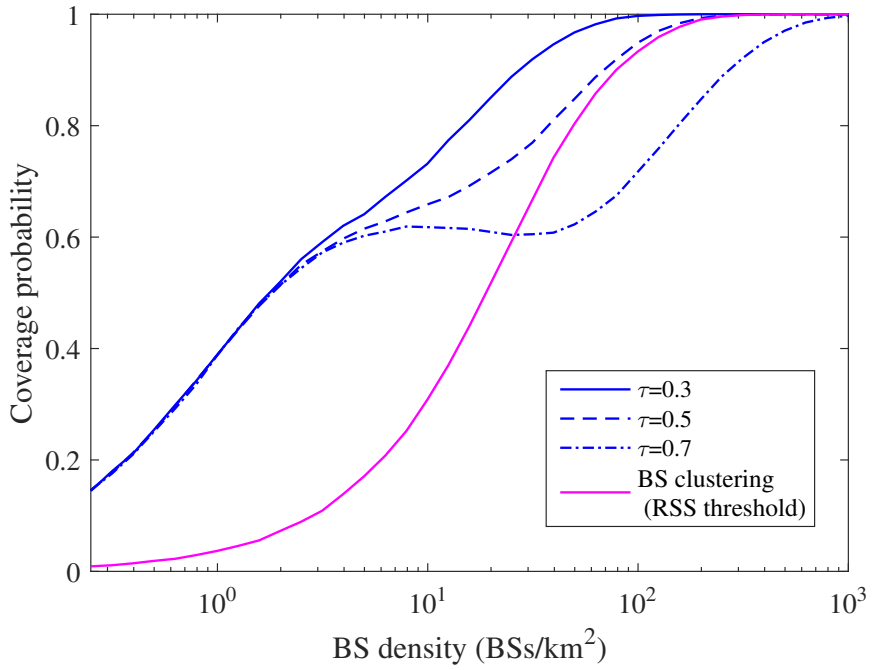

(a) Case 1

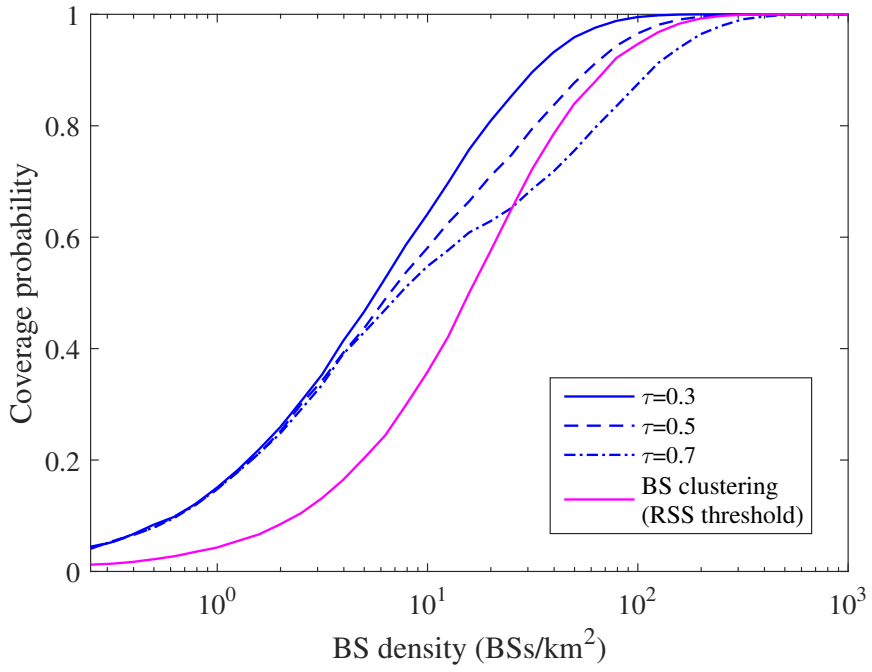

(b) Case 2

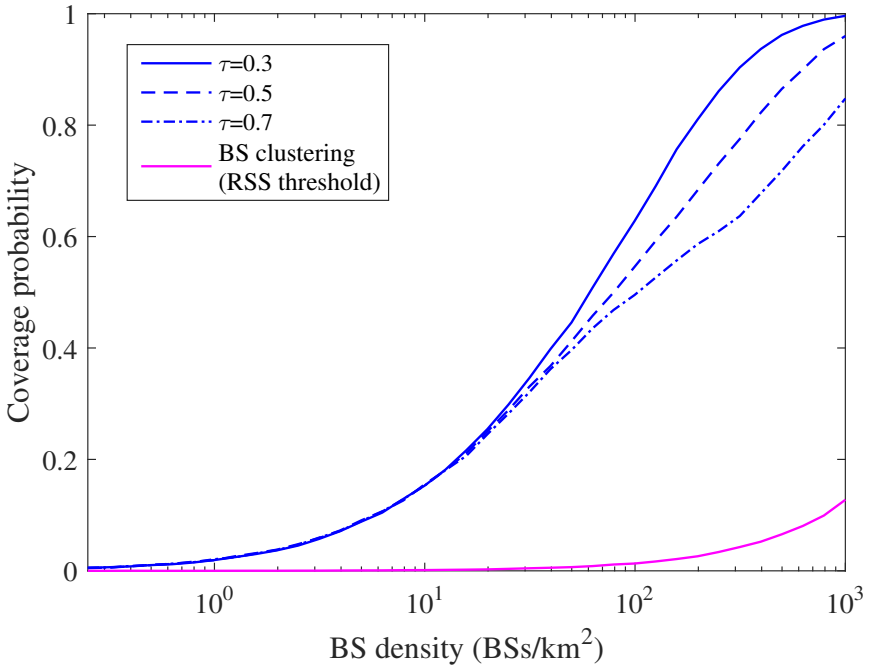

(c) Case 3

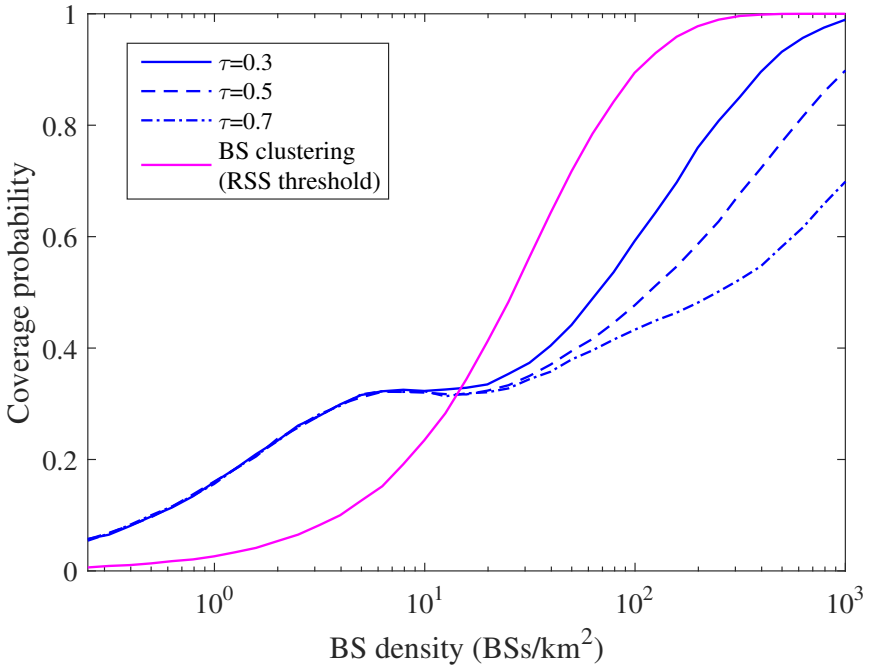

(d) Case 4

Figure 5.5: Coverage probability vs. BS density of BS clustering in four Cases

offered by LoS BSs inside the cooperative cluster, thus slowing down the increase of coverage probability with the BS density. In case 2, more smooth increase of our proposed clustering strategy is observed compared to that in case 1. In Case 3, the RSS threshold based BS clustering shows the lowest coverage probability. This is due to the fact that in millimetre wave transmissions, the fast attenuating transmit signal power can not meet the RSS threshold for clustering. Thus, the pre-defined RSS threshold should be dynamically adapted to the realistic transmission scenario. In case 4, the RSS based BS clustering shows a much faster increasing rate towards full coverage probability than our proposed LoS based BS clustering at higher BS densities. This is because apart from the LoS BSs, the nearby NLoS BSs are more likely to be selected by the RSS based BS cluster, which further enhance the aggregated transmitting signal power, thus resulting a better coverage probability.

Fig. 5.6 shows the coverage probability versus the small-cell BS density of our proposed user-centric BS clustering strategy, with $\tau = 0.3$ and 0.7 in the four studied cases. The coverage probabilities in all four cases increase to reach 1 with the raise of the BS density. In Cases 1, 2 and 4, a drop in the increasing rate of the coverage probability occurs in the middle range of the BS density ($10^{0.5} \sim 10^{1.5}$ BS/km^2). This is because the increase of the number of BSs leads to a fast increase of the interference, which slows down the increasing rate or even degrades the coverage probability. It is also noticed that there is an increasing gap between the curves of Case 2 and 4 at relatively high BS densities, and an almost constant gap between the curves of Cases 1 and 4. Compared with the coverage probability of Case 1 and 2, the 3D path loss model in Case 4 results in longer transmission links, which results in worse received signal powers at the user, which causes a worse performance in terms of SINR and coverage probability. In Case 3, the millimetre wave transmissions

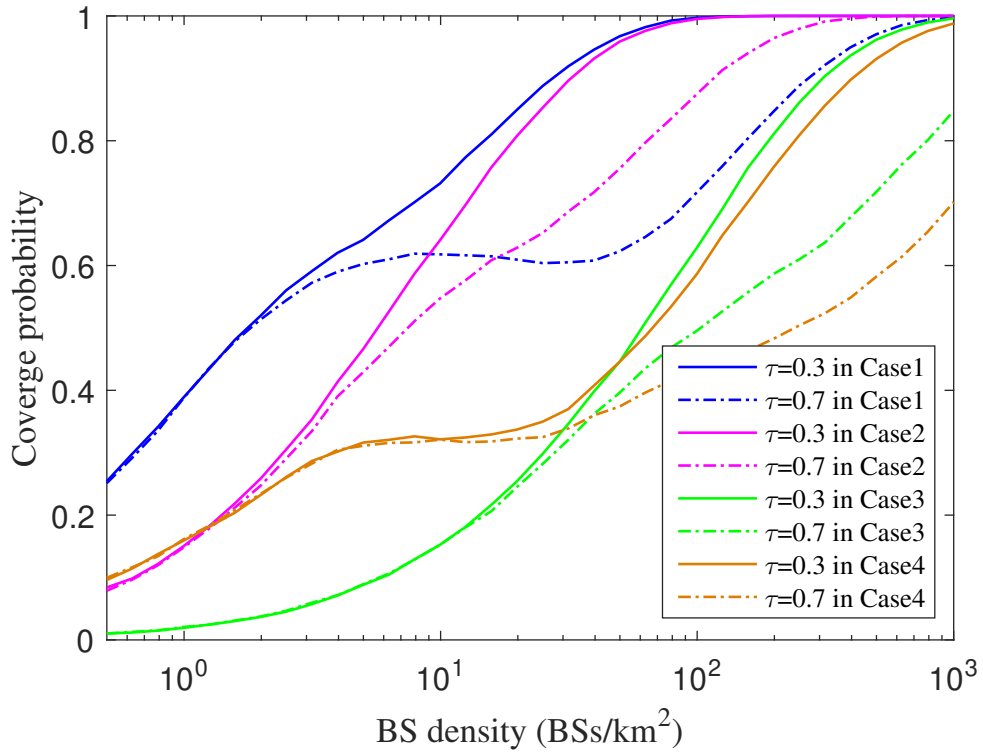

Figure 5.6: Coverage probability vs. BS density of proposed BS clustering in four Cases

at $\tau = 0.3$ and 0.7 have the lowest coverage probability at low BS densities, but increase fast when the BS density goes beyond 10 BS/km^2. This is because the fast attenuating millimetre wave signal power causes much less interference from nearby BSs that are not in the cluster.

Fig. 5.6 shows the number of clustered BSs in the proposed clustering method versus the LoS probability threshold under the four cases. From this figure, it can be seen that the number of BSs in the cluster sharply decreases with the increase of the clustering LoS probability threshold for cases 2, 3 and 4. This is due to the more abrupt nature of the LoS probability function in these case (see Fig. 5.1), The the coverage probability depends on the number of BSs in the serving cluster. The decrease is the

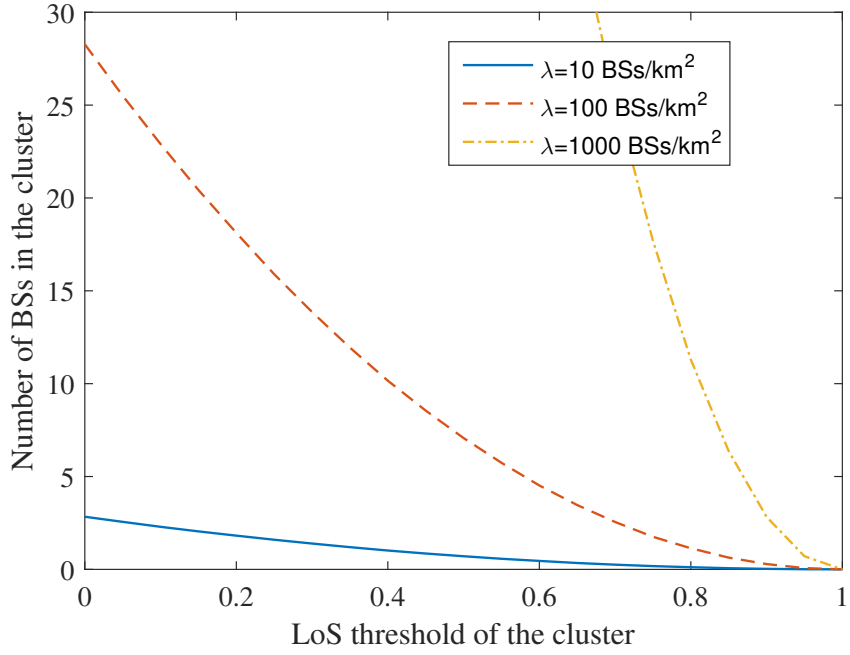

(a) Case1

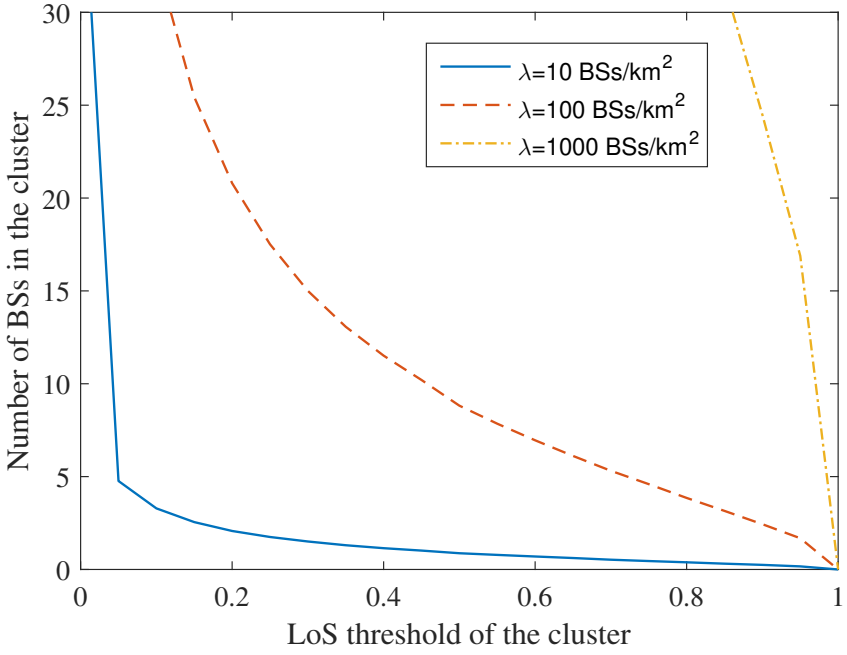

(b) Case2

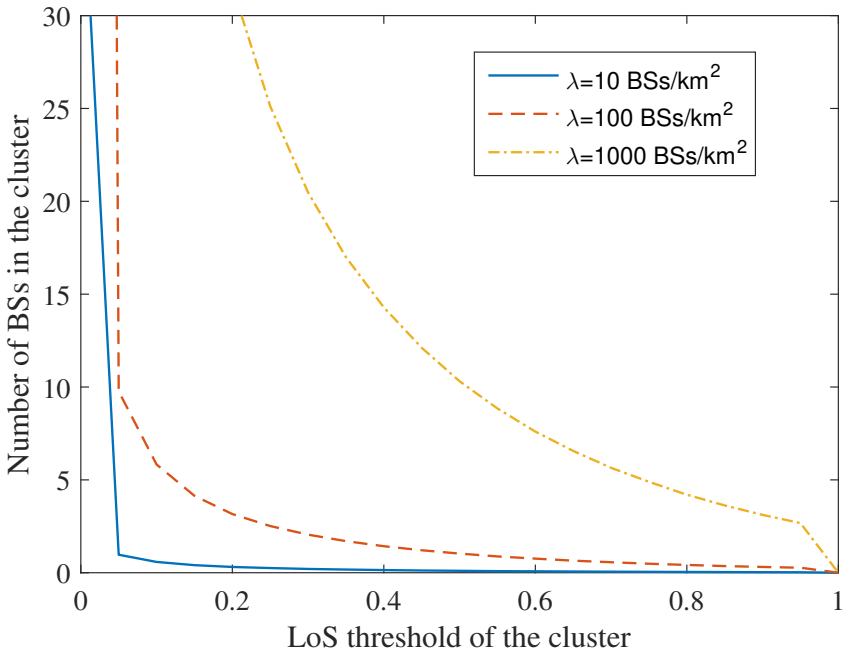

(c) Case3

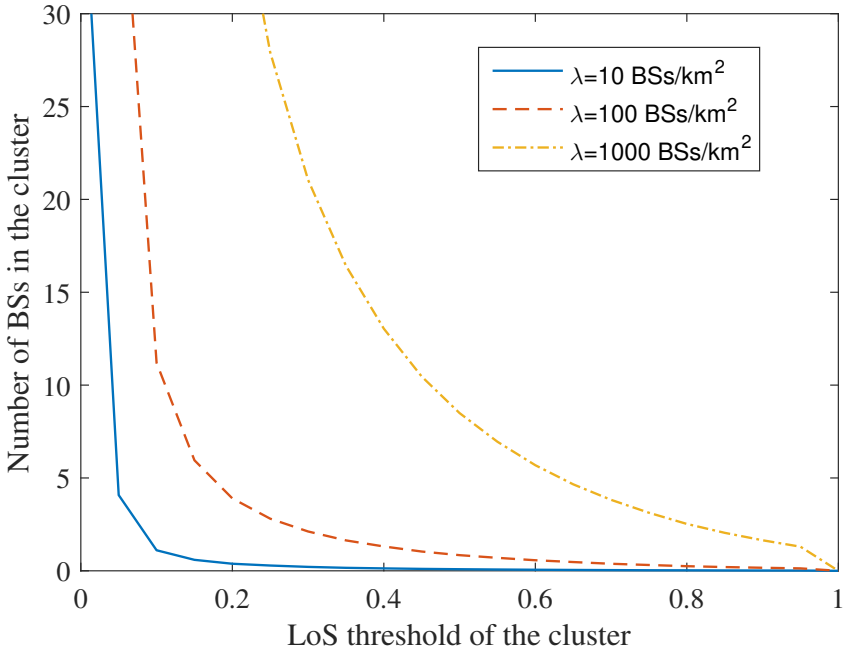

(d) Case4

Figure 5.6: No. of BSs in the cluster against the LoS probability threshold for BS clustering in four Cases

fastest for Case 3 and 4 due to the exponential decreases of LoS probability function with the link distance. It is important to note that the more BSs selected for the cluster, the better coverage probability can be achieved at the user. However, this comes at a cost, the more BSs in the cluster, the higher implementation complexity of the JTs. For example, the user's required data must be available at all BSs in the cluster. Moreover, the spatial reuse may be affected. Therefore, moderately decreasing the LoS probability threshold to cluster the right number of BSs may be helpful to reach a good trade off between network performance, implementation complexity and spatial reuse.

Fig. 5.6 shows the spectrum efficiency of the proposed user-centric BS clustering and the RSS-based BS clustering strategy with the BS density for the four studied cases. As compared to the RSS-based BS clustering strategy, our proposed BS clustering strategy achieves performance gains in Cases 1, 2 and 3. Especially in Case 3, the RSS based BS clustering is not functioning. This is because in millimetre wave transmissions, the fast attenuating signal power can hardly meet the RSS threshold. In contrast, the RSS-based BS clustering achieves a better performance than our proposed BS clustering at high BS densities in Case 4. This is due to the fact that nearby NLoS BSs, which are not selected by our proposed BS clustering, produce a large amount of interference, which slows down the increasing rate of spectrum efficiency. In the proposed scheme, the spectrum efficiency generally first increases to its local maximum value, followed by a slight drop, until it finally reaches a constant increasing rate again. The slow down occurs because the fast-increasing interference from NLoS BSs slows down the increasing rate of spectrum efficiency. The drop is severe for for $\tau = 0.7$.

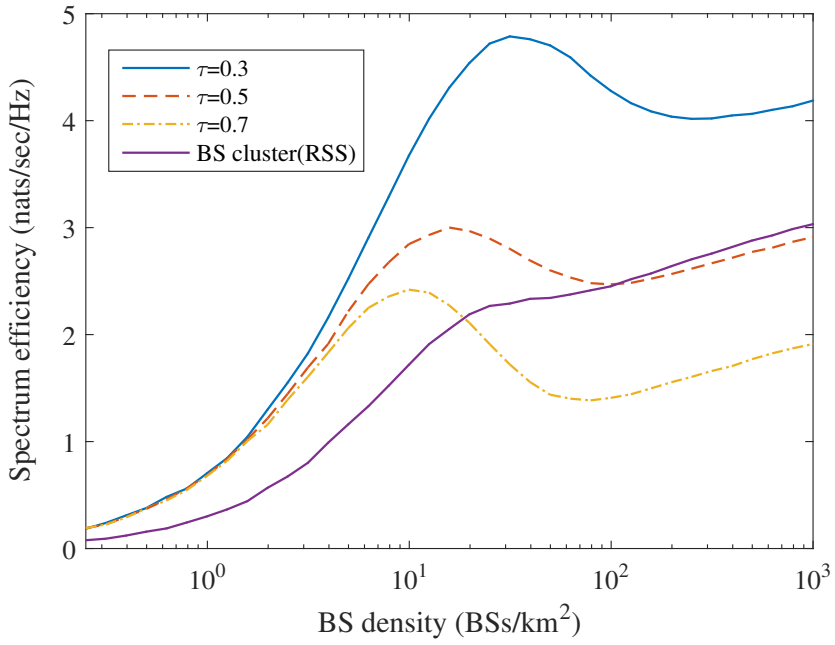

(a) Case1

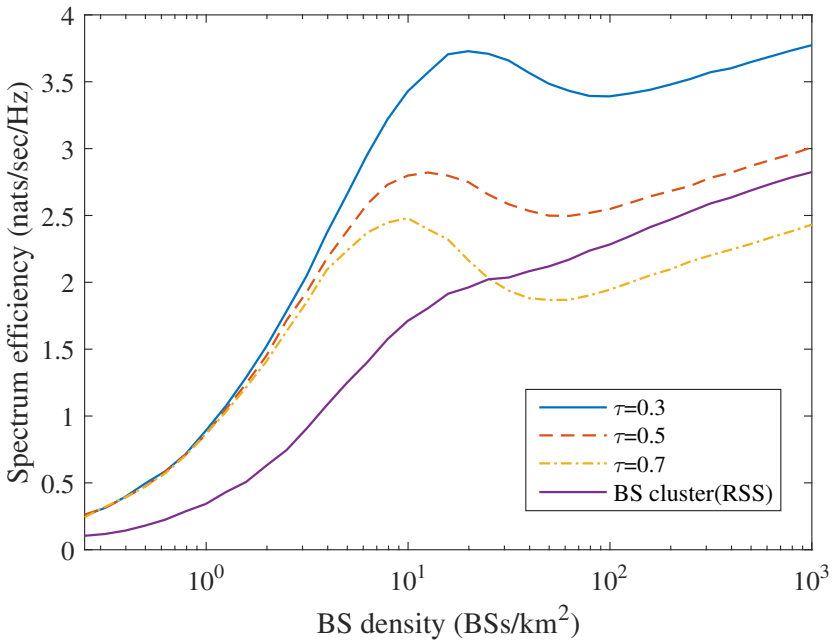

(b) Case2

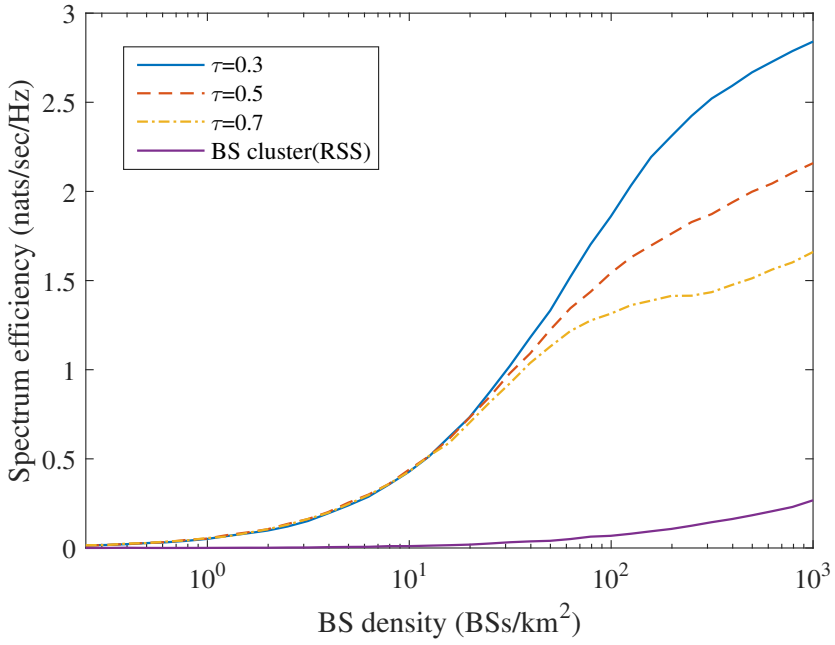

(c) Case3

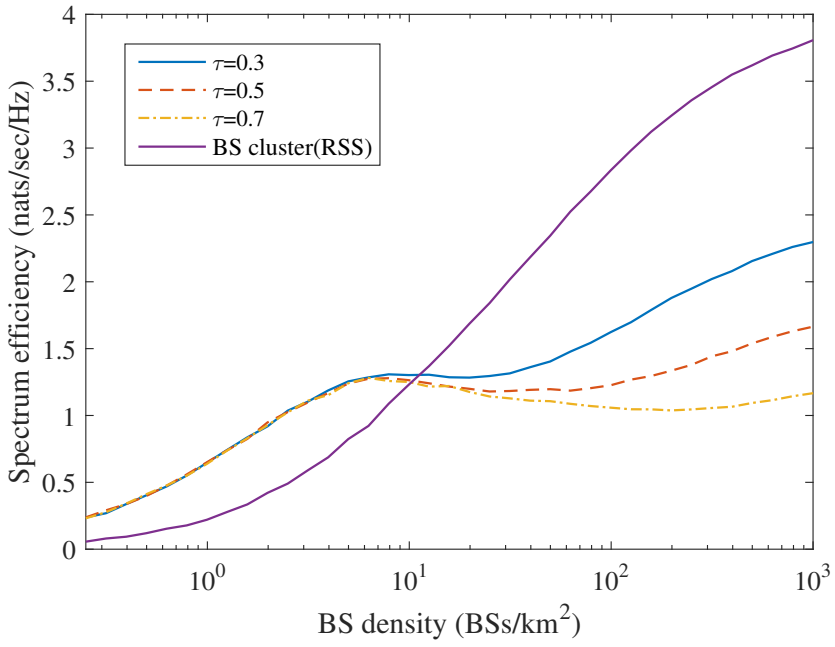

(d) Case4

Figure 5.6: spectrum efficiency vs. BS density in four Cases

5.5 Summary

In this chapter, we have analysed the probabilistic events of LoS/NLoS transmission in four transmission scenarios with different path loss models, including a linear LoS probability function, a suburban area, a millimetre wave transmission and a 3D path loss model. A new user-centric BS clustering strategy has been proposed for non-coherent JT to overcome the severe inter-cell interference in dense small-cell networks. The simulation results have shown that the coverage probability and spectrum efficiency achieved by our proposed BS clustering strategy increase with the BS density even at extremely high densities of BSs. In our future work, we will consider explore the trade-off between BS clustering and area spectrum reuse and extend the proposed user-centric BS clustering strategy to be combined with multi-user JT so as to enhance ASE.

Chapter 6

Multi-BS Multi-UE Clustering

Following from previous chapter, in order to enhance the ASE in a user-centric BS clustering strategy, we further propose a multi-BS multi-UE clustering. The tractable approach is derived by using stochastic geometry. The performance analysis is presented in terms of coverage probability and ASE.

6.1 Introduction

According to the traffic forecast in [3], the growth rate of mobile data traffic in 2017 is 12 exabytes per month, which will have a seven-fold increase until 2022. The trend of increasing demand for high quality at the UE requires more advanced wireless communication techniques to mitigate inter-cell interference [85].

For interference limited cellular networks, Coordinated multipoint (CoMP) with joint transmission (JT) has been widely considered as a promising technique to increase the SINR at the UE. One UE connects to multiple BSs that provide the maximum average received power [98]. CoMP transmission is realized from ex-

changing coordination information between a set of transmission nodes [71]. It can therefore achieve higher SE by by exploiting cooperative diversity gains and mitigating inter-cell interference [99]. In [76], a closed-form expressions and accurate approximations of average data rate of CoMP cluster with imperfect channel state information (CSI) is derived. CoMP transmission techniques is proved to enhance the network performance of the coverage probability in [77, 100].

Continually researching on CoMP of non-coherent JT, in this chapter we propose a new multi-BS multi-UE clustering strategy for non-coherent JT in dense small-cell networks, where a number of UEs and BSs are grouped in a cluster. BSs in the cluster are able to serve multiple UEs simultaneously. Each UE in the cluster can receive an aggregated signal from all BSs in the cluster with non-coherent JT. We develop a tractable approach to reach the closed form expression of the network performance. The resulting coverage probability, achievable SE and ASE are evaluated through system level simulations.

6.2 System Model and Coverage Probability

6.2.1 Clustering Strategy in Small-cell Network

We consider a homogeneous dense small-cell network, where each small-cell BS transmits at the same power level. The spatial distribution of the small cells, which are grouped in the BS set Φ, follows a PPP with a spatial density of λ_{BS}. UEs are distributed over the network area following another independent homogeneous PPP with the density of λ_{UE}.

In this paper, the cluster form a disk area with a radius of d to cover a random

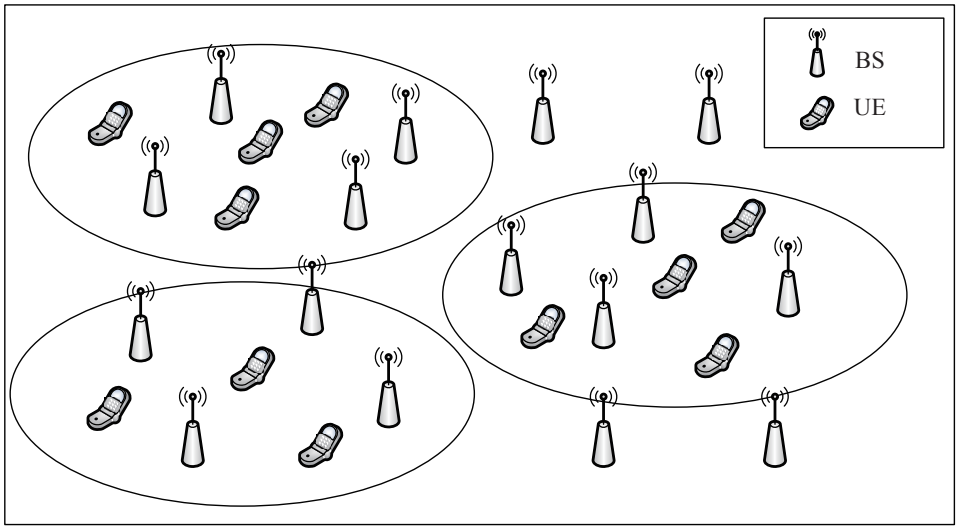

Figure 6.1: Illustration of a multi-BS multi-UE cluster

area as shown in Fig. 6.2. BSs inside cluster are denoted by $n = 1, 2, 3, ..., N$, are simultaneously serving multiple UEs. UEs inside the cluster are denoted by $k = 1, 2, 3, ..., K$, experience the aggregated transmit signal power from all BSs in the cluster with non-coherent JT. We define the SINR for one UE as,

$$\text{SINR} = \frac{\sum_{i=1}^{N} p h_i l(r_i)}{\sum_{j \in \Phi, j \neq n} p h_j l(r_j) + \sigma^2} \tag{6.1}$$

where p is the small-cell BS transmit power, h_i is the channel fading power gain of the link between the i^{th} BS and the UE, which follows a unit-mean exponential distribution, r_i is the distance from the i^{th} BS to the UE, and σ^2 is the additive White Gaussian Noise (AWGN) power at the UE.

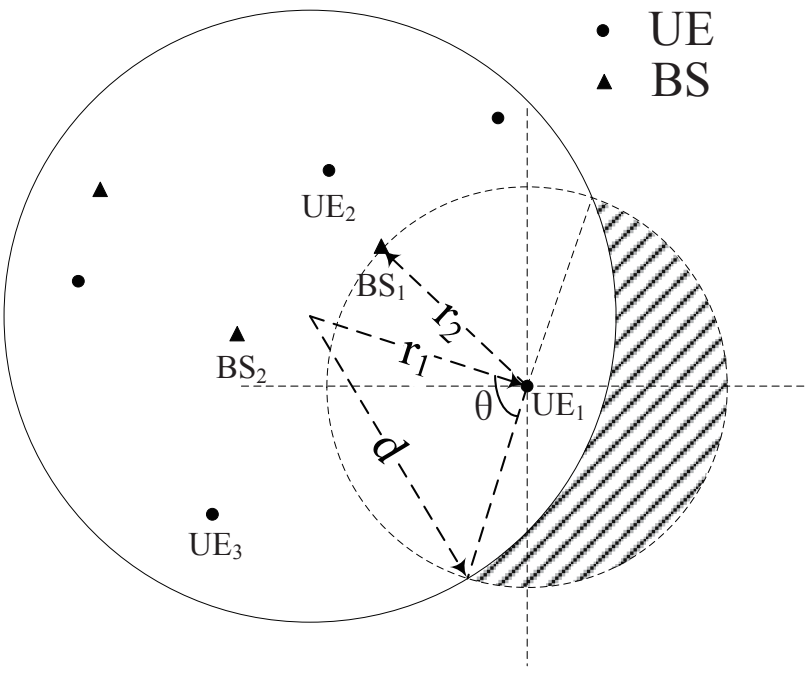

Figure 6.2: The k^{th} UE is connected with the n^{th} BS

6.2.2 Probabilistic BS Density

In this section, we propose probabilistic BS density from the view of a UE according to the spatial distributions of UEs and BSs in the cluster. As shown in Fig. 6.2, we define the distance between the center of the cluster and a UE in the cluster is r_1, and the distance between a random BS in the plane and the UE in the cluster is r_2. From the Fig. 6.2, a BS located away r_2 from the UE can be either in or not in the cluster. We therefore define a multi-slope probability of the BS to be in the cluster as ϵ. The density of serving BSs in the cluster and interference BSs outside the cluster is rewritten as $\epsilon\lambda_{\text{BS}}$ and $(1-\epsilon)\lambda_{\text{BS}}$ respectively.

From the view of a UE in Fig. 6.2, a BS to be certainly the serving BSs in the cluster only if this BS located within the range of $[0, d-r_1]$, i.e. $r2 < d - r_1$. If

a BS located within the range of $[d - r_1, \infty]$, the BS is belong to interference BSs located outside the cluster. When a BS located in the range of $[d - r_1, d + r_1]$, the probability of the BS to be in the cluster (ϵ) is calculated by the proportion of the arc (in the angle of 2θ) in the entire circle (of radius r_2). The multi-slope probability of ϵ is defined as,

$$\epsilon = \begin{cases} 1 & \text{when} \quad r_2 < d - r_1 \\ \frac{\theta}{\pi} & \text{when} \quad d + r_1 < r_2 < d + r_1 \\ 0 & \text{when} \quad r_2 > d + r_1 \end{cases} \tag{6.2}$$

The angle θ is calculated from trigonometric function.

$$\theta = \arccos\left(\frac{{r_1}^2 + {r_2}^2 - d^2}{2r_1 r_2}\right) \tag{6.3}$$

6.3 Theoretical Analysis in Multi-BS Multi-UE Clustering

To evaluate the coverage probability of a small-cell network, we aims to calculate the expectation of the coverage probability of all UEs in the cluster, i.e.

$$\mathcal{C} = \mathbb{E}[\mathcal{C}_k | r_1]$$

where $\mathcal{C}_k$ is the coverage probability experienced at the k^{th} UE. From Campbell's theorem,

$$\mathcal{C} = \int_0^d \mathcal{C}_k(r_1)\delta \quad \mathrm{d}r_1 \tag{6.4}$$

From the view of the center of the cluster, the probability of a UE located r_1 away is given as, $\Delta = e^{-\lambda_{\mathrm{UE}}\pi {r_1}^2}$ Thus, the PDF is,

$$\delta = 2\pi\lambda_{\mathrm{UE}} r_1 e^{-\lambda_{\mathrm{UE}}\pi {r_1}^2} \tag{6.5}$$

From the difference of the BS density in range $[0, \infty]$ presented in last section, $\mathcal{C}_k$ is then divided into two slopes.

$$\mathcal{C}_k = \mathcal{C}_k^1 + \mathcal{C}_k^2 \tag{6.6}$$

where the coverage probability of the k^{th} UE in two slopes is composed of the following two parts

$$\begin{aligned} \mathcal{C}_k^1 &= \int_0^{d-r_1} \mathbb{P}[\mathrm{SINR}_k > T] f_{R_2}^1(r_2) \quad \mathrm{d}r_2 \\ \mathcal{C}_k^2 &= \int_{d-r_1}^{d+r_1} \mathbb{P}[\mathrm{SINR}_k > T] f_{R_2}^2(r_2) \quad \mathrm{d}r_2 \end{aligned} \tag{6.7}$$

From the view of the k^{th} UE, the PDF function of finding at least n points within the range of r_2 is given in [96].

$$f_{R_2}^1(r_2) = \frac{2(\lambda_{\mathrm{BS}}\pi)^n r^{2n-1}}{(n-1)!} \exp(-\lambda_{\mathrm{BS}}\pi r^2) \tag{6.8}$$

$$f_{R_2}^2(r_2) = \frac{2(\epsilon\lambda_{\mathrm{BS}}\pi)^n r^{2n-1}}{(n-1)!} \exp(-\epsilon\lambda_{\mathrm{BS}}\pi r^2) \tag{6.9}$$

The coverage probability is calculated from the SINR experienced at k^{th} UE greater than a pre-defined threshold T. The interference from the BSs outside the cluster is denoted by I, and $I = \sum_{j\in\Phi, j\neq n} p h_j l(r_j)$. By following Gamma approximation

in [83], the probability of SINR greater than T is shown as

$$\begin{aligned}
\mathbb{P}[\text{SINR} > T] &= \mathbb{P}\left[\sum_{i=n}^{N} h_i > \frac{T(I+\sigma^2)}{\sum^N pl(r_2)}\right] \\
&\overset{(a)}{=} 1 - \mathbb{E}\left[\frac{\gamma(n,\mu)}{\Gamma(n)}\right] \\
&= 1 - \mathbb{E}\left[\int_0^{\mu} \frac{t^{n-1}e^{-t}}{\Gamma(n)} dt\right] \\
&\overset{(b)}{\leq} 1 - \mathbb{E}[(1-e^{-b\mu})^n] \\
&= \sum_{m=1}^{n} \binom{n}{m} (-1)^{m+1} \mathbb{E}[e^{-mb\mu}]
\end{aligned} \tag{6.10}$$

(a) follows from the sum of mutually independent random variables having exponential is a Gamma random variable [83], and $\mu = \frac{T(I+\sigma^2)}{\sum^N pl(r_2)}$. Note that $\gamma(n,\mu)$ is the lower incomplete gamma function. (b) follows the inequalities of Gamma distribution introduced in [101].

Theorem 6.1 ***Inequalities of Gamma distribution***

The inequalities of Gamma distribution introduced in [101],

$$(1-e^{-bx})^p < \int_0^x \frac{t^{p-1}e^{-t}}{\Gamma(p)} \quad dt < (1-e^{-ax})^p \tag{6.11}$$

where

$$a = 1, \quad b = (\Gamma(1+p))^{-1/p}, \quad \textit{if} \quad 0 < \frac{1}{p} < 1 \tag{6.12}$$

By substitute μ in the expectation, we have

$$\begin{aligned}&\mathbb{E}[e^{-mb\mu}]\\&=\exp\Big(-\frac{mbT\sigma^2}{\sum_{m<n}pl(r_2)}\Big)\mathbb{E}\Big[\exp\Big(-\frac{mbIT}{\sum_{m<n}pl(r_2)}\Big)\Big]\end{aligned}\tag{6.13}$$

The calculation of Laplace transform of the interference is shown as,

$$\begin{aligned}&\mathbb{E}\Big[\exp\Big(-\frac{mbIT}{\sum_{n<N}pl(r_2)}\Big)\Big]\\&=\exp\Big(-2\pi\lambda_{\mathrm{BS}}\int_{d-r1}^{d+r1}\frac{x(1-\epsilon(x))}{1+(spx^{-\alpha})^{-1}}\mathrm{d}x\Big)\\&\times\exp\Big(-2\pi\lambda_{\mathrm{BS}}\int_{d+r1}^{\infty}\frac{x}{1+(spx^{-\alpha})^{-1}}\mathrm{d}x\Big)\end{aligned}\tag{6.14}$$

where $s=\frac{mbT}{\sum_{m<n}pl(r_2)}$

The network performance of the proposed clustering strategy can be further analyzed from the average data rate and ASE, which are given as,

$$\mathcal{R}=\int_0^{\infty}\log_2(1+T)\frac{\mathrm{d}(1-\mathcal{C}(T))}{\mathrm{d}T}\mathrm{d}T\tag{6.15}$$

and the ASE is calculated by the total data rate achieved by all UEs in the cluster divided by the area of the cluster.

$$\mathrm{ASE}=\frac{\mathcal{R}_{\mathrm{total}}}{\mathrm{Area}}=\lambda_{\mathrm{UE}}\mathcal{R}\tag{6.16}$$

6.4 Numerical Results

In this section, we present numerical results and further study the performance of the proposed multi-BS multi-UE clustering strategy in a small-cell network. we adopt the following parameters: the transmit power of the small cells is $p = 23$dBm, AWGN power is $\sigma^2 = -95$dBm and the path loss exponent is modelled as $\alpha = 3.09$. The density of the UE is defined as the multiple density of the BS.

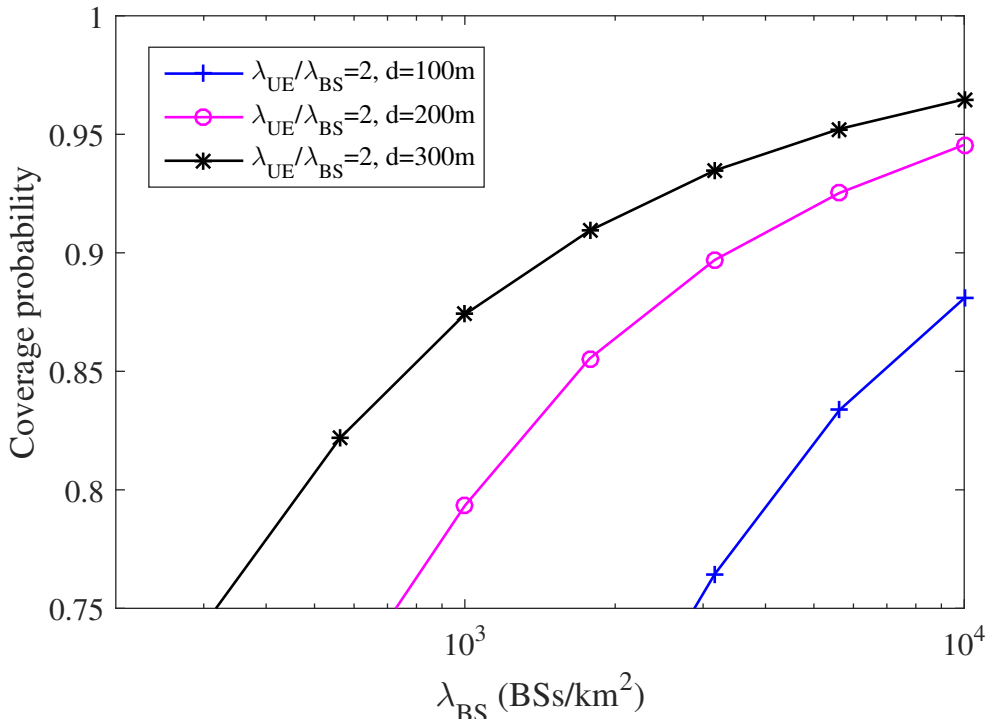

Figure 6.3: Coverage probability vs. BS density in multi-BS multi-UE clustering

Fig. 6.3 shows the coverage probability versus the BS density in the proposed clustering strategy. The coverage increases fast to approach the maximum value 1 at high BS density. This is because the increase of the BS density cause more number of BSs in the cluster. A typical UE in the cluster is able to be simultaneously served by multiple BSs from the non-coherent JTs, and the received signal is the

summation of transmitting signals from all BSs in the cluster. At same BS and UE densities, the coverage probability increases as the cluster range expands. This is simple due to that the cluster range from 100m to 300m, the more BSs are grouped in the cluster. A UE in the cluster experiences a much higher received signal from more serving BSs in the cluster.

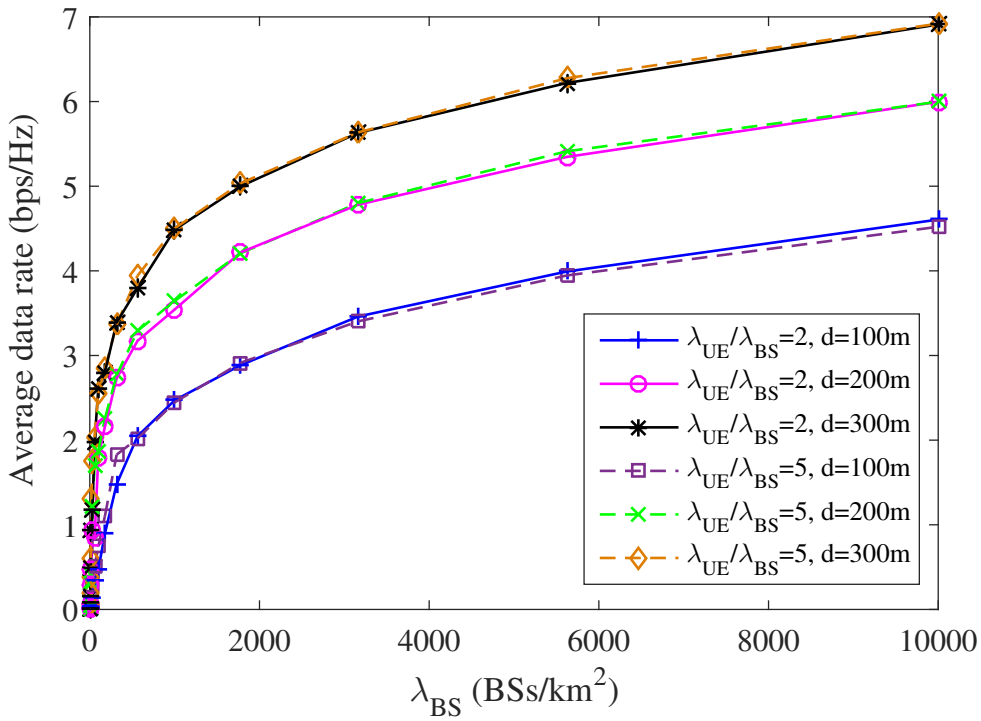

Figure 6.4: Average data rate vs. BS density in multi-BS multi-UE clustering

Fig. 6.4 shows the average data rate at UEs versus the BS density in the proposed clustering strategy. The the average data rates in all cases achieve a high increasing rate at low BS density, and gradually reach to a linear increase at high BS density. This is because at low BS density (< 1000BSs/km^2), the number of BS in the cluster is usually less than 10. The increase of each BS in the cluster give a significant boost of RSS at the UE, which results the fast increasing average data rate. When the BS

density is relatively high, the aggregated received signal at the UE is proportional to the number of BSs in the cluster, which thus results the linear increase of the data rate at UEs.

Moreover, We study the average data rate by different cluster range in proposed clustering strategy and proportion of UE and BS densities. Similar as the coverage probability, the average data rate increases with the cluster range grows. The expansion of the cluster range groups more nearby BSs resulting extreme high total received signal power at UEs, raises the SINR for UEs in the cluster, thus better average data rate for better QoS. When the proportion of UE and BS densities increases from 2 to 5, the data rate at UEs remains constant. The reason behind is due to that all UEs in the cluster are assumed to be serving simultaneously at same spectrum under non-coherent JTs. Each UE is isolated from other UEs with no intra-interference in the cluster.

In Fig. 6.5, we study the linearly increasing ASE of the proposed clustering strategy versus the BS density. Comparing the different proportion of UE and BS densities, the higher UE density the better ASE can be achieved. This is because that when the UE density increases, the number of UEs being served in the cluster is also increasing. Recalling the eq. (6.16), the ASE the is calculated from the total achieving data rate divided by cluster area. The more UEs can be served simultaneously, the higher total data rate can be achieved, and thus the better ASE of the proposed clustering. Moreover, the ASE increases as the cluster range expands, which is because of the similar reason to serve more UEs in the cluster.

Fig. 6.6 shows the EE versus the BS density. Comparing the cluster radius under same UE and BS ratio, we find the smaller of the BS cluster the higher EE can be

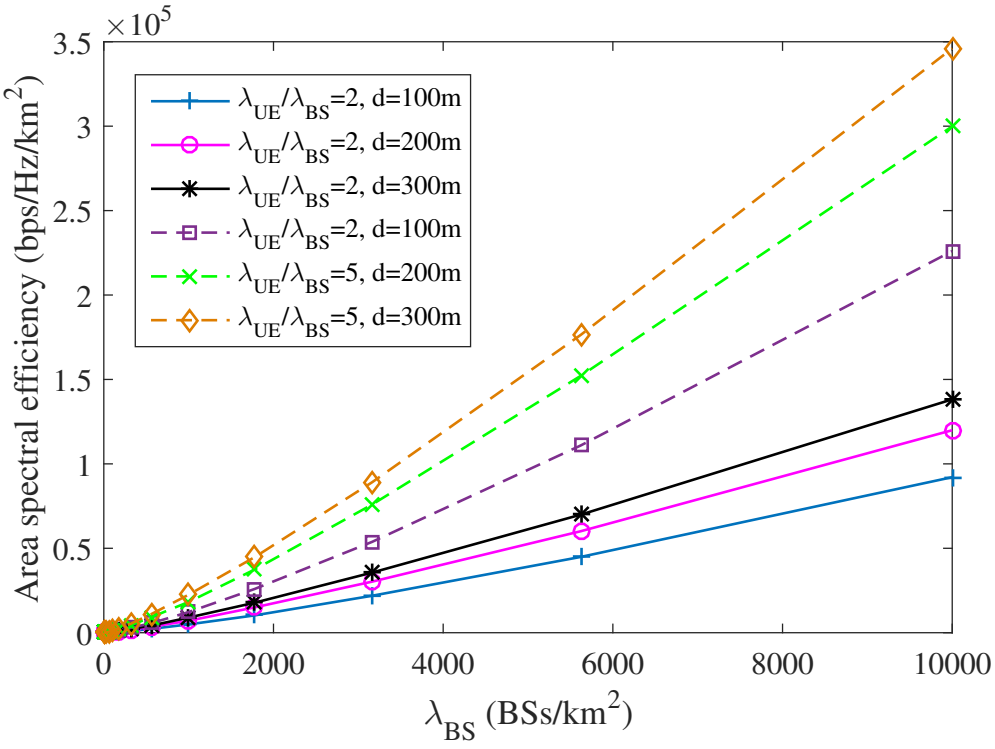

Figure 6.5: ASE vs. BS density in multi-BS multi-UE clustering

reached. Moreover, comparing the different UE and BS ratio at same cluster radius, it is obvious that the lower of the ratio is benefit for the EE. The reason is because the smaller BS clusters or larger number of BSs allow a much lower working load of required UE data for each BS, which thus cause less power to be consumed for each BS. In general, the EE increases with the less number UEs, the more number of BSs and smaller cluster radius, which is exactly opposite to the ASE shown in Fig. 6.5. Thus, a reasonable balance between ASE and EE can be reached in the proposed BS clustering.

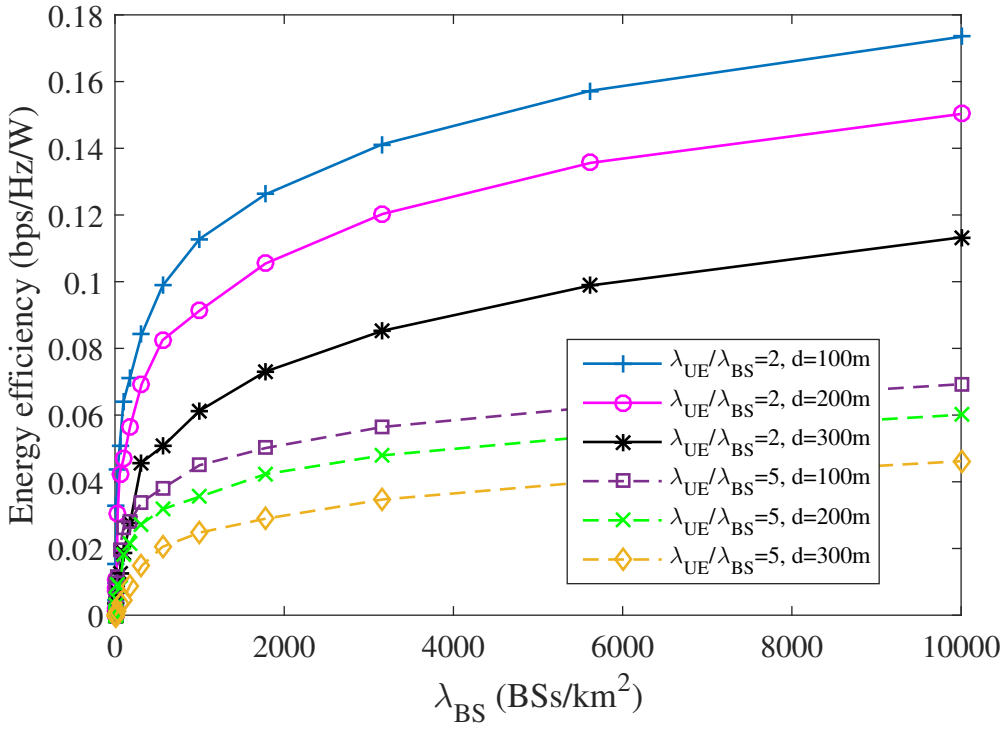

Figure 6.6: EE vs. BS density in multi-BS multi-UE clustering

6.5 Summary

In this chapter, we proposed a multi-BS multi-UE clustering. In the theorems of probabilistic density theorem and gamma approximation of summation fading, the tractable approach is derived in stochastic geometry. The results show the SE increases fast at low BS density and reach a linear increase at relatively high BS density. Meanwhile, the ASE can achieve a high increasing rate in higher UE density and larger cluster range.

Chapter 7

Conclusions and Future Work

7.1 Conclusions

This thesis has investigated the performance analysis of the current HetNets for providing high quality of service to mobile users. The coverage probability, SE, ASE and EE are treated as the key features to evaluate a cellular network. The related closed form expressions are derived in various scenarios. In the meantime, the background of deploying more small-cell BSs in HetNets to meet the exponential increasing user data demand raise the concern of the LoS links in the path loss model. The more practical path loss model is investigated to have multiple slopes with both LoS and NLoS links. The high possible occurrence of the LoS links is demonstrated to degrade the coverage probability in small cell network, but still remains fast linear increase in ASE.

Inspire of that the complex path loss model with multiple slopes and probabilistic LoS and NLoS path losses is facilitated in a HetNets. The PPP is introduced according to the randomness of the BS location. Utilizing the stochastic geometry, the

closed form expressions of K-tier HetNets are derived to the analyze the network performance, such as coverage probability, ASE and EE. For feasible comparison in network performance, The analytical model is further simplified in a two-tier HetNets with simplified linear LoS and NLoS path loss model. The results demonstrate that at relatively high small-cell densities, the excessive inter-cell interference caused by LoS and NLoS blocked almost all desired links. The increasing small-cell transmit power will not improve the ASE, but will degrade the EE significantly. Even in an extremely dense HetNet both the ASE and EE of the HetNet will drop quickly.

Following the investigating of LoS transmissions, the the probabilistic events of LoS and NLoS transmissions are studied in four transmission scenarios with different path loss models, including a linear LoS probability function, a suburban area, a millimetre wave transmission and a 3D path loss model. The network performance is numerically evaluated in a small-cell network. The simulation results show the severe degradation of both coverage probability and SE appeared at high BS density. Accordingly, A new user-centric BS clustering strategy is proposed for non-coherent JT to overcome the severe inter-cell interference in dense small-cell networks. The simulation results show that the coverage probability and spectrum efficiency achieved by the proposed BS clustering strategy increases with the BS density even at high densities of BSs.

Furthermore, the enhancement of the ASE in the clustering strategy called multi-BS multi-UE clustering is then proposed. The tractable approach is derived in stochastic geometry according to the probabilistic density theorem and gamma approximation of summation fading. The performance analysis is presented in terms of coverage probabiltiy, SE and ASE. The proposed clustering strategy achieves high coverage

probability and linear increasing SE at high BS density without sacrificing the ASE.

7.2 Future Work

The future work of this thesis is discussed according to the remaining issues and challenges in each chapter.

In chapter 4, a closed form expression for HetNets has been developed in the consideration of LoS and NLoS transmissions. There are a number of potential improvements requiring further investigations. Firstly, the bias factor mentioned in the user association exists in closed form expressions in K-tier HetNets, which enable the analysis of load balancing between different tiers. Moreover, the cell range expansion technology can be realized by having larger bias in small cell. As the number of small-cell BSs increases, it is reasonable to offload from macrocells to small cells. Secondly, the LoS probability in the path loss is modeled as a linear function in proposed theoretical expressions. The more realistic path loss model can be fitted in the closed form expressions, such as the path loss models mentioned in chapter 5. In addition, the HetNets are assumed in the outdoor environment only. As LoS transmissions are highly likely to appear in the indoor environment. The theoretical analysis can be further extended to a mixed outdoor and indoor scenario.

In chapter 5, LoS and NLoS path loss models are simulated in four transmission environments. The corresponding user-centric BS clustering strategy is proposed to mitigate the inference at the user, which thus improve the network performance. The potential work in the future will first to reach a tractable approach of closed form expressions rather than the current analysis is based on simulation results only. Secondly, the proposed BS clustering strategy assumes there is enough space

between each cluster, so the problem of overlapping BS clusters has not address and can be considered in future work [102]. Moreover, both BSs and UEs are currently modeled with independent Poisson point process (PPP). However, with defined cluster in point process, the Poisson cluster process (PCP) is more positive to exhibit attractive point patterns [103]. Moreover, the comparison between PPP and PCP in analysis of BS clustering strategy can be investigated.

In chapter 6, the multi-BS multi-UE clustering is proposed, and the closed form expressions is derived for evaluating network performance in terms of coverage probability, SE, ASE and EE. The proposed strategy is currently facilitated in small-cell network only. The closed form expressions can be further derived for HetNets with multiple types of BSs. In current clustering strategy, the UEs and BSs are the randomly located in the cluster, which will result the UEs at cluster center will have better QoS than cluster-edge UEs, because the cluster-center UEs are likely to have shorter distances to BSs. Therefore, the further analysis of cluster-center and cluster-edge performance is needed. Lastly, the proposed strategy assume the spectrum is shared by all UEs. In this case, the coherent JTs are expected to be analyzed for signal coordination and synchronization between BSs in the cluster.

Chapter 8

Appendix

8.1 Discussion of parameter b and c

Following the similar process in eq. 4.27 and eq. 4.32 in chapter 4, we discuss the relationship between b and d_1 and c and d_1.

If $0 < b \leq d_1$, the second multiplier in eq. (4.26), i.e. $\tilde{b}$ is given as

$$\tilde{b} = \exp\Big(- \int_0^b \frac{u}{d_1} 2\pi u \lambda_1 du \Big) \tag{8.1}$$

and the interference from NLoS BSs in 1^{th} tier is shown as,

$$\begin{aligned}
&\mathcal{L}_{I_1^{\mathrm{NL}}}(s) = \exp\Big(- 2\pi\lambda_1 \int_b^{d_1} (\frac{u}{d_1}) \frac{u}{1 + (sP_1 A^{\mathrm{NL}})^{-1} u^{\alpha^{\mathrm{NL}}}} du \Big) \\
&\times \exp\Big(- 2\pi\lambda_1 \int_{d_1}^{\infty} (\frac{u}{d_1}) \frac{u}{1 + (sP_1 A^{\mathrm{NL}})^{-1} u^{\alpha^{\mathrm{NL}}}} du \Big) \\
&= \exp\Big(- \frac{2\pi\lambda_1}{d_1} \Big\{ \xi_1 \left[\alpha^{\mathrm{NL}}, 2, (\frac{P_2 A^{\mathrm{NL}}}{P_1 A^{\mathrm{L}}} \gamma r^{\alpha^{\mathrm{L}}})^{-1}, d_1 \right] - \xi_1 \left[\alpha^{\mathrm{NL}}, 2, (\frac{P_2 A^{\mathrm{NL}}}{P_1 A^{\mathrm{L}}} \gamma r^{\alpha^{\mathrm{L}}})^{-1}, b \right] \Big\} \\
&- 2\pi\lambda_1 \xi_2 \left[\alpha^{\mathrm{NL}}, 1, (\frac{P_2 A^{\mathrm{NL}}}{P_1 A^{\mathrm{L}}} \gamma r^{\alpha^{\mathrm{L}}})^{-1}, d_1 \right] \Big)
\end{aligned} \tag{8.2}$$

If $b > d_1$, we have

$$\tilde{b} = \exp\Big(- \int_0^{d_1} \frac{u}{d_1} 2\pi u \lambda_1 du - \int_{d_1}^{b} 2\pi u \lambda_1 du \Big) \tag{8.3}$$

and,

$$\begin{aligned} \mathcal{L}_{I_1^{\mathrm{NL}}}(s) &= \exp\Big(- 2\pi\lambda_1 \int_b^{\infty} \frac{u}{1 + (sP_1 A^{\mathrm{NL}})^{-1} u^{\alpha^{\mathrm{NL}}}} du \Big) \\ &= \exp\Big(- 2\pi\lambda_1 \xi_2 \left[\alpha^{\mathrm{NL}}, 1, (\frac{P_2 A^{\mathrm{NL}}}{P_1 A^{\mathrm{L}}} \gamma r^{\alpha^{\mathrm{L}}})^{-1}, b \right] \Big) \end{aligned} \tag{8.4}$$

Moreover, if $0 < c \leq d_1$, the third multiplier in eq. (4.26), i.e. $\tilde{c}$ is given as

$$\tilde{c} = \exp\Big(- \int_0^{c} (\frac{u}{d_1}) 2\pi u \lambda_2 du \Big) \tag{8.5}$$

and the interference from NLoS BSs in 2^{th} tier is,

$$\begin{aligned} &\mathcal{L}_{I_2^{\mathrm{NL}}}(s) = \exp\Big(- 2\pi\lambda_2 \int_c^{d_1} (\frac{u}{d_1}) \frac{u}{1 + (sP_2 A^{\mathrm{NL}})^{-1} u^{\alpha^{\mathrm{NL}}}} du \Big) \\ &\times \exp\Big(- 2\pi\lambda_2 \int_{d_1}^{\infty} (\frac{u}{d_1}) \frac{u}{1 + (sP_2 A^{\mathrm{NL}})^{-1} u^{\alpha^{\mathrm{NL}}}} du \Big) \\ &= \exp\Big(- \frac{2\pi\lambda_2}{d_1} \Big\{ \xi_1 \left[\alpha^{\mathrm{NL}}, 2, (\frac{P_2 A^{\mathrm{NL}}}{P_1 A^{\mathrm{L}}} \gamma r^{\alpha^{\mathrm{L}}})^{-1}, d_1 \right] - \xi_1 \left[\alpha^{\mathrm{NL}}, 2, (\frac{P_2 A^{\mathrm{NL}}}{P_1 A^{\mathrm{L}}} \gamma r^{\alpha^{\mathrm{L}}})^{-1}, c \right] \Big\} \\ &- 2\pi\lambda_2 \xi_2 \left[\alpha^{\mathrm{NL}}, 1, (\frac{P_2 A^{\mathrm{NL}}}{P_1 A^{\mathrm{L}}} \gamma r^{\alpha^{\mathrm{L}}})^{-1}, d_1 \right] \Big) \end{aligned} \tag{8.6}$$

If $c > d_1$, we have

$$\tilde{c} = \exp\Big(- \int_0^{d_1} \frac{u}{d_1} 2\pi u \lambda_2 du - \int_{d_1}^{c} 2\pi u \lambda_2 du \Big) \tag{8.7}$$

and,

$$\begin{aligned}\mathcal{L}_{I_2^{\mathrm{NL}}}(s) &= \exp\Big(-2\pi\lambda_2 \int_c^{\infty} \frac{u}{1+(sP_2A^{\mathrm{NL}})^{-1}u^{\alpha^{\mathrm{NL}}}} du\Big) \\ &= \exp\Big(-2\pi\lambda_2\xi_2 \left[\alpha^{\mathrm{NL}}, 1, (\frac{P_2A^{\mathrm{NL}}}{P_1A^{\mathrm{L}}}\gamma r^{\alpha^{\mathrm{L}}})^{-1}, c\right]\Big)\end{aligned} \tag{8.8}$$

By plugging eq. (4.27, 4.32, 8.1, 8.3, 8.5 and 8.7) into eq. (4.26), we have the $f_{1,1}^{\mathrm{L}}$. Moreover, plugging eq. (4.28, 8.2, 8.4, 8.6 and 8.8) and eq. (4.26) into eq. (4.25), we have the $T_{1,1}^{\mathrm{L}}$.

References

[1] J. Wang, X. Chu, M. Ding, and D. López-Pérez, "On the performance of multi-tier heterogeneous networks under los and nlos transmissions," in *2016 IEEE Globecom Workshops (GC Wkshps)*. IEEE, 2016, pp. 1–6.

[2] J. Wang, X. Chu, M. Ding, and D. López-Pérez, "The effect of los and nlos transmissions on base station clustering in dense small-cell networks," in *2019 IEEE 90th Vehicular Technology Conference (VTC2019-Fall)*, 2019, pp. 1–6.

[3] C. V. N. Index, "Global mobile data traffic forecast update, 2017–2022 white paper," *Cisco: San Jose, CA, USA*, Feb. 2019.

[4] M. Jackson, "EE prepare first live uk trial of 5g wireless broadband in london." [Online]. Available: `ISP News`

[5] M. Ding, P. Wang, D. López-Pérez, G. Mao, and Z. Lin, "Performance impact of LoS and NLoS transmissions in dense cellular networks," *IEEE Trans. Wireless Commun.*, vol. 15, no. 3, pp. 2365–2380, Mar. 2016.

[6] Q. Ye, B. Rong, Y. Chen, M. Al-Shalash, C. Caramanis, and J. G. Andrews, "User association for load balancing in heterogeneous cellular networks," *IEEE Transactions on Wireless Communications*, vol. 12, no. 6, pp. 2706–2716, 2013.

[7] Z. Zheng, X. Zhang, L. X. Cai, R. Zhang, and X. Shen, "Sustainable communication and networking in two-tier green cellular networks," *IEEE Wireless*

Communications, vol. 21, no. 4, pp. 47–53, Aug. 2014.

[8] H. Zhang, C. Jiang, N. C. Beaulieu, X. Chu, X. Wen, and M. Tao, "Resource allocation in spectrum-sharing ofdma femtocells with heterogeneous services," *IEEE Transactions on Communications*, vol. 62, no. 7, pp. 2366–2377, Jul. 2014.

[9] L. Wu, Y. Zhong, and W. Zhang, "Spatial statistical modeling for heterogeneous cellular networks-an empirical study," in *2014 IEEE 79th Vehicular Technology Conference (VTC Spring)*, 2014, pp. 1–6.

[10] Z. Gao, Z. Li, N. Wang, D. Wang, and X. Mu, "On sinr biasing for optimal cell range expansion in two-tier wireless hetnets," 2017.

[11] A. Ghosh, N. Mangalvedhe, R. Ratasuk, B. Mondal, M. Cudak, E. Visotsky, T. A. Thomas, J. G. Andrews, P. Xia, H. S. Jo *et al.*, "Heterogeneous cellular networks: From theory to practice," *IEEE communications magazine*, vol. 50, no. 6, pp. 54–64, 2012.

[12] D. Cao, S. Zhou, and Z. Niu, "Optimal combination of base station densities for energy-efficient two-tier heterogeneous cellular networks," *IEEE Transactions on Wireless Communications*, vol. 12, no. 9, pp. 4350–4362, 2013.

[13] T. D. P. Perera, D. N. K. Jayakody, S. K. Sharma, S. Chatzinotas, and J. Li, "Simultaneous wireless information and power transfer (swipt): Recent advances and future challenges," *IEEE Communications Surveys & Tutorials*, vol. 20, no. 1, pp. 264–302, 2017.

[14] V. M. Nguyen and M. Kountouris, "Coverage and capacity scaling laws in downlink ultra-dense cellular networks," in *2016 IEEE International Conference on Communications (ICC)*, 2016, pp. 1–7.

[15] R. F. Guiazon, K.-K. Wong, and M. Fitch, "Coverage probability of cellular

networks using interference alignment under imperfect CSI," *Digital Communications and Networks*, vol. 2, no. 4, pp. 162–166, 2016.

[16] T. D. Novlan, H. S. Dhillon, and J. G. Andrews, "Analytical modeling of uplink cellular networks," *IEEE Transactions on Wireless Communications*, vol. 12, no. 6, pp. 2669–2679, 2013.

[17] J. G. Andrews, F. Baccelli, and R. K. Ganti, "A tractable approach to coverage and rate in cellular networks," *IEEE Transactions on communications*, vol. 59, no. 11, pp. 3122–3134, 2011.

[18] W. Wang and G. Shen, "Energy efficiency of heterogeneous cellular network," in *2010 IEEE 72nd Vehicular Technology Conference - Fall*, 2010, pp. 1–5.

[19] Z. Zhang, Y. Li, K. Huang, S. Zhou, and J. Wang, "Energy efficiency analysis of cellular networks with cooperative relays via stochastic geometry," *China Communications*, vol. 12, no. 9, pp. 112–121, Sep. 2015.

[20] H.-S. Jo, Y. J. Sang, P. Xia, and J. G. Andrews, "Heterogeneous cellular networks with flexible cell association: A comprehensive downlink sinr analysis," *IEEE Transactions on Wireless Communications*, vol. 11, no. 10, pp. 3484–3495, Oct. 2012.

[21] D. Lopez-Perez, I. Guvenc, G. de la Roche, M. Kountouris, T. Quek, and J. Zhang, "Enhanced intercell interference coordination challenges in heterogeneous networks," *IEEE Wireless Communications*, vol. 3, no. 18, pp. 22–30, 2011.

[22] A. K. Gupta, H. S. Dhillon, S. Vishwanath, and J. G. Andrews, "Downlink coverage probability in mimo hetnets with flexible cell selection," in *2014 IEEE Global Communications Conference*, 2014, pp. 1534–1539.

[23] C. Li, J. Zhang, M. Haenggi, and K. B. Letaief, "User-centric intercell in-

terference nulling for downlink small cell networks," *IEEE Transactions on Communications*, vol. 63, no. 4, pp. 1419–1431, 2015.

[24] R. W. Heath, M. Kountouris, and T. Bai, "Modeling heterogeneous network interference using poisson point processes," *IEEE Transactions on Signal Processing*, vol. 61, no. 16, pp. 4114–4126, 2013.

[25] B. Błaszczyszyn, M. K. Karray, and H. P. Keeler, "Using poisson processes to model lattice cellular networks," in *2013 Proceedings IEEE INFOCOM*, 2013, pp. 773–781.

[26] A. Guo and M. Haenggi, "Spatial stochastic models and metrics for the structure of base stations in cellular networks," *IEEE Transactions on Wireless Communications*, vol. 12, no. 11, pp. 5800–5812, 2013.

[27] P. Madhusudhanan, J. G. Restrepo, Y. Liu, and T. X. Brown, "Downlink coverage analysis in a heterogeneous cellular network," in *2012 IEEE Global Communications Conference (GLOBECOM)*, 2012, pp. 4170–4175.

[28] P. T. V. Bhuvaneswari, S. Indu, N. L. Shifana, D. Arjun, and A. S. Priyadharshini, "An analysis on cell range expansion in 4g lte networks," in *2015 3rd International Conference on Signal Processing, Communication and Networking (ICSCN)*, 2015, pp. 1–6.

[29] Z. Gao, Z. Li, N. Wang, D. Wang, and X. Mu, "On sinr biasing for optimal cell range expansion in two-tier wireless hetnets," in *7th IET International Conference on Wireless, Mobile Multimedia Networks (ICWMMN 2017)*, 2017, pp. 77–82.

[30] Y. Wu, Y. Cui, and B. Clerckx, "Analysis and optimization of inter-tier interference coordination in downlink multi-antenna HetNets with offloading," *IEEE Transactions on Wireless Communications*, vol. 14, no. 12, pp. 6550–

6564, 2015.

[31] H. S. Dhillon *et al.*, "Modeling and analysis of k-tier downlink heterogeneous cellular networks," in *IEEE J. Sel. Areas Commun*, vol. 30, no. 3, Apr. 2011, pp. 550–560.

[32] S. Sadr and R. S. Adve, "Tier association probability and spectrum partitioning for maximum rate coverage in multi-tier heterogeneous networks," *IEEE Communications Letters*, vol. 18, no. 10, pp. 1791–1794, 2014.

[33] H. Tabassum, Z. Dawy, E. Hossain, and M.-S. Alouini, "Interference statistics and capacity analysis for uplink transmission in two-tier small cell networks: A geometric probability approach," *IEEE Transactions on Wireless Communications*, vol. 13, no. 7, pp. 3837–3852, 2014.

[34] S. Singh, X. Zhang, and J. G. Andrews, "Joint rate and SINR coverage analysis for decoupled uplink-downlink biased cell associations in HetNets," *IEEE Transactions on Wireless Communications*, vol. 14, no. 10, pp. 5360–5373, 2015.

[35] M. Di Renzo and P. Guan, "Stochastic geometry modeling and system-level analysis of uplink heterogeneous cellular networks with multi-antenna base stations," *IEEE Transactions on Communications*, vol. 64, no. 6, pp. 2453–2476, 2016.

[36] D. Cao, S. Zhou, and Z. Niu, "Improving the energy efficiency of two-tier heterogeneous cellular networks through partial spectrum reuse," *IEEE Transactions on Wireless Communications*, vol. 12, no. 8, pp. 4129–4141, 2013.

[37] Z. Chen, L. Qiu, and X. Liang, "Area spectral efficiency analysis and energy consumption minimization in multiantenna poisson distributed networks," *IEEE Transactions on Wireless Communications*, vol. 15, no. 7, pp. 4862–

4874, 2016.

[38] M. Z. Shakir and M.-S. Alouini, "On the area spectral efficiency improvement of heterogeneous network by exploiting the integration of macro-femto cellular networks," in *2012 IEEE International Conference on Communications (ICC)*, 2012, pp. 5695–5700.

[39] C. Li, J. Zhang, J. G. Andrews, and K. B. Letaief, "Success probability and area spectral efficiency in multiuser MIMO hetnets," *IEEE Transactions on Communications*, vol. 64, no. 4, pp. 1544–1556, 2016.

[40] M. Z. Shakir, H. Tabassum, and M.-S. Alouini, "Analytical bounds on the area spectral efficiency of uplink heterogeneous networks over generalized fading channels," *IEEE Transactions on Vehicular Technology*, vol. 63, no. 5, pp. 2306–2318, 2014.

[41] L. Yang, S. Song, and K. B. Letaief, "Jointly optimal spectrum deployment and cognitive access for ase maximization of macro-femto hetnets," in *2015 IEEE International Conference on Communication Workshop (ICCW)*, 2015, pp. 100–105.

[42] Z. Chen, L. Qiu, and X. W. Liang, "Area spectral efficiency analysis of multi-antenna two-tier cellular networks," *IEEE Communications Letters*, vol. 21, no. 1, pp. 108–111, 2017.

[43] P. Xia, C.-H. Liu, J. G. Andrews *et al.*, "Downlink coordinated multi-point with overhead modeling in heterogeneous cellular networks," *IEEE Transactions on Wireless Communications*, vol. 12, no. 8, pp. 4025–4037, 2013.

[44] K. Davaslioglu, C. C. Coskun, and E. Ayanoglu, "Energy-efficient resource allocation for fractional frequency reuse in heterogeneous networks," *IEEE Transactions on Wireless Communications*, vol. 14, no. 10, pp. 5484–5497,

Oct. 2015.

[45] W. Wang and G. Shen, "Energy efficiency of heterogeneous cellular network," in *2010 IEEE 72nd Vehicular Technology Conference-Fall*, 2010, pp. 1–5.

[46] Z. Hasan, H. Boostanimehr, and V. K. Bhargava, "Green cellular networks: A survey, some research issues and challenges," *arXiv preprint arXiv:1108.5493*, 2011.

[47] C. Li, J. Zhang, and K. B. Letaief, "Throughput and energy efficiency analysis of small cell networks with multi-antenna base stations," *IEEE Transactions on Wireless Communications*, vol. 13, no. 5, pp. 2505–2517, 2014.

[48] M. Wildemeersch, T. Q. Quek, C. H. Slump, and A. Rabbachin, "Cognitive small cell networks: Energy efficiency and trade-offs," *IEEE Transactions on Communications*, vol. 61, no. 9, pp. 4016–4029, 2013.

[49] Y. S. Soh, T. Q. Quek, M. Kountouris, and H. Shin, "Energy efficient heterogeneous cellular networks," *IEEE Journal on selected areas in communications*, vol. 31, no. 5, pp. 840–850, 2013.

[50] Y. Cai, Y. Ni, J. Zhang, S. Zhao, and H. Zhu, "Energy efficiency and spectrum efficiency in underlay device-to-device communications enabled cellular networks," *China Communications*, vol. 16, no. 4, pp. 16–34, 2019.

[51] H. H. Yang, G. Geraci, and T. Q. Quek, "Energy-efficient design of MIMO heterogeneous networks with wireless backhaul," *IEEE Transactions on Wireless Communications*, vol. 15, no. 7, pp. 4914–4927, 2016.

[52] W. Liu, S. Han, and C. Yang, "Energy efficiency comparison of massive MIMO and small cell network," in *2014 IEEE Global Conference on Signal and Information Processing (GlobalSIP)*, 2014, pp. 617–621.

[53] R. Ramamonjison and V. K. Bhargava, "Energy efficiency maximization

framework in cognitive downlink two-tier networks," *IEEE Transactions on Wireless Communications*, vol. 14, no. 3, pp. 1468–1479, 2015.

[54] R. Ramamonjison and V. K. Bhargava, "Sum energy-efficiency maximization for cognitive uplink networks with imperfect CSI," in *2014 IEEE wireless communications and networking conference (WCNC)*, 2014, pp. 1012–1017.

[55] L. Xiang, X. Ge, C.-X. Wang, F. Y. Li, and F. Reichert, "Energy efficiency evaluation of cellular networks based on spatial distributions of traffic load and power consumption," *IEEE Transactions on Wireless Communications*, vol. 12, no. 3, pp. 961–973, 2013.

[56] X. Zhao, J.-B. Wang, J.-Y. Wang, M. Chen, M. Feng, and M. Sheng, "System outage probability analysis in uplink multi-hop cellular systems over composite channels," *EURASIP Journal on Wireless Communications and Networking*, vol. 2011, no. 1, pp. 1–8, 2011.

[57] A. K. Gupta, X. Zhang, and J. G. Andrews, "SINR and throughput scaling in ultradense urban cellular networks," *IEEE Wireless Communications Letters*, vol. 4, no. 6, pp. 605–608, 2015.

[58] J. G. Andrews, X. Zhang, G. D. Durgin, and A. K. Gupta, "Are we approaching the fundamental limits of wireless network densification?" *IEEE Communications Magazine*, vol. 54, no. 10, pp. 184–190, 2016.

[59] M. Ding, D. López-Pérez, G. Mao, and Z. Lin, "Ultra-dense networks: Is there a limit to spatial spectrum reuse?" in *2018 IEEE International Conference on Communications (ICC)*. IEEE, 2018, pp. 1–6.

[60] Z. Zhang and R. Q. Hu, "Dense cellular network analysis with los/nlos propagation and bounded path loss model," *IEEE Communications Letters*, vol. 22, no. 11, pp. 2386–2389, 2018.

[61] 3rd Generation Partnership Project (3GPP), "3GPP TR 36.814 (v9.0.0): Further advancements for E-UTRA physical layer aspects (release 9)," Mar. 2010.

[62] M. K. Samimi, T. S. Rappaport, and G. R. MacCartney, "Probabilistic omnidirectional path loss models for millimeter-wave outdoor communications," *IEEE Trans. Wireless Commun. Letters*, vol. 4, no. 4, pp. 357–360, Aug. 2015.

[63] 3rd Generation Partnership Project (3GPP), "3GPP TR 36.873 (v12.7.0): Study on 3D channel model for LTE (release 12)," Dec. 2017.

[64] C. Galiotto, N. K. Pratas, N. Marchetti, and L. Doyle, "A stochastic geometry framework for LOS/NLOS propagation in dense small cell networks," in *2015 IEEE International Conference on Communications (ICC)*. IEEE, 2015, pp. 2851–2856.

[65] C. Galiotto, I. Gomez-Miguelez, N. Marchetti, and L. Doyle, "Effect of LOS/NLOS propagation on area spectral efficiency and energy efficiency of small-cells," in *2014 IEEE Global Communications Conference*. IEEE, 2014, pp. 3471–3476.

[66] M. Di Renzo, "Stochastic geometry modeling and analysis of multi-tier millimeter wave cellular networks," *IEEE Transactions on Wireless Communications*, vol. 14, no. 9, pp. 5038–5057, 2015.

[67] T. Ding, M. Ding, G. Mao, Z. Lin, D. López-Pérez, and A. Y. Zomaya, "Uplink performance analysis of dense cellular networks with LoS and NLoS transmissions," *IEEE Transactions on Wireless Communications*, vol. 16, no. 4, pp. 2601–2613, 2017.

[68] X. Zhang and J. G. Andrews, "Downlink cellular network analysis with multi-slope path loss models," *IEEE Transactions on Communications*, vol. 63, no. 5, pp. 1881–1894, May 2015.

[69] B. Yang, G. Mao, M. Ding, X. Ge, and X. Tao, "Dense small cell networks: From noise-limited to dense interference-limited," *IEEE Transactions on Vehicular Technology*, vol. 67, no. 5, pp. 4262–4277, 2018.

[70] W. Nie, F.-C. Zheng, X. Wang, W. Zhang, and S. Jin, "User-centric cross-tier base station clustering and cooperation in heterogeneous networks: Rate improvement and energy saving," *IEEE J. Sel. Areas Commun.*, vol. 34, no. 5, pp. 1192–1206, May 2016.

[71] A. Davydov, G. Morozov, I. Bolotin, and A. Papathanassiou, "Evaluation of joint transmission CoMP in C-RAN based LTE-A HetNets with large coordination areas," in *2013 IEEE Globecom Workshops (GC Wkshps)*. IEEE, 2013, pp. 801–806.

[72] M. Sawahashi, Y. Kishiyama, A. Morimoto, D. Nishikawa, and M. Tanno, "Coordinated multipoint transmission/reception techniques for LTE-Advanced," *IEEE Wireless Communications*, vol. 17, no. 3, p. 26, 2010.

[73] R. Irmer, J. Droste, P. Marsch, M. Grieger, G. Fettweis, S. Brueck, H.-P. Mayer, L. Thiele, and V. Jungnickel, "Coordinated multipoint: Concepts, performance, and field trial results," *IEEE Communications Magazine*, vol. 49, no. 2, pp. 102–111, 2011.

[74] K. Huang and J. G. Andrews, "A stochastic-geometry approach to coverage in cellular networks with multi-cell cooperation," in *2011 IEEE Global Telecommunications Conference-GLOBECOM 2011*. IEEE, 2011, pp. 1–5.

[75] J.-B. Seo, S.-Y. Kim, and V. C. Leung, "Outage probability characterization of CoMP-joint transmission with path-loss and rayleigh fading," *IEEE Communications Letters*, vol. 19, no. 1, pp. 78–81, 2015.

[76] D. Jaramillo-Ramirez, M. Kountouris, and E. Hardouin, "Coordinated multi-

point transmission with imperfect CSI and other-cell interference," *IEEE Transactions on Wireless Communications*, vol. 14, no. 4, pp. 1882–1896, 2015.

[77] M. Xu, X. Tao, F. Yang, and H. Wu, "Enhancing secured coverage with CoMP transmission in heterogeneous cellular networks," *IEEE Communications Letters*, vol. 20, no. 11, pp. 2272–2275, 2016.

[78] S. Geirhofer and P. Gaal, "Coordinated multi point transmission in 3GPP LTE heterogeneous networks," in *2012 IEEE Globecom Workshops*. IEEE, 2012, pp. 608–612.

[79] A. H. Sakr and E. Hossain, "Location-aware cross-tier coordinated multipoint transmission in two-tier cellular networks," *IEEE Transactions on Wireless Communications*, vol. 13, no. 11, pp. 6311–6325, 2014.

[80] B. Du, C. Pan, W. Zhang, and M. Chen, "Distributed energy-efficient power optimization for CoMP systems with max-min fairness," *IEEE Communications Letters*, vol. 18, no. 6, pp. 999–1002, 2014.

[81] G. Grebla, B. Birand, P. van de Ven, and G. Zussman, "Joint transmission in cellular networks with CoMP—stability and scheduling algorithms," *Performance Evaluation*, vol. 91, pp. 38–55, 2015.

[82] S. Li, Q. Cui, H. Haas, X. Tao, and X. Chen, "Joint power allocation for coherent downlink coordinated transmission," in *2012 IEEE Vehicular Technology Conference (VTC Fall)*. IEEE, 2012, pp. 1–5.

[83] X. Yu, Q. Cui, and M. Haenggi, "Coherent joint transmission in downlink heterogeneous cellular networks," *IEEE Wireless Communications Letters*, vol. 7, no. 2, pp. 274–277, 2018.

[84] E. Dahlman, S. Parkvall, and J. Skold, *4G: LTE/LTE-Advanced for mobile broadband*. Academic press, 2013.

[85] J. Lee, Y. Kim, H. Lee, B. L. Ng, D. Mazzarese, J. Liu, W. Xiao, and Y. Zhou, "Coordinated multipoint transmission and reception in LTE-Advanced systems," *IEEE Communications Magazine*, vol. 50, no. 11, pp. 44–50, 2012.

[86] P. Liu, S. Gazor, I.-M. Kim, and D. I. Kim, "Noncoherent relaying in energy harvesting communication systems," *IEEE Transactions on Wireless Communications*, vol. 14, no. 12, pp. 6940–6954, 2015.

[87] G. Nigam, P. Minero, and M. Haenggi, "Coordinated multipoint joint transmission in heterogeneous networks," *IEEE Trans. Commun.*, vol. 62, no. 11, pp. 4134–4146, Nov. 2014.

[88] R. Tanbourgi, S. Singh, J. G. Andrews, and F. K. Jondral, "A tractable model for noncoherent joint-transmission base station cooperation," *IEEE Transactions on Wireless Communications*, vol. 13, no. 9, pp. 4959–4973, 2014.

[89] R. Tanbourgi, S. Singh, J. G. Andrews, and F. K. Jondral, "Analysis of noncoherent joint-transmission cooperation in heterogeneous cellular networks," *IEEE ICC 2014*, pp. 5160–5165, Jun. 2014.

[90] N. Lee, R. W. Heath, D. Morales-Jimenez, and A. Lozano, "Base station cooperation with dynamic clustering in super-dense cloud-ran," in *2013 IEEE Globecom Workshops (GC Wkshps)*, 2013, pp. 784–788.

[91] M. Hong, R.-Y. Sun, H. Baligh, and Z.-Q. Luo, "Joint base station clustering and beamformer design for partial coordinated transmission in heterogenous networks," *arXiv preprint arXiv:1203.6390*, 2012.

[92] P. D. Mankar, G. Das, and S. S. Pathak, "Modeling and coverage analysis of BS-centric clustered users in a random wireless network," *IEEE Wireless Communications Letters*, vol. 5, no. 2, pp. 208–211, 2016.

[93] R. Corvaja, J. J. G. Fernandez, and A. G. Armada, "Mean achievable rates in

clustered coordinated base station transmission with block diagonalization," *IEEE Transactions on Communications*, vol. 61, no. 8, pp. 3483–3493, 2013.

[94] M. Haenggi, *Stochastic geometry for wireless networks*. Cambridge University Press, 2012.

[95] F. Baccelli and B. Błaszczyszyn, *Stochastic Geometry and Wireless Networks*. Now Publishers, Inc., 2010.

[96] D. Moltchanov, "Distance distributions in random networks," *Ad Hoc Networks*, vol. 10, no. 6, pp. 1146–1166, 2012.

[97] D. López-Pérez, M. Ding, H. Claussen, and A. H. Jafari, "Towards 1 Gbps/ue in cellular systems: Understanding ultra-dense small cell deployments," *IEEE Communications Surveys & Tutorials*, vol. 17, no. 4, pp. 2078–2101, 2015.

[98] M. Kamel, W. Hamouda, and A. Youssef, "Performance analysis of multiple association in ultra-dense networks," *IEEE Transactions on Communications*, vol. 65, no. 9, pp. 3818–3831, 2017.

[99] C. Khirallah, D. Vukobratović, and J. Thompson, "On energy efficiency of joint transmission coordinated multi-point in lte-advanced," in *2012 International ITG Workshop on Smart Antennas (WSA)*. IEEE, 2012, pp. 54–61.

[100] Y. Zhang, S. Bi, and Y.-J. A. Zhang, "User-centric joint transmission in virtual-cell-based ultra-dense networks," *IEEE Transactions on Vehicular Technology*, vol. 67, no. 5, pp. 4640–4644, 2018.

[101] H. Alzer, "On some inequalities for the incomplete gamma function," *Mathematics of Computation of the American Mathematical Society*, vol. 66, no. 218, pp. 771–778, 1997.

[102] H. S. Kang and D. K. Kim, "User-centric overlapped clustering based on anchor-based precoding in cellular networks," *IEEE Communications Letters*,

vol. 20, no. 3, pp. 542–545, 2016.

[103] N. Miyoshi, "Downlink coverage probability in cellular networks with poisson–poisson cluster deployed base stations," *IEEE Wireless Communications Letters*, vol. 8, no. 1, pp. 5–8, 2018.

[104] S. Hashima, O. Muta, M. Alghonimey, H. Shalaby, H. Frukawa, S. Elnoubi, and I. Mahmoud, "Area spectral efficiency performance comparison of downlink fractional frequency reuse schemes for mimo heterogeneous networks," in *2014 International Conference on Information Science, Electronics and Electrical Engineering*, vol. 2, Apr. 2014, pp. 1005–1010.

[105] Y. Huang, X. Zhang, J. Zhang, J. Tang, Z. Su, and W. Wang, "Energy-efficient design in heterogeneous cellular networks based on large-scale user behavior constraints," *IEEE Transactions on Wireless Communications*, vol. 13, no. 9, pp. 4746–4757, Sep. 2014.

[106] M. Hong, R. Sun, H. Baligh, and Z.-Q. Luo, "Joint base station clustering and beamformer design for partial coordinated transmission in heterogeneous networks," *IEEE J. Sel. Areas Commun.*, vol. 31, no. 2, pp. 226–240, Feb. 2013.

[107] F. Baccelli and A. Giovanidis, "A stochastic geometry framework for analyzing pairwise-cooperative cellular networks," *IEEE Trans. Wireless Commun.*, vol. 14, no. 2, pp. 794–808, Feb. 2015.

[108] Y. Zhong, P. Qiao, W. Zhang, and F.-c. Zheng, "No blind spot: network coverage enhancement through joint cooperation and frequency reuse," *J. Commun. Netw.*, vol. 18, no. 5, pp. 773–783, Oct. 2016.

[109] 3rd Generation Partnership Project (3GPP), "3GPP TR 36.828 (v11.0.0): Further enhancements to LTE Time Division Duplex (TDD) for Downlink-

Uplink (DL-UL) interference management and traffic adaptation," Jan. 2012.

[110] B. Yang, G. Mao, M. Ding, X. Ge, and X. Tao, "Performance analysis of dense SCNs with generalized shadowing/fading and NLoS/LoS transmissions," *arXiv preprint arXiv:1701.01544*, Jan. 2017.

[111] H. Zhang, H. Liu, C. Jiang, X. Chu, A. Nallanathan, and X. Wen, "A practical semidynamic clustering scheme using affinity propagation in cooperative picocells," *IEEE Trans. Veh. Technol.*, vol. 64, no. 9, pp. 4372–4377, Sep. 2015.

[112] Q. Zhang, H. H. Yang, T. Q. Quek, and J. Lee, "Heterogeneous cellular networks with LoS and NLoS transmissions—The role of massive mimo and small cells," *IEEE Transactions on Wireless Communications*, vol. 16, no. 12, pp. 7996–8010, Sep. 2017.

[113] X. Ge, T. Han, Y. Zhang, G. Mao, C.-X. Wang, J. Zhang, B. Yang, and S. Pan, "Spectrum and energy efficiency evaluation of two-tier femtocell networks with partially open channels," *IEEE Transactions on Vehicular Technology*, vol. 63, no. 3, pp. 1306–1319, 2014.

[114] M. Bacha, Y. Wu, and B. Clerckx, "Downlink and uplink decoupling in two-tier heterogeneous networks with multi-antenna base stations," *IEEE Transactions on Wireless Communications*, vol. 16, no. 5, pp. 2760–2775, 2017.

[115] H. Ding, D. B. da Costa, X. Wang, U. S. Dias, R. T. de Sousa, and J. Ge, "On the effects of los path and opportunistic scheduling in energy harvesting relay systems," *IEEE Transactions on Wireless Communications*, vol. 15, no. 12, pp. 8506–8524, 2016.

[116] W. Xi, X. Yun, S. Nagata, Y. Kishiyama, and L. Chen, "An enhanced interference measurement scheme for CoMP in LTE-Advanced downlink," in *2013*

IEEE International Conference on Communications (ICC). IEEE, 2013, pp. 4870–4874.

[117] H. Ding, D. B. da Costa, X. Wang, U. S. Dias, R. T. de Sousa, and J. Ge, "Energy harvesting relay systems in mixed Rician and Rayleigh fading: The effects of LOS path component," in *2016 IEEE Wireless Communications and Networking Conference*, 2016, pp. 1–6.

[118] N. Lee, D. Morales-Jimenez, A. Lozano, and R. W. Heath, "Spectral efficiency of dynamic coordinated beamforming: A stochastic geometry approach," *IEEE Transactions on Wireless Communications*, vol. 14, no. 1, pp. 230–241, 2015.